

## **INFORMATION TO USERS**

**This manuscript has been reproduced from the microfilm master. UMI films the text directly from the original or copy submitted. Thus, some thesis and dissertation copies are in typewriter face, while others may be from any type of computer printer.**

**The quality of this reproduction is dependent upon the quality of the copy submitted. Broken or indistinct print, colored or poor quality illustrations and photographs, print bleedthrough, substandard margins, and improper alignment can adversely affect reproduction.**

**In the unlikely event that the author did not send UMI a complete manuscript and there are missing pages, these will be noted. Also, if unauthorized copyright material had to be removed, a note will indicate the deletion.**

**Oversize materials (e.g., maps, drawings, charts) are reproduced by sectioning the original, beginning at the upper left-hand corner and continuing from left to right in equal sections with small overlaps. Each original is also photographed in one exposure and is included in reduced form at the back of the book.**

**Photographs included in the original manuscript have been reproduced xerographically in this copy. Higher quality 6" x 9" black and white photographic prints are available for any photographs or illustrations appearing in this copy for an additional charge. Contact UMI directly to order.**

# **UMI**

**A Bell & Howell Information Company  
300 North Zeeb Road, Ann Arbor MI 48106-1346 USA  
313/761-4700 800/521-0600**



**University of Alberta**

**A Thermodynamic Automaton and Some Applications**

by

Dongsong Yang



**A THESIS  
SUBMITTED TO THE FACULTY OF GRADUATE STUDIES AND RESEARCH  
IN PARTIAL FULFILLMENT OF THE REQUIREMENTS FOR THE DEGREE  
OF  
DOCTOR OF PHILOSOPHY  
IN  
GEOPHYSICS**

**DEPARTMENT OF PHYSICS**

**EDMONTON, ALBERTA**

**SPRING 1997**



**National Library  
of Canada**

**Acquisitions and  
Bibliographic Services**

**395 Wellington Street  
Ottawa ON K1A 0N4  
Canada**

**Bibliothèque nationale  
du Canada**

**Acquisitions et  
services bibliographiques**

**395, rue Wellington  
Ottawa ON K1A 0N4  
Canada**

*Your file Votre référence*

*Our file Notre référence*

The author has granted a non-exclusive licence allowing the National Library of Canada to reproduce, loan, distribute or sell copies of his/her thesis by any means and in any form or format, making this thesis available to interested persons.

The author retains ownership of the copyright in his/her thesis. Neither the thesis nor substantial extracts from it may be printed or otherwise reproduced with the author's permission.

L'auteur a accordé une licence non exclusive permettant à la Bibliothèque nationale du Canada de reproduire, prêter, distribuer ou vendre des copies de sa thèse de quelque manière et sous quelque forme que ce soit pour mettre des exemplaires de cette thèse à la disposition des personnes intéressées.

L'auteur conserve la propriété du droit d'auteur qui protège sa thèse. Ni la thèse ni des extraits substantiels de celle-ci ne doivent être imprimés ou autrement reproduits sans son autorisation.

0-612-21658-6

**University of Alberta**

**Library Release Form**

**Name of Author:** Dongsong Yang

**Title of Thesis:** A Thermodynamic Automaton and Some  
Applications

**Degree:** Doctor of Philosophy

**Year this Degree Granted:** 1997

Permission is hereby granted to the University of Alberta Library to reproduce single copies of this thesis and to lend or sell such copies for private, scholarly, or scientific research purpose only.

The author reserves other publication rights, and neither the thesis nor extensive extracts from it may be printed or otherwise reproduced without the author's prior written permission.

Dongsong Yang

# 509, 9747-104 Street


Edmonton, Alberta

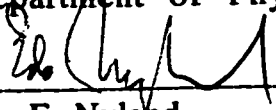
T5K 0Y6


December 5, 1996

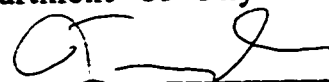
**University of Alberta**  
**Faculty of Graduate Studies and Research**

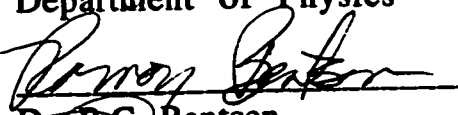
The undersigned certify that they have read, and recommend to the Faculty of Graduate Studies and Research for acceptance, a thesis entitled **A Thermodynamic Automaton and Some Applications** submitted by **Dongsong Yang** in partial fulfillment of the requirements for the degree of **Doctor of Philosophy** in **Geophysics**.

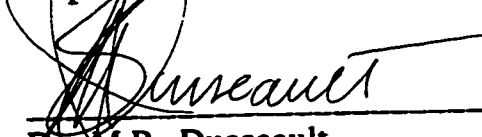
  
\_\_\_\_\_  
Dr. T.J.T. Spanos (Supervisor)  
Department of Physics

  
\_\_\_\_\_  
Dr. E. Nyland  
Department of Physics

  
\_\_\_\_\_  
Dr. T. Evans  
Department of Physics

  
\_\_\_\_\_  
Dr. J.C. Tuszynski  
Department of Physics

  
\_\_\_\_\_  
Dr. R.G. Bentsen  
Department of Mining Met & Pet Engin

  
\_\_\_\_\_  
Dr. M.B. Dusseault  
External Examiner

Date: *Oct 30, 1996*

## **Abstract**

In this study, a thermodynamic automaton model is constructed and used to simulate a number of physical processes associated with diffusion, one phase flow, and dispersion. In addition, megascopic concentration and capillary pressure in porous media are considered from a theoretical point of view.

In Chapter 2, a thermodynamic automaton model is constructed which allows for a continuous distribution of particle velocities and thus yields a clear definition of temperature.

In Chapter 3, the validity of the thermodynamic automaton model is checked by modeling the thermal equilibrium state, initialization of a thermal equilibrium state and diffusion in a tube. The simulation results are found to be consistent with theoretical predictions.

In Chapter 4, the automaton model is used to simulate plane Poiseuille flow with no-slip (insulator) and thermal boundary (heat bath) conditions. Two distinct thermodynamic processes of the flow

with the two boundary conditions are observed. The simulation results are consistent to the predictions of the kinetic theory of gases. In Chapter 5, the automaton model is utilized to simulate one phase flow, diffusion and dispersion in porous media at the megascopic scale. The simulation results show that (1) one phase flow simulations in porous media are consistent with Darcy's law; (2) the apparent diffusion coefficient decreases with a decrease in permeability; (3) small scale heterogeneity did not affect diffusion and dispersion processes significantly; (4) dispersion increases with an increase in flow velocity.

In Chapter 6, dispersion in porous media is simulated at both the pore scale and the mega-scale with enhanced rules. The enhanced rules allow for large scale phase separation. Also they reflect pore scale information that the solid has a higher probability to collide with the displaced fluid, and incorporate pore structure and pressure difference between the displacing and displaced fluids. The simulation results are consistent with both theoretical predictions and experimental results.



In Chapter 7, a megascopic capillary pressure equation is derived by starting from the complete system of equations for compressible phases and taking the incompressible limit.

## **ACKNOWLEDGEMENTS**

I am extremely grateful to my supervisor, Dr. T.J.T. Spanos for his guidance, support and encouragement during the course of my work. His valuable discussions and excellent suggestions have contributed to this research.

I am grateful to Dr. E. Nyland, Dr. M.E. Evans, Dr. J.A. Tuszynski, Dr. R.G. Bentsen and Dr. M.B. Dusseault for their comprehensive and constructive critiquing of my research. My appreciation is extended to my colleagues Dr. J. Eastwood, Dr. C. Hickey, Dr. D. Shim for their scientific help and friendship.

My special thanks go to Dr. V. de la Cruz for his fruitful discussion and insight into the physics in porous media, and Dr. N. Udey for his great help in terms of coding in C and for his insight into the whole project.

The financial support for the project was provided by Natural Sciences and Engineering Research Council and Graduate Teaching Grants from the University of Alberta.

Finally, I would like to express my deep gratitude to my wife, Minghui, for her love, support and understanding I received during my studies.

## **TABLE OF CONTENTS**

<b>CHAPTER</b>	<b>PAGE</b>
<b>1. INTRODUCTION</b>	<b>1</b>
1.1 Thesis Organization	5
1.2 Bibliography	6
 <b>2. EVOLUTION OF CELLULAR AUTOMATA AND CONSTRUCTION     OF A THERMODYNAMIC AUTOMATON</b>	 <b>9</b>
2.1 Introduction	9
2.2 Concepts of Cellular Automata and Lattice Gas Models	11
2.3 Literature Review	13
 2.4 Description and Evolution of the Cellular Automata Lattice Gas Models	  20
2.4.1 HPP Model	21
2.4.2 FHP Model	22
2.4.3 FCHC Model	23
2.4.4 Multi-Speed Model	23
2.5 Construction of a Thermodynamic Automaton Model	25
2.6 Summary and Conclusions	31

2.7 Bibliography	33
3. THERMODYNAMIC AUTOMATON SIMULATION OF THERMAL EQUILIBRIUM STATE AND DIFFUSION IN A TUBE	42
3.1 Introduction	42
3.2 Theoretical Background	44
3.3 The Model and Simulation Experiments	52
3.4 Results and Discussion	56
3.4.1 Simulation of Thermal Equilibrium State	56
3.4.2 Simulation of Initialization of Thermal Equilibrium State	64
3.4.3 Simulation of Diffusion in a Tube	69
3.5 Conclusions	76
3.6 Bibliography	77
4. FLOW SIMULATION USING A THERMODYNAMIC AUTOMATON MODEL	78
4.1 Introduction	78
4.2 Theoretical Background	80
4.3 The Model and Simulation Experiments	83
4.4 Results and Discussion	86

4.4.1 Simulation of Thermal Dynamic Process of Plane Poiseuille Flow	86
4.4.2 Fluid Viscosity Determination	89
4.5 Conclusions	92
4.6 Bibliography	93
 5. THERMODYNAMIC AUTOMATON SIMULATIONS OF FLUID FLOW, DIFFUSION AND DISPERSION IN POROUS MEDIA	95
5.1 Introduction	95
5.2 Theoretical Background	96
5.3 The Model and Simulation Experiments	101
5.4 Results and Discussion	105
5.4.1 One Phase Flow in Porous Media	105
5.4.2 Diffusion in Porous Media	113
5.4.3 Dispersion in Porous Media	116
5. 5. Conclusions	120
5.6. Bibliography	121
 6. AUTOMATON SIMULATION OF DISPERSION IN POROUS MEDIA WITH ENHANCED RULES	124
6.1 Introduction	124

6.2 Theoretical Background	126
6.3 The Model and Simulation Experiments	127
6.4 Results and Discussion	133
6.4.1 Pore Scale Dispersion Simulation	133
6.4.2 Mega-Scale Dispersion Simulation	135
6.5 Conclusions	141
6.6 Bibliography	142
 7. MEGASCOPIC CAPILLARY PRESSURE	 143
7.1 Introduction	143
7.2 The Flow of Two Compressible Fluids	146
7.3 A Megascopic Capillary pressure Equation	150
7.4 Conclusions	156
7.5 Bibliography	158
 8. CONCLUSIONS	 160
8.1 Bibliography	164
 APPENDIX	 165

## LIST OF FIGURES

FIGURE	PAGE
3.1 Analytic solution to the evolution of concentration $C$ with the parameter $Dt$ being 0.01, 0.02, 0.03, 0.05, 0.07, 0.09, 0.1, 0.2, 0.3, 0.5, 0.7, 0.9, 1, 2, 3, 5, 7, and 9.	51
3.2 The speed distributions of particles after 1000 iterations. 6000 particles with the same mass and speed were initialized with random angles. Relativistic collision rules were applied in these simulations.	57
3.3 The speed distributions of particles after 1000 iterations. The initial configuration for the simulations was the same as in Figure 3.2. Non-relativistic collision rules were employed in these simulations.	58
3.4 A plot of probability density of particles versus speed and angle after 1000 iterations. The speed distribution which is invariant with angle demonstrates that isotropy is maintained in the relativistic cases.	59

- 3.5 A plot of probability density of particles versus speed and angle after 1000 iterations. The speed distribution which is invariant with angle demonstrates that isotropy is maintained in the non-relativistic cases. 60
- 3.6 Corresponding plots of  $\ln(P(E))$  versus Energy  $E$  for the particle speed distributions with  $v_0=0.1$ , and  $0.2$  for Figure 3.3. The plots are straight lines as expected. Temperatures can be determined from the slopes of the lines. 61
- 3.7 Initialization of a thermal equilibrium state with 60000 particles with  $m=1$ ,  $\beta=200$  and  $50$ . The speed distribution curves represent "snapshots" of a thermal equilibrium state. 65
- 3.8 Initialization of a thermal equilibrium state with 60000 particles with  $m=2$ ,  $\beta=100$  and  $25$ . The speed distribution curves represent "snapshots" of a thermal equilibrium state. 66



3.9	Corresponding plots of $\ln(P(E))$ versus Energy $E$ for Figure 3.7. Temperatures can be determined from the slopes of the lines.	67
3.10	Corresponding plots of $\ln(P(E))$ versus Energy $E$ for Figure 3.8. Temperatures can be determined from the slopes of the lines.	68
3.11	Simulation results of the evolution of concentration profiles at iterations of 0, 40, 80, 200, 400, 700 for self-diffusion at a temperature of 0.005.	70
3.12	Nonlinear error function best fits of the evolution of concentration profiles in Figure 3.11.	71
3.13	Simulation results of the evolution of concentration profiles at iterations of 0, 400, 700, 1000, 1180, 2000 for self-diffusion at a temperature of 0.00005.	73
3.14	Nonlinear best fits of evolution of tracer concentration profiles in Figure 3.13.	74

4.1	Simulation and comparison of thermal dynamic processes of plane Poiseuille flow with no-slip boundary conditions i.e. thermal insulator (left column) and thermodynamic boundary conditions i.e. heat bath (right column).	87
4.2	Fluid viscosity vs. $\sqrt{T}$ . Viscosity is proportional to $\sqrt{T}$ .	90
5.1	Flow velocity profiles with two different probabilities of a solid collision at lattice sites (0.1 and 0.5).	106
5.2	Flow velocity vs. pressure drop for one phase flow in a porous medium.	107
5.3	The change of flow velocity profiles with changes in $1/\text{permeability}$ .	109
5.4	A flow velocity profile with the probability of a solid collision being zero.	110
5.5	A flow velocity profile with a low flow velocity (0.001).	111

- 5.6 A flow velocity profile with a very low flow velocity  
(0.00006). 112
- 5.7 Diffusion in a homogeneous porous medium. The  
concentration profiles are plotted after 200 iterations  
with the probabilities of a solid collision being 0.9, 0.5  
and 0.0. 114
- 5.8 Comparison of diffusion in porous media with different  
distributions of the probability of a solid collision but the  
same mean probability of a solid collision. 115
- 5.9 Dispersion in porous media with a no-slip boundary  
condition for the solid collision. The concentration profiles  
are plotted after 1500 iterations with different flow rates  
and different distributions of the probability of a solid  
collision. 117
- 5.10 Dispersion in porous media with a thermal boundary  
condition for the solid collision. The concentration profiles  
are plotted after 1500 iterations with different flow rates

and different distributions of the probability of a solid collision.	118
6.1 Schematic diagram of tube models A and B.	128
6.2 Pore scale dispersion in both the homogeneous and heterogeneous porous media models shown in Figure 6.1. The concentration profiles are plotted after 300 iterations and at two different temperatures.	134
6.3 Mega-scale dispersion in both a homogeneous and a heterogeneous porous medium with both the flipping probability and the beta factor being zero. The concentration profiles are plotted after 1500 iterations.	136
6.4 Mega-scale dispersion in both a homogeneous and a heterogeneous porous medium with the flipping probability being zero and the beta factor being 0.001. The concentration profiles are plotted after 1500 iterations.	137

6.5 Mega-scale dispersion in both a homogeneous and a heterogeneous porous medium with the flipping probability being zero and the beta factor being 0.01. The concentration profiles are plotted after 1500 iterations. 138

6.6 Mega-scale dispersion in both a homogeneous and a heterogeneous porous medium with the flipping probability being 1 and the beta factor being 0.01. The concentration profiles are plotted after 1500 iterations. 139

## **LIST OF TABLES**

<b>TABLE</b>	<b>PAGE</b>
2.1 Classifications of model types.	30
3.1 Theoretical values for beta, T, ln (beta) and -beta.	46
3.2 Simulation values for beta, T, ln(beta) and -beta.	63
3.3 Diffusion coefficients of a diffusion process at different time steps at temperature 0.005.	72
3.4 Diffusion coefficients of the diffusion process at different time steps at temperature 0.00005.	75
4.1 Calculated fluid viscosity based on Experiment 2.	89
5.1 Average flow rate vs. pressure drop.	108

## LIST OF SYMBOLS

### Chapter 2

#### Roman

$N$	total number of iterations
$N_a$	number of iterations for particle moving along a
$N_b$	number of iterations for particle moving along b
$P$	probability
$P_0, P_a$ and $P_b$	probabilities defined by $v_a$ and $v_b$
$v$	particle velocity
$v_a$	particle vleocity along a
$v_b$	particle velocity along b
$\langle \Delta \rangle$	mean particle displacement

### Chapter 3

#### Roman

$C$	concentration of the tracer
$C_0$	initial concentration of the tracer
$D$	diffusion coefficient
$E$	particle energy
$i$	diffusion flux
$m$	particle mass
$P(E)$	probability density of finding a particle in energy range $E+dE$ .
$t$	time or iteration
$T$	temperature

$v$	particle velocity
$v_0$	initial particle velocity
$x$	univariate random variable

## Chapter 4

### Roman

$h$	half separation distance between two parallel plates
$p$	pressure
$Q$	flux of fluid
$\sqrt{T}$	square root of temperature
$t$	time
$T$	temperature
$u$	velocity
$u_a$	mean velocity of fluid
$u_x$	velocity along $x$

### Greek

$\rho$	fluid density
$\mu$	fluid viscosity
$\Phi$	viscous dissipation of kinetic energy
$\tau$	shear stress

## Chapter 5

### Roman

$C$	concentration of tracer
$D$	diffusion coefficient



	$D_a$	apparent diffusion coefficient
	$D_l$	longitudinal dispersion coefficient
	$F$	formation electric resistivity
	$g$	acceleration of gravity
	$K$	permeability of porous media
	$p$	pressure
	$q$	volumetric flow rate/unit area
	$Q_{ij}$	mobility ratio
	$T$	temperature
Greek		
	$\rho$	fluid density
	$\eta$	porosity of the porous medium
	$\mu$	fluid viscosity
<b>Chapter 6</b>		
Roman		
	$B$	blue particle
	$B_0$	segregated blue particles
	$B_l$	mixed blue particles
	$HO$	homogeneous model
	$HE$	heterogeneous model
	$m$	particle mass
	$n$	particle number at present time
	$n'$	particle number at the previous time
	$R$	red particle
	$R_0$	segregated red particles
	$R_l$	mixed red particles

	T	temperature
	v	particle velocity
Greek		
	$\beta'$	beta factor
<b>Chapter 7</b>		
Roman		
	C	concentration of fluid
	J	Leverett J function
	$K_i$	bulk modulus of fluid i (i=1, 2)
	$K_s$	bulk modulus of solid
	K	permeability
	P	fractional porosity of the wetting phase (in Leverett J function)
	$P_i$	macroscopic pressure of fluid i (i=1, 2)
	$Q_{ij}$	Mobilities (i, j=1,2) (cf. de la Cruz and Spanos, 1983)
	$S_i$	saturation of fluid i (i=1, 2)
	$\mathbf{v}_i$	macroscopic velocity vector of fluid i (i=1, 2)
Greek		
	$\alpha$	surface tension
	$\alpha_i$	compliance factor for fluid i (i=1, 2) for incompressible flow defined in equations (7.29) and (7.30) (process-dependent)

$\beta$	compliance factor for the flow of two incompressible fluids (cf. eqns. (7.32) and (7.33) for relation to $\alpha_i$ )
$\beta'$	beta factor defined in Equation (7.36)
$\delta_i$	compliance factor for a compressible fluid ( $i=1, 2$ ) (process-dependent) (cf. de la Cruz et al., 1989, 1993)
$\delta_i^a$	modification to static compliance factor for fluid $i$ ( $i=1, 2$ ) as a result of quasi-static flow
$\eta$	porosity of the porous medium
$\eta_i$	fraction of space occupied by fluid $i$ ( $i=1, 2$ ) measured dynamically
$\eta_i^o$	fraction of space occupied by fluid ( $i=1, 2$ ) measured statically
$\mu_i$	shear viscosity of fluid $i$ ( $i=1, 2$ )
$\xi_i$	bulk viscosity of fluid $i$ ( $i=1, 2$ )
$\rho_i$	density of fluid $i$ ( $i=1, 2$ )

## **CHAPTER 1 INTRODUCTION**

This dissertation includes automata simulations and a discussion of the associated physical theory. The automata section of this study consists of three parts: (1) construction of a thermodynamic automaton model; (2) writing the associated computer program in C; and (3) simulations of physical processes such as fluid flow in porous media using the automaton model. The theoretical study consists of a derivation of megascopic capillary pressure in porous media.

With the advent of powerful computers, cellular automata simulations, with simple collision and propagation rules for particles on a lattice, have been applied extensively to simulate hydrodynamics processes (Kadanoff, 1985; D'Humières et al., 1986; Frisch et al., 1987; Rothman, 1988; Hayot, 1991; Boghosian, 1993; Gao and Sharma, 1994a and 1994b; and Gutfraind and Hansen, 1995). Cellular automata models are ideal for parallel computing and are able to model nonlinear processes and complicated boundaries. Since the first cellular automaton model was constructed by Von Neumann (1966), many variant automata models including lattice gas models (Hardy, et al., 1976; Frisch, et al., 1986; and D'Humières, et al., 1986) were developed. However, for these conventional lattice gas models, thermal effects are difficult to incorporate due to discrete particle velocities used in the simulations.

A primary concern of this thesis is to construct a thermodynamic automaton model using continuous particle velocities. This model has a clear definition of temperature (Maxwell-Boltzmann distribution), is able to model thermodynamic boundaries and maintains isotropy in any lattice geometry. The construction of such models is not only of academic but also of practical importance. For instance, this model is able to simulate physical processes such as the motion of ground water contaminants and oil recovery by miscible flooding.

After constructing the thermodynamic automaton model, the model is applied to simulate the following physical processes:

- (1) thermal equilibrium state for one phase;
- (2) initialization of a thermal equilibrium state;
- (3) diffusion in a tube;
- (4) plane Poiseuille flow;
- (5) fluid flow, diffusion and dispersion in porous media; and
- (6) dispersion in porous media with enhanced rules.

Note, diffusion is caused by random motion of molecular particles and dispersion is caused by molecular diffusion and mechanical mixing due to fluid velocity gradients.

The purpose of modeling simple physical processes where analytical solutions are available is to compare the simulation results with analytical results, thus providing a check on the validity of the model. Once exhaustive comparisons strongly support the validity of the model, processes where analytic solutions do not exist are modelled.

The thermal equilibrium state for one phase is first simulated by allowing the particle velocities to evolve naturally. The objectives of this simulation are two-fold: (1) checking the validity of the model and (2) examining if temperature is an internal property of the model. A related issue is to initialize a thermal equilibrium state prior to modeling a physical process, since many physical processes start from a thermal equilibrium state. The initialization of a thermal equilibrium state can be accomplished by initializing the particle velocity distribution to fit the Maxwell-Boltzmann distribution. Subsequently, simulation of diffusion in a tube is considered. This simulation allows one to check the validity of the model by comparing the simulation results with analytic solutions and to determine the diffusion coefficient.

In the second simulation, plane Poiseuille flow with two different boundary conditions is considered. The no-slip boundary condition used in standard lattice gas models is compared to a thermodynamic boundary condition developed for the current model. Fluid viscosity is determined from a steady state flow and the effect of temperature on viscosity is investigated.

In the third simulation, mega-scale one-phase fluid flow and miscible flow in porous media are investigated. The porous medium is introduced into the model by allowing fluid-solid collisions. The effect of permeability on flow, diffusion and dispersion processes is studied. The effect of heterogeneity of the porous medium on diffusion and dispersion as well as the influence of flow rates on

dispersion is studied. For the dispersion simulations, both no-slip and thermal boundary conditions are utilized for fluid-solid collisions and a comparison of the simulation results is made.

In the fourth simulation, both macro-scale (pore scale) and mega-scale dispersion incorporating pore structure effects are studied. The main purpose of the macro-scale dispersion simulations is to illustrate the pore structure effect on dispersion. To include the pore structure effects in a mega-scale dispersion simulation, some additional rules must be added. The justification for these additional rules is discussed and the mega-scale dispersion is modeled with the enhanced rules.

## 1.1 Thesis Organization

Chapter 1 of this thesis provides an introduction and outline to the entire thesis. Chapter 2 provides a detailed description of the evolution of automaton models and the construction of the thermodynamic automaton model. Chapter 3 presents detailed simulations of (1) the thermal equilibrium state for one phase; (2) initialization of the thermal equilibrium state; and (3) diffusion in one dimension. These simulations all use the same periodic boundary conditions and simulation results can be compared with analytic solutions. Chapter 4 presents simulations of channel flow with the standard no-slip boundaries (which act as an insulator) and thermodynamic boundaries (which act as a heat bath). Two distinct processes are observed and a comparison of the two processes is discussed. Fluid viscosity is determined from channel flow with the thermodynamic boundary condition where a steady-state flow is obtained. The effect of temperature on fluid viscosity is examined. In Chapter 5, simulations of single-phase and miscible fluid flow in porous media are presented. For one phase flow in porous media, the simulation results are compared with Darcy's law (Darcy, 1856). For the diffusion simulation, the effect of permeability and heterogeneity on the apparent diffusion coefficients is discussed. For the dispersion simulations, the effect of flow rate on dispersion is analyzed. In Chapter 6, a simulation of macro-scale and mega-scale dispersion is presented. In Chapter 7, a theoretical study of megascopic capillary pressure is presented and, finally, Chapter 8 provides general discussion and the conclusions of this study.



## 1.2 Bibliography

Boghosian, B. M., 1993. Lattice Gas Hydrodynamics. Nuclear Physics B (Proc. Suppl.) 30, 204-210.

Darcy, H., 1856. Les Fontaines Publiques de la Ville Dijon, Dalmont, Paris.

D'Humières, D., Lallemand, P. and Frisch, U., 1986. Lattice Gas Model for 3D Hydrodynamics. Europhys. Lett., Vol. 2, No. 4, 291-297.

Frisch, U., D'Humières, D., Hasslacher, B., Lallemand, P., Pomeau, Y. and Rivet, J.P., 1987. Lattice Gas Hydrodynamics in Two and Three Dimensions. Complex System, Vol. 1, 649-707.

Frisch, U., Hasslacher, B. and Pomeau, Y., 1986. Lattice-Gas Automata for the Navier-Stokes Equation. Physical Review Letters, Vol. 56, No. 14, 1505-1508.

Gao, Y. and Sharma, M.M., 1994a. A LGA Model for Fluid Flow in Heterogeneous Porous Media. Transport in Porous Media. Vol.17, 1 - 17.

Gao, Y. and Sharma, M.M., 1994b. A LGA Model for Dispersion in Heterogeneous Porous Media. *Transport in Porous Media*. Vol. 17, 19-32.

Gutfraind, R. and Hansen, A., 1995. Study of Fracture Permeability Using Lattice Gas Automata. *Transport in Porous Media*. Vol. 18, 131-149.

Hardy, J., de Pazzis, O. and Pomeau, Y., 1976. Molecular Dynamics of a Classical Lattice Gas Transport Properties and Time Correlation Functions. *Physical Review A*, Vol. 13, No. 5, 1949-1961.

Hayot, F., 1991. Fingering Instability in a Lattice Gas. *Physica D* 47. 64-71.

Kadanoff, L.P., 1985. Simulating Hydrodynamics: A Pedestrian Model. *Journal of Statistical Physics*, Vol. 39, Nos. 3-4, 267-283.

Rothman, D.H., 1988. Cellular-Automata Fluids: A Model for Flow in Porous Media. *Geophysics*, Vol. 53, No. 4, 509-518.

Von Neumann, J., 1966. Theory of Self-Reproducing Automata (edited and completed by Burks, A.), University of Illinois Press.

## **CHAPTER 2**

### **EVOLUTION OF CELLULAR AUTOMATA AND CONSTRUCTION OF A THERMODYNAMIC AUTOMATON**

#### **2.1 Introduction**

Cellular automata were originally constructed by Von Neumann (1966) as self-reproducing cellular arrays of computers. They can be regarded as an alternative or complementary approach to the use of mathematical equations for modeling physical systems (Toffoli, 1984). The lattice gas automaton is based on cellular automaton rules and is a variant of cellular automata.

Recently, cellular automata lattice gas models have emerged as a very powerful tool for simulating complex dynamic systems. These models are conceptually simple and ideally suited for parallel computing. They are able to model and provide solutions for nonlinear processes with complicated boundaries, for example, fluid flow through porous media. In those cases where non-unique solutions exist, the output of the cellular automata is also non-unique.

Many advances have been made in the use of lattice gas automata since the first lattice gas model (HPP model) was constructed by Hardy, Pazzis and Pomeau (1976). However, most of these models did not incorporate thermal effects (Hardy, et al., 1976; Wolfram, 1986; Frisch, et al., 1986; and D'Humières, et al., 1986) and those that did include temperature (D'Humières, et al., 1986; Chopard, and Droz, 1987; and Chen, et al., 1989) were severely constrained by discrete particle velocities. Also, a specific lattice (triangular lattice for 2D modeling and face-centered-hypercubic lattice for 3D modeling) had to be used in order to maintain isotropy.

The primary objective of this study was to design a thermodynamic automaton model which is capable of integrating thermal effects into the simulation processes, and to apply the new model to simulate physical processes such as diffusion and dispersion in porous media (as discussed in the following chapters). The new model was constructed by allowing a continuous distribution of particle velocities and using Lorentz invariant elastic collision rules for very high temperatures and non-relativistic elastic scattering for lower temperatures.

## 2.2 Concepts of Cellular Automata and Lattice Gas Models

The word automaton has been used to refer to mathematical models of devices which provide responses by processing and synthesizing given inputs (Salomaa, 1969). Cellular automata have been referred to as the computer scientists counterpart to the physicist's concept of "field" (Toffoli and Margolus, 1987). Boghosian (1989) defined cellular automata as dynamic systems with discretization in space, time and dependent variables. They differ from partial differential equations in that space, time and the dependent variables are discrete. They differ from finite difference approximations in which space and time are discretized but the dependent variables are continuous (Boghosian and Levermore, 1987). A cellular automaton model is specified by initializing arrays of cells and the associated cell states on a lattice in conjunction with rules. These rules govern the evolution of cell states at a specific time interval as a function of its own states and the states of its neighbours at the initial time.

Deterministic cellular automata have a single initial state with a deterministic rule which yields a unique evolution of each state. In contrast, probabilistic cellular automata use a probability distribution

to determine the evolution of each state. Deterministic automata can be regarded as a special case of probabilistic cellular automata.

Lattice gas models also called lattice gas automata, are a special class of cellular automata with particles initialized in cells on a lattice (triangular or square lattice, etc.). The evolution of such a system is associated with the interaction (or collision) of particles within the same cell and in their neighbouring cells, and the propagation of particles. For the simulation of incompressible fluids, a lattice gas can be made to evolve according to the incompressible Navier-Stokes equation in the limit of a large lattice size and low particle velocity (Frisch, et al., 1986).

Since lattice gases are sufficiently interesting and useful to be regarded separately (Boghosian, 1989), there has been a plea to stop referring to lattice gases as cellular automata (Henon, 1988). Therefore, it is not surprising to find various terminology in the literature, such as cellular automata, lattice gases or lattice gas automata, to refer to the same system.

## 2.3 Literature Review

Cellular automata were first introduced in the late forties by John Von Neumann. He was stimulated by Stan Ulam (1952) to provide a cellular model of self-reproduction for the behaviour of complex systems (Von Neumann, 1966). John Conway's "game of life" which is introduced by Gardner (1971) had a major impact on cellular automata research and rendered the word cellular automata very popular.

Cellular automata have been applied in various fields such as mathematics, computer science, biology, communication and engineering. At present, they are becoming increasingly popular for modeling physical systems (Wolfram, 1986) and particularly in hydrodynamics (Kadanoff, 1985; D'Humières et al., 1986; Frisch et al., 1987; Ladd et al., 1988; Rothman, 1988a, 1988b and 1989; Apert and Zaleski, 1990; Vianney and Koelman, 1990; Appert et al., 1991; Chen et al., 1991a; Hayot, 1991; Boghosian, 1993; Gao and Sharma, 1994a and 1994b; and Gutfraind and Hansen, 1995).

Hardy et al. (1976) constructed a lattice gas model which is the so-called HPP model. One of its most important properties is the



existence of an equilibrium state. Based on the HPP model, Frish, Hasslacher and Pomeau (1986) developed a modified lattice gas model which is the so-called FHP model. They gave a concrete example of how cellular automata could be utilized to simulate classical nonlinear fields.

Wolfram (1984) used cellular automata for the description of mathematical systems. He suggested four qualitative classes of cellular automata. They are (1) the spatially homogeneous state; (2) a sequence with a simple stable or periodic structure; (3) chaotic aperiodic behaviour; and (4) complicated localized structure with some propagation.

Later on, Wolfram (1986) conducted a thorough study of the basic theory for cellular automaton fluids. He used kinetic theory to demonstrate that the macroscopic behavior of certain cellular automata corresponded to the Navier-Stokes equation for hydrodynamics.

Kadanoff (1985) used a 2D lattice model to simulate Hele-Shaw experiments for hydrodynamic instability, using a discretized version of hydrodynamic equations implemented in terms of the motion of

so-called "random walkers". His simulation results are in qualitative agreement with the results of Hele-Shaw experiments.

Rothman (1988a) used the cellular automaton FHP model to estimate numerically permeability and verify Darcy's law for 2D fluid flow in porous media. Later on, Rothman and Keller (1988) introduced deterministic collision rules for a lattice gas model and successfully demonstrated the separation of two immiscible fluids. The rule is based on a minimization law and conservation of mass, momentum and particle type. Their numerical results indicated that the surface tension coefficient obeyed Laplace's equation.

Rothman (1988b) applied a lattice gas model to two-phase flow in porous media and Rayleigh-Taylor instability. His numerical results showed the existence of a critical capillary pressure in simulations of two-phase flow in a channel and that predictions of linear stability theory were observed in a simulation of Rayleigh-Taylor instability.

Rothman (1989) extended his studies to macroscopic laws for immiscible two phase flow in porous media, using a lattice gas model. The results indicated that the macroscopic flow is a nonlinear

function of the applied forces for a small applied force but linear thereafter.

Somers and Rem (1991) developed a coloured particle scheme (Rothman and Keller, 1988) by introducing coloured holes in the lattice model. This new model extended the original nearest-neighbour particle interaction to several lattice lengths. Their programming codes for all features of the processes including collision and propagation were optimized for a parallel machine, which improved the computational efficiency.

Chen et al. (1991b) modified the model of Somers and Rem by permitting the coloured particles to move only along the opposite direction of the local colored hole flux. They applied their model to simulate phase separation, surface tension and the contact angle between the fluids and the solid wall.

Gunstensen (1989) extended the two-phase immiscible lattice gas model to a model for three immiscible phases, for instance, oil, gas and water. Two examples of a phase separation of three fluids in 2D were provided. One case was characterized by the three surface

tensions being equal, and in the other case, one surface tension was greater than the sum of the other two.

Gunstensen (1991) used a 3D lattice model to study two phase flow in porous media. He found that the usual description of flow is applicable under conditions of high pressure gradients but is not applicable at low pressure gradients.

Cheng and Ebner (1993) carried out a study of the dynamics of liquid-droplet spreading, using a Monte Carlo simulation based on an Ising lattice gas model. They found that there existed a precursor film with microscopic thickness and a cross-over from a regime where spreading rates relied on the strength of the long-range potential to one where it didn't.

Gao and Sharma (1994a and 1994b) proposed a lattice gas automaton to simulate fluid flow, and flow with dispersion and diffusion in heterogeneous porous media. They demonstrated that effective permeability and the local fluid flow field can be obtained and the longitudinal dispersion coefficient can be computed for heterogeneous porous media.

Gutfraind and Hansen (1995) investigated the problem of flow permeability of fracture joints using lattice gas automata simulations. They further pointed out that a natural extension of their work, i.e., seeking a solution of boundary value problems in the presence of surface roughness and investigating tracer dispersion in a channel with rough walls, can best be attacked by a lattice gas automaton model.

More recently, a lattice Boltzmann model has been used widely to study hydrodynamic properties (McNamara and Zanetti, 1988; Higuera and Succi, 1989; Higuera et al., 1989; Succi et al., 1991; Lavallée et al., 1991; Gunstensen and Rothman, 1991; Gunstensen, 1991; Gunstensen et al., 1991; Benzi et al., 1992; Grunau et al., 1993; Rybka et al., 1993; Martinez et al., 1993; and Sone and Takata, 1994). This model is based on the Boltzmann transport equation and has the advantage of by-passing the averaging step utilized in the lattice gas model and thus eliminating statistical fluctuation or noise. A further advantage has been demonstrated by Rybka et al. (1993) in studies of flow in a confined geometry. The disadvantage of the lattice Boltzmann model is its round-off error due to the floating point arithmetic.

Adler, D'Humières and Rothman (1994) used a Boltzmann approximation to calculate surface tension as a function of population density in a 2D lattice gas model of immiscible fluids. They found that generally good agreement exists between the theory and the data calculation for surface tension.

In summary, the cellular automaton lattice gas model has been applied to diverse subjects, particularly in fluid flow in porous media. Recent studies have been advanced to 3D modeling of immiscible fluid displacement in porous media.

## **2.4 Description and Evolution of the Cellular Automata Lattice Gas Models**

In this section, the common core characteristics of cellular automata lattice gas models are presented and descriptions of the specific models are provided. The differences among those models are emphasized and the evolution of these models is highlighted.

The lattice gas model, as its name indicates, consists of a lattice (triangular, square, hexagonal), cells, and "gas particles". The particles reside in cells on the lattice. The main simulation processes include

- (1) initialization of particles, cells, lattice, and boundary conditions for lattice;
- (2) particle collision;
- (3) particle propagation;
- (4) iterations in discrete time steps; and
- (5) averaging procedures in order to obtain a macroscopic description.

All the lattice gas models possess most of these characteristics but differ in the rules used to incorporate the above five processes.

### 2.4.1 HPP Model

The regular, square, 2D lattice with unit link lengths was utilized in the HPP model (Hardy, Pazzis and Pomeau, 1976). Up to four indistinguishable particles lie on each vertex. The particles have equal mass, unit speed, unit velocity and a direction coinciding with one of the four link directions, i.e., east, south, west, or north. The simultaneous occupation of a vertex by identical particles is not allowed.

Evolution of the system includes two steps, e.g., binary (two particle) collisions and propagation. The conservation of the number of particles and momentum are respected throughout the whole process. At each time step, the particle moves to the neighbouring site to which its velocity was pointing. When two particles with opposite directions collide (head on collisions) at a site, the configuration is replaced by another one at a right angle to the original one. In all the other cases, the configurations remain unchanged.

The HPP model is a deterministic model. The collision and propagation rules obey conservation of particle number, mass and



momentum. The total energy is also conserved but is associated with conservation of mass since velocity is constant. Thus, it does not play any dynamic role.

One of the main flaws of the HPP model is its lack of isotropy because of the square lattice symmetry. This renders the HPP automaton invariant under 90 degree rotations but is insufficient to guarantee the isotropy of the fourth degree tensor relating the momentum flux to quadratic terms in the velocity. It is noted that in the discrete model, the structure of the lattice effects the direction of the propagation of the particles. Thus, the only 2D lattice able to maintain isotropy is a triangular lattice (Frish et al., 1986). However, in the probabilistic model (see Section 2.5), the lattice only records the position of particles and the structure of the lattice has no effect on particle motions after sufficiently large distance.

#### **2.4.2 FHP Model**

A triangular instead of square lattice is employed in the FHP model (Frish et al., 1986) to ensure isotropy. The site at the centre of each cell is connected to its six hexagonal neighbouring cells and the particle velocities point in one of the six link directions. The particles

on the six links at each site are arranged according to rules which conserve the number and total momentum of the particles. The Fermi exclusion rule also applies.

The set-up is similar to the HPP lattice gas model with modified collisions, and both binary and triple collisions being allowed. For example, two particles meeting head on might rotate through  $60^\circ$  and a triple of particles through  $120^\circ$ . These collision features are important in determining some parameters such as viscosity. This model can be regarded as a non-deterministic model since the collision rule is non-deterministic. Again, there is no independent energy conservation law as in the HPP model. Since the particle speed is discrete, i.e., 0 or 1, this model did not incorporate thermal effects.

### **2.4.3 FCHC Model**

The above HPP and FHP models are used for 2D modelling. Since there is no regular lattice with enough symmetry to maintain macroscopic isotropy in three dimensions, D'Humières, Lallemand and Frisch (1986) introduced a pseudo-three-dimensional model for 3D

simulations. That is the so-called face-centred-hypercubic (FCHC) model. It resides on a general cubic lattice with a unit lattice constant. The residing lattice is a three-dimensional projection of a FCHC model with unit periodicity in the fourth direction. This model extends the 2D FHP model to 3D and retains the isotropic property.

#### **2.4.4 Multi-Speed Model**

In order to incorporate thermal effects, D'Humières et al. (1986), Chopard and Droz (1987), and Chen et al. (1989) introduced multi-speed models. In these models, particles have discrete speeds of 0.1. or  $\sqrt{2}$ . Mass, momentum and energy are conserved during the collisions. Furthermore, energy conservation is independent of mass conservation.

## **2.5 Construction of a Thermodynamic Automaton Model**

To integrate temperature, a thermodynamic automaton model which allows a continuous distribution of particle velocities is constructed.

The model can be constructed using the following procedures:

1. One proceeds from the premise that one can introduce physical laws such as conservation of momentum, energy and particle types at the particle level.
2. The particles are allowed to populate a discretized space with a lattice connecting discrete positions.
3. The particles undergo elastic collisions and propagate along the lattice probabilistically. Effectively, particles carry out free movement on lattice space.
4. The particle velocities evolve to the Maxwell-Boltzmann distribution very quickly, yielding a clear definition of temperature.
5. The boundary conditions of simulation are set up to be thermodynamic quantities.
6. A porous medium may be introduced into the model by allowing a probability for a fluid-solid collision at each point in space. Permeability is adjusted by changing that probability. Heterogeneity is introduced by allowing that probability to change in space.

7. Additional fluid phases are introduced by allowing different particle types. Fluid viscosity can be changed by adjusting the probability of fluid particle collisions.

8. Body forces and surface tension are introduced through the collision rules. For instance, to model surface tension, when two different types of particles collide with each other, the particles have a tendency to move towards neighbouring particles of their own type. Body forces can be simulated by defining different probabilities for particles moving downward.

The main features and consequences of the model are :

(1) The lattice simply acts as a book keeper to keep track of particle positions and to enforce rules. Thus, no restriction for lattice geometry exists. The model is compatible with virtually any lattice without losing isotropy.

(2) A site in a lattice represents an area (or in three dimensions a volume of space). No exclusion principle is applied. Thus a large number of particles can be initialized, which provides a better representation of the statistics.

(3) Particle momentum is continuous, allowing thermal effects to be captured.

(4) Isotropy is maintained and it is straightforward to extend to 3D modelling.

(5) Collision and propagation rules are probabilistic rather than deterministic as in the previous models. Since "gas particles" undergo elastic collisions, probabilistic rules which represent the nature of the particle collision and propagation are used in the model. Only binary elastic collisions are applied. Since binary collisions are the prominent collisions, it is felt that the simulation should not be affected significantly by the absence of triple collision modelling.

(6) Relativistic effects can be incorporated. In the relativistic case, Lorentz invariant elastic collision rules are applied and the particle velocity consists of a speed between 0.0 to 1.0 which corresponds to the speed of light.

The thermodynamic automaton simulation proceeds from the initial configuration through a series of evolution processes including a collision step and a propagation step. The detailed procedures of the thermodynamic automaton simulation are as follows:

- (1) Initialization of cells and lattice (either triangular or square) with boundary conditions (periodic, no-slip or thermal boundaries).
- (2) Using a random number generator (see Recipe C) to generate stochastically additional random number generators which are

assigned to each cell, respectively. Note, when a single random number generator was used in a systematic fashion across the lattice for the description of collision and propagation, an asymmetric flow profile was obtained. Whereas a new random number generator was generated at each lattice site, the profile became symmetric. Therefore, it is important to use a different random number generator in each cell.

(3) Initialization of a set of particles (say 100 particles in each cell). the particle speed and direction of which can be randomly assigned by the random number generator in each cell. The particles can also be initialized such that their velocities fit a Maxwell-Boltzmann distribution.

(4) Pairs of particles in each cell are randomly picked up and removed from the cell until no more than two particles are left in the cell. The selected pair of particles then collide in the centre mass frame according to either a Lorentz invariant elastic collision rule or a non-relativistic elastic scattering rule. The outcome of this collision is found by generating a random deflection angle, ranging from 0 to 360 degrees in the centre mass frame, and then transforming the results back to the lab frame or lattice frame.

(5) After a collision, and with the definition of probabilities (P)  $P_0=(1-v_a)(1-v_b)$ ,  $P_a=v_a(1-v_b)$ ,  $P_b=v_b(1-v_a)$  and  $P_{ab}=v_av_b$ , where a

and  $\mathbf{b}$  represent the two principal directions which correspond to the  $x$  and/or  $y$  axes for a square lattice; particles propagate according to the following rules:

- (a) the particle does not move if  $P < P_0$ ;
- (b) the particle moves along  $\mathbf{a}$  if  $P_0 < P < P_0 + P_a$ ;
- (c) the particle moves along  $\mathbf{b}$  if  $P_0 + P_a < P < P_0 + P_a + P_b$ ;
- (d) the particle moves along  $\mathbf{a}$  and  $\mathbf{b}$  if  $P_0 + P_a + P_b < P$ .

Note that the sum of all the probabilities is one and particles move as "random walkers" and drunkman's walk is an automaton. The position of a particle is  $\mathbf{x} = N_a \mathbf{a} + N_b \mathbf{b} + N_{ab}(\mathbf{a} + \mathbf{b})$  where  $N_a = N \cdot P_a$ ,  $N_b = N \cdot P_b$ ,  $N_{ab} = N \cdot P_{ab}$  and  $N$  is the total number of iterations. After a large time elapses, the average motion of the particle is a straight line since, on average,  $N_a = N P_a$ , etc..., and  $\langle \mathbf{x} \rangle = \mathbf{v}t$ . It should be noted that this propagation rule requires that a particle's velocity cannot be greater than 1.

- (6) iterate in time and repeat the collision and propagation cycles.
- (7) output results and the macroscopic values can be obtained by averaging procedures.

Table 2.1 shows the classification of different types of models according to their characterizations in space and momentum phases.



A lattice gas automaton model is discrete in both the space and the momentum domains, a thermodynamic automaton is discrete in the space domain but continuous in the momentum domain, and a molecular dynamics model is continuous in both the space and the momentum domains.

Table 2.1 Classification of model types.

---

	DP	CP
DS	lattice gas automaton	thermodynamic automaton
CS	?	molecular dynamics

---

Where D=discrete, P=momentum, C=continuous, and S=space.

It is emphasized that the automaton models are quite distinct from molecular dynamics simulations (cf. Koplick et al., 1988 and 1989) in that they make no attempt to simulate the actual microscopic fields associated with the particles in a real fluid. Molecular dynamics simulations attempt to model faithfully the microscopic behaviour of a real fluid including molecular interactions, while automaton models extract only the minimal amount of microscopic properties required to obtain the desired macroscopic properties. The particle in the

automaton model is not a "molecular particle" but can be regarded as an information carrier.

Another important issue is the scale at which the physical processes are modelled. In the context of this study, unless otherwise specified, the molecular scale is defined as the microscopic scale, the scale at which single continuum equations (such as the Navier-Stokes equation) hold as the macroscopic scale, the scale at which porous media equations hold as the megascopic scale, and the automaton scale as the intermediate scale or meso-scale which is either between the microscopic scale and the macroscopic scale, or between the macroscopic scale and the megascopic scale.

## 2.6 Summary and Conclusions

In summary, a thermodynamic automaton model has been constructed which allows for a continuous particle velocity distribution. The advantages of the model over previous ones are:

- (1) capturing thermal effects;
- (2) integrating relativistic effects;
- (3) no lattice gas constraint or isotropy problem;
- (4) no exclusion principle and a better representation of the statistics; and
- (5) it can be easily extended to 3D modelling. That is, a cubic lattice can be used.

The disadvantage of this model is the relatively slow computational speed because of the substitution of Boolean (integer) operations by floating-point operations and the use of continuous particle speed distribution. However, this problem can be alleviated or solved by a sufficiently powerful computer such as the Scalable Power Parallel Computer (SP2) located at the University of Alberta, Edmonton.

## 2.7 Bibliography

Adler, C., D'Humières, D. and Rothman, D.H., 1994. Surface Tension and Interface Fluctuations in Immiscible Lattice Gases. J. Phys. I France 4; 29-46.

Appert, C., Rothman, D.H. and Zaleski, S., 1991. A Liquid-Gas Model on a Lattice. Physica D 47, 85-96.

Appert, C. and Zaleski, S., 1990. Lattice Gas with a Liquid-Gas Transition. Phys. Rev. Lett., Vol. 64, No. 1, 1-4.

Benzi, R., Succi, S. and Vergassola, M., 1992. The Lattice Boltzmann Equation: Theory and Applications. Physics Reports, Vol. 222, No. 3. 145-197.

Boghosian, B. M., 1989. Lattice Gases. 295-307. 1989 Lectures in Complex Systems. Edited by Erica J. Addison-Wesley, 1990.

Boghosian, B. M., 1993. Lattice Gas Hydrodynamics. Nuclear Physics B (Proc. Suppl.) 30, 204-210.

Boghosian, B. M. and Levermore, C.D., 1987. Complex Systems. Vol.1. 1-17.

Chen, S., Diemer, K., Doolen, G.D., Eggert, K., Fu, C., Gutman, S. and Travis, B.J., 1991a. Lattice Gas Automata for Flow through Porous Media. *Physica D* 47, 72-84.

Chen, S., Doolen, G.D., Eggert, K., Grunau, D. and Loh, E.Y., 1991b. Local Lattice-Gas Model for Immiscible Fluids. *Physical Review A*. Vol. 43. No. 12, 7053-7056.

Chen, S., Lee, M., Zhao, K.H. and Doolen, G.D., 1989. A Lattice Gas Model with Temperature. *Physica D* 37, 42-59.

Cheng E. and Ebner, C., 1993. Dynamics of Liquid-Droplet Spreading: A Monte Carlo Study. *Physical Review B*, Vol. 47, No. 20, 13808-13811.

Chopard, B. and Droz, M., 1987. Cellular Automata Model for Thermo-Hydrodynamics. 302-306. *Chaos and Complexity*, edited by Livi, R., Ruffo, S., Ciliberto, S. and Buiatti, M. World Scientific Publishing Co Pte Ltd.

D'Humières, D., Lallemand, P. and Frisch, U., 1986. Lattice Gas Model for 3D Hydrodynamics. *Europhys. Lett.*, Vol. 2, No. 4, 291-297.

Frisch, U., D'Humières, D., Hasslacher, B., Lallemand, P., Pomeau, Y. and Rivet, J.P., 1987. Lattice Gas Hydrodynamics in Two and Three Dimensions. *Complex Systems*, Vol. 1, 649-707.

Frisch, U., Hasslacher, B. and Pomeau, Y., 1986. Lattice-Gas Automata for the Navier-Stokes Equation. *Physical Review Letters*, Vol. 56, No. 14, 1505-1508.

Gao, Y. and Sharma, M.M., 1994a. A LGA Model for Fluid Flow in Heterogeneous Porous Media. *Transport in Porous Media*. V. 17, 1-17.

Gao, Y. and Sharma, M.M., 1994b. A LGA Model for Dispersion in Heterogeneous Porous Media. *Transport in Porous Media*. Vol. 17, 19-32.

Gardner, M., 1971. On Cellular Automata, Self-Reproduction, the Garden of Eden and the Game of 'Life'. *Sci. Amer.* Vol. 224, No. 2, 112-117.

Grunau, D., Chen, S. and Eggert, K., 1993. A Lattice Boltzmann Model for Multiphase Fluid Flow. *Phys. Fluids A*, Vol. 5, No. 10, 2557-2562.

Gunstensen, A.K., 1989. A Three-Phase Immiscible Lattice Gas. MIT Porous Flow Project, Report No. 2, 33-48.

Gunstensen, A.K., 1991. Lattice-Boltzmann Studies of Two-Phase Flow through Three-Dimensional Models of Porous Media. MIT Porous Flow Project, Report No. 4, 1-19.

Gunstensen, A.K. and Rothman, D. H., 1991. Microscopic Modelling of Immiscible Fluids in Three Dimensions by a Lattice-Boltzmann Method. MIT Porous Flow Project, Report No. 4, 20-29.

Gunstensen, A.K., Rothman, D.H., Zaleski, S. and Zanetti, G., 1991. Lattice Boltzmann Model of Immiscible Fluids. *Physical Review A*, Vol. 43, No. 8, 4320-4327.

Gutfraind, R. and Hansen, A. 1995. Study of Fracture Permeability Using Lattice Gas Automata. *Transport in Porous Media*. V. 18, 131-149.

Hardy, J., de Pazzis, O. and Pomeau, Y., 1976. Molecular Dynamics of a Classical Lattice Gas Transport Properties and Time Correlation Functions. *Physical Review A*, Vol. 13, No. 5, 1949-1961.

Hayot, F., 1991. Fingering Instability in a Lattice Gas. *Physica D* 47. 64-71.

Henon, M., 1988. On the Relation between Lattice Gases and Cellular Automata. *Proceedings of the Workshop on Discrete Kinetic Theory, Lattice Gas Dynamics and Foundations of Hydrodynamics*. Torino, Italy. 160-161.

Higuerá, F.J. and Succi, S., 1989. Simulating the Flow around a Circular Cylinder with a Lattice Boltzmann Equation. *Europhys. Lett.*, Vol. 8, No. 6, 517-521.

Higuerá, F.J., Succi, S. and Benzi, R., 1989. Lattice Gas Dynamics with Enhanced Collisions. *Europhys. Lett.*, Vol. 9, No. 4, 345-349.

Kadanoff, L.P., 1985. Simulating Hydrodynamics: A Pedestrian Model. *Journal of Statistical Physics*, Vol. 39, Nos. 3-4, 267-283.



Koplick, J., Banavar, J.R. and Willemsen, J.F., 1988. Molecular Dynamics of Poiseuille Flow and Moving Contact Lines. *Physical Review Letters*, Vol. 60, No. 13, 1282-1285.

Koplick, J., Banavar, J.R. and Willemsen, J.F., 1989. Molecular Dynamics of Fluid Flow at Solid Surfaces. *Phys. Fluids A*, Vol. 1, No. 5, 781-794.

Ladd, A.J.C., Colvin, M.E. and Frenkel, D., 1988. Application of Lattice-Gas Cellular Automata to the Brownian Motion of Solid in Suspension. *Phys. Rev. Lett.*, Vol. 60, No. 11, 975-978.

Lavallée, P., Boon, J.P. and Noullez, A., 1991. Boundaries in Lattice Gas Flows. *Physica D* 47, 233-240.

Martinez, D.O., Matthaeus, W.H., Chen, S. and Montgomery, D.C., 1993. Comparison of Spectral Method and Lattice Boltzmann Simulations of Two-Dimensional Hydrodynamics. *Phys. Fluids*, Vol. 6, No. 3, 1285-1298.

McNamara, G.R. and Zanetti, G, 1988. Use of the Boltzmann Equation to Simulate Lattice-Gas Automata. *Physical Review Letters*. Vol. 61, No. 20, 2332-2335.

Rothman, D.H., 1988a. Cellular-Automata Fluids: A Model for Flow in Porous Media. *Geophysics*, Vol. 53, No. 4, 509-518.

Rothman, D.H., 1988b. Lattice-Gas Automata for Immiscible Two-Phase Flow. MIT Porous Flow Project. Report No. 1, 11-25.

Rothman, D.H., 1989. Macroscopic Laws for Immiscible Two-Phase Flow in Porous Media: Results from Numerical Experiments. MIT Porous Flow Project. Report No. 2, 1-32.1-33.

Rothman, D.H. and Keller, J.M., 1988. Immiscible Cellular-Automaton Fluids. MIT Porous Flow Project, Report No. 1, 1-10.

Rybka, R.B., Cieplak, M., D'Ortona, U., Salin, D. and Banavar, J.R., 1993. Cellular-Automata Studies of Circular Couette Flows and Chaotic Mixing. *Physical Review E*, Vol. 48, No. 2, 757-766.

Salomaa, A., 1969. Theory of Automata. Pergamon Press. 1-6.

Somers, J. A. and Rem, P.C., 1991. Analysis of Surface Tension in Two-Phase Lattice Gases. Physica D 47, 39-46.

Sone, Y. and Takata, S., 1994. Numerical Analysis of a Rarefied Gas Flow past a Volatile Particle Using the Boltzmann Equation for Hard-Sphere Molecules. Phys. Fluids, Vol. 6, No. 5, 1914-1928.

Succi, S., Benzi, R. and Higuera, F., 1991. The Lattice Boltzmann Equation: A New Tool for Computational Fluid Dynamics. Physica D 47, 219-230.

Toffoli, T., 1984. Cellular Automata as An Alternative to (Rather Than An Approximation of) Differential Equations in Modeling Physics. Physica 10D. 117-127.

Toffoli, T. and Margolus, N., 1987. Cellular Automata Machines. The MIT Press, Cambridge, Massachusetts. 5-11.

Ulam, S., 1952. Random Process and Transformations. Proc. Int. Congr. Mathem. 264-275.

Viannes, J.M. and Koelman, A., 1990. Cellular-Automaton-Based Simulation of 2D Polymer Dynamics. Phys. Rev. Lett. Vol. 64, No. 16, 1915-1918.

Von Neumann, J., 1966. Theory of Self-Reproducing Automata (edited and completed by Burks, A.), University of Illinois Press, Urbana, Illinois.

Wolfram, S., 1984. Cellular Automata as Models of Complexity. Review Article, Nature, Vol. 311, 419-424.

Wolfram, S., 1986. Cellular Automaton Fluids 1: Basic Theory. Journal of Statistical Physics, Vol. 45, Nos. 3-4, 471-526.

## **CHAPTER 3**

### **THERMODYNAMIC AUTOMATON SIMULATION OF THERMAL EQUILIBRIUM STATE AND DIFFUSION IN A TUBE**

#### **3.1 Introduction**

In Chapter 2, a thermodynamic automaton model was constructed. Here, the model is used to simulate the thermal equilibrium state for one phase, the initialization of a thermal equilibrium state, and diffusion in a tube. The overall objective of the simulations is to check the validity of the model.

As an initial step, the speed distribution of a single type of gas molecule in a thermal equilibrium state is simulated. One objective of this work is to compare the simulation results against analytic solutions for both relativistic and non-relativistic collision rules at different particle velocities. The other objective of this simulation is to determine the temperature of a given equilibrium state.

Next, initialization of a thermal equilibrium state prior to modeling a physical process is demonstrated. This is important since the physical

processes analyzed in this study start from a thermal equilibrium state. For example, when hot and cold objects are put in contact, heat will be transferred from the hot object to the cold object. However, before the hot object touches the cold one, each object is in a thermal equilibrium state. Thus, in order to model the heat transfer process, the hot and cold objects must be initialized with thermal equilibrium states.

Finally, diffusion in a tube is simulated. The simulation results can be compared with analytical results. Also, the diffusion coefficient can be determined.

It should be noted that the following unit specification rules were adopted:

- (1) variables and parameters are specified by SI units for analytical results;
- (2) for automata simulations, length is specified by lattice units, time by iteration units, and mass by the mass of a single particle. All the other quantities are derived from these basic units.

### 3.2 Theoretical Background

The speed distribution of gas molecules in thermal equilibrium obeys the relativistic Boltzmann distribution for particle speeds close to the speed of light and the non-relativistic Maxwell-Boltzmann distribution for much lower particle speeds.

In the non-relativistic case, the probability density  $P(E)$  of finding a particle in the energy range  $E+dE$  is related to  $\beta$  (beta) and  $E$  by the following formula:

$$P(E) = C e^{-\beta E} \quad (3.1)$$

where  $C$  is a constant that can be determined by the normalization condition

$$\int_0^{\infty} P(E) dE = 1 \quad (3.2)$$

Upon substituting Equation 3.1 into Equation 3.2, one has

$$C = \beta \quad (3.3)$$

Thus, Equation (3.1) becomes

$$P(E) = \beta e^{-\beta E} \quad (3.4)$$

Taking the natural logarithm on both sides, one gets

$$\ln(P(E)) = \ln(\beta) - \beta E \quad (3.5)$$

Equation (3.5) is linear and a plot of  $\ln(P(E))$  vs.  $E$  is a straight line with slope  $-\beta$  and intercept  $\ln(\beta)$ . In this model, temperature is defined as  $T=1/\beta$  by letting Boltzmann's constant  $k=1$ . Thus,  $T$  can be immediately determined once  $\beta$  is known.

For a closed system, the average energy should remain constant and is the average kinetic energy in our simulation. The average kinetic energy is

$$\langle E \rangle = \int_0^{\infty} E P(E) dE = 1/\beta \quad (3.6)$$

When particles are initialized with the same mass  $m$  and the same particle velocity  $v_0$ , the average energy is

$$\langle E \rangle = 0.5 m v_0^2 \quad (3.7)$$

Comparing Equations (3.6) with (3.7), one gets

$$\beta = 2/m v_0^2 \quad (3.8)$$

Table 3.1 lists the theoretical values for beta,  $T$ , intercept  $\ln(\beta)$  and slope  $-\beta$  for  $m=1.00$  and  $2.00$  and  $v_0 = 0.10$  and  $0.20$ .



Table 3.1 Theoretical values for  $\beta$ ,  $T$ ,  $\ln(\beta)$  and  $-\beta$ .

m	$v_0$	$\beta$	$T$	$\ln(\beta)$	$-\beta$
1.00	0.10	200.00	0.005	5.30	-200.00
1.00	0.20	50.00	0.02	3.91	-50.00
2.00	0.10	100.00	0.01	4.61	-100.00
2.00	0.20	25.00	0.04	3.22	-25.00

A thermal equilibrium state is constructed by initializing the Maxwell-Boltzmann distribution (exponential function  $\beta e^{-\beta K}$ ). From Numerical Recipes in C (Press et al., 1992), a relationship between a univariate random variable  $x$  and an exponential variable  $E$  can be established by requiring that their corresponding areas under their curves are the same. That is

$$\int_0^x u(t) dt = \int_0^E \beta \exp(-\beta t) dt \quad (x \text{ in } [0,1]) \quad (3.9)$$

where  $u(t)$  is a uniform distribution in  $[0, 1)$  and satisfies

$$\int_0^1 u(t) dt = 1 \quad (3.10)$$

From Equation (3.9), one has

$$x = 1 - e^{-\beta E} \quad (3.11)$$

Thus

$$E = - \ln(1-x)/ \beta \quad (3.12)$$

Diffusion is the equalization of concentration by a direct change in composition of every small portion of a fluid (Landau and Lifshitz, 1959). In a diffusion process, a change in composition occurs due to the molecular transfer of the phases. When there is macroscopic motion of the fluids, small portions may move without a change in composition of these portions. This change in the macroscopic composition is due purely to the mechanical mixing of the phases. The interaction of these two processes which is dispersion will be considered in Chapter 5.

For a given diffusion system without external pressure, the diffusion coefficient is a function of temperature only. If the temperature is not altered, then the diffusion coefficient is constant for a given diffusion process.

Consider a liquid in a narrow tube of infinite length with a tracer concentrated in the centre of the tube ( $l_0 < x < l_2$ ), at time  $t=0$ . In the course of time, the distribution of the concentration of the tracer will change.

From the equation of the continuity for one component, one obtains

$$\frac{\partial C}{\partial t} + \bar{v} \cdot \nabla C = -\bar{\nabla} \cdot \bar{i} \quad (3.13)$$

where  $C$  is the concentration of the component, i.e., the mass of that component in a unit volume and  $\bar{i}$  is the diffusion flux, i.e., the amount of that component which is transferred through a unit area and in a unit time by diffusion.

Landau and Lifshitz (1959) argued that if no macroscopic motion occurs in the fluid except that which may be caused by concentration, then the velocity of this motion is proportional to the gradient. Thus the term containing the velocity in Equation (3.13) is a quantity of second order, and can be neglected if a small concentration gradient is assumed. The continuity equation (Equation (3.13)) becomes

$$\frac{\partial C}{\partial t} = -\bar{\nabla} \cdot \bar{i} \quad (3.14)$$

The first quantitative study of diffusion was made by the physiologist Adolf Fick in 1855, by adapting Fourier's heat equation

in order to describe diffusion processes. He determined experimentally that the flux of one component in a mixture is directly proportional to its concentration gradient, and is given by the phenomenological relation which is called Fick's law

$$\vec{i} = -D\nabla C \quad (3.15)$$

Substituting Equation (3.15) into Equation (3.14), and considering only one dimension with constant  $D$ , one obtains the diffusion equation in the form

$$\frac{\partial^2 C}{\partial x^2} - \frac{1}{D} \frac{\partial C}{\partial t} = 0 \quad (3.16)$$

where  $C$  = concentration of the tracer ( $\text{kg/m}^3$  or particle number/unit volume, if all particles are of equal mass),

$D$  = diffusion coefficient ( $\text{m}^2/\text{s}$ ).

Since the diffusion equation is of exactly the same form as the equation of heat flow (Carslaw and Jaeger, 1959, P. 50), the solution (Carslaw and Jaeger, 1959, P. 54) to the equation of heat flow can be directly applied to the diffusion equation. If the region  $l_0 < x < l_2$  is initially at constant tracer concentration,  $C_0$ , and the other region is

initially at zero, the solution to Equation (3.16) is associated with the Gauss-error function. That is,

$$C = 0.5C_0 \left( \operatorname{erf} \frac{1-x}{2\sqrt{Dt}} + \operatorname{erf} \frac{1+x}{2\sqrt{Dt}} \right), -\infty < x < \infty \quad (3.17)$$

where  $C$  and  $D$  are defined as in Eq. (3.16)

$x$  = distance away from the center of the tracer along the tube (m).

$t$  = time (s),

$C_0$  = initial concentration of the tracer (particle number/unit volume).

Using Mathematica (version 2.2) and for the given values of the parameter  $Dt$  of 0.01, 0.02, 0.03, 0.05, 0.07, 0.09, 0.1, 0.2, 0.3, 0.5, 0.7, 0.9, 1, 2, 3, 5, 7 and 9, the above analytical solutions of concentration profiles were plotted (see Figure 3.1). Figure 3.1 indicates that for a given diffusion process i.e. constant  $D$ , the concentration profile of the tracer, which has a bell shape, flattens out with time.

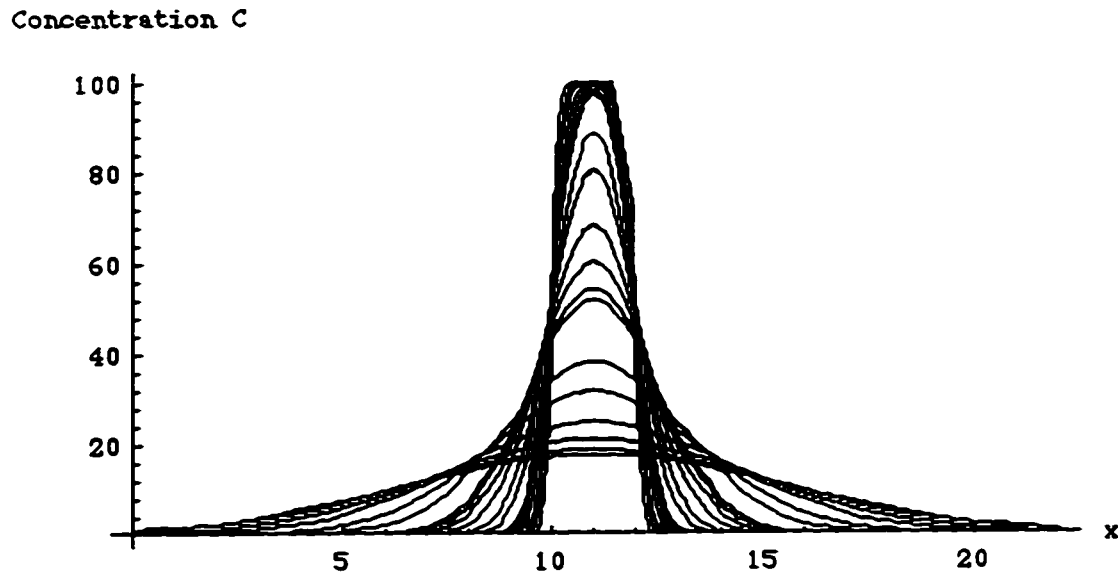


Figure 3.1 Analytic solution to the evolution of concentration  $C$  with the parameter  $Dt$  being 0.01, 0.02, 0.03, 0.05, 0.07, 0.09, 0.1, 0.2, 0.3, 0.5, 0.7, 0.9, 1, 2, 3, 5, 7, and 9. Furthermore, the bell shape concentration profile flattens out with time during the diffusion process.

### 3.3 The Model and Simulation Experiments

A detailed description of this model is given in Chapter 2. Three main types of simulation experiments were conducted.

1. thermal equilibrium state for one phase.
2. initialization of the thermal equilibrium state.
3. diffusion in a tube.

For Experiment 1, an initial configuration is constructed with a random initialization of particles with the same speed and mass ( $m=1.00$ ). The lattice size was  $100 \times 100$ . Each cell was populated by 6 particles, so that the total number of particles was 60000.

Periodic boundary conditions were employed at the top, bottom, left and right lattice boundaries. That is, when a particle moves out of the lattice from the left or the top end, it will wrap around and come back from the right or the bottom end and vice versa. The simulations were run for different initial particle speeds, i.e., 0.1, 0.2, 0.3, using Lorentz invariant elastic collision and non-relativistic elastic scattering rules, respectively. After 1000 time iterations, the configuration evolved to a thermal equilibrium state.

For Experiment 2, a thermal equilibrium state is obtained by initializing particles with random energies,  $-\ln(1-x)/\beta$ , random angles and constant mass (note that particle velocity can be calculated from energy, angle and mass). Since the total energy should not be larger than that obtained by initializing all particles with a speed  $v$  (note that  $v$  can be calculated from  $\beta$  by Equation (3.8)), the total energy was monitored and once it reached the required total energy, all the remaining particles were initialized with zero energy. In this simulation, a total number of 6000 particles was initialized. The simulations were run for the following four sets of parameters:

- (1)  $m = 1$ ,  $\beta = 200$ , corresponding to average velocity  $v=0.1$ .
- (2)  $m = 1$ ,  $\beta = 50$ , corresponding to  $v=0.2$ .
- (3)  $m=2.0$ ,  $\beta = 100$ , corresponding to  $v=0.1$ .
- (4)  $m=2.0$ ,  $\beta = 25$ , corresponding to  $v=0.2$ .

For Experiment 3, a  $23 \times 12$  lattice was divided into three parts, i.e., a left part (Columns 0 to 9), a middle part (Columns 10 to 12) and a right part (Columns 13 to 22). A total of 100 particles (mass=1) was assigned to each cell. The particles in the left and right parts of the cell were given the colour blue and the particles in the middle part



were given the colour red. Note that here the red particles act as a tracer. The initial configuration was such that the particles in each part were initialized in the thermal equilibrium state. Periodic boundary conditions were applied. After each iteration, in modelling the diffusion process, an average (accumulative or time average) of the red particle (tracer) number in each cell was calculated and the column average was determined from the cell average. The evolution of the tracer concentration along one dimension ( $x$ ) was monitored.

The diffusion simulations were run with two different temperatures, 0.005 and 0.00005. Using Mathematica 2.2 (Wolfram Research, 1994), the evolution of concentration profiles from the simulations can be plotted. Also, the nonlinear best fit curves for the profiles and a parameter ( $Dt$ ) related to the best fit function were determined. Note that since it is a nonlinear fit, the Statistical 'NonlinearFit' package (refer to Mathematical Technical Report-Guide to Standard Mathematical Packages, Version 2.2, 1993, P. 396-399) was input before calculating the curves.

The simulation codes were written in the C programming language due to its flexibility and portability. In particular, using the structure

variables in the C language, the particles (containing information on mass, momentum and so on), cell and lattice (containing particles) can be coded readily. The programs were initially tested and run on a Sun Sparc Station 5 with small particle numbers and a small lattice size. For a large number of particles and a large lattice size, the SP2 was used. Generally, each simulation takes less than 120 CPU minutes.

### **3.4 Results and Discussion**

In this section, simulation results for Experiment 1 is first presented. The simulation results are checked with the theoretical predictions. Also, temperature is computed. Then, simulation results for Experiment 2 is provided. The initialization of the particle velocity distribution is discussed. Finally, the simulation results for Experiment 3 is presented. The simulation results are compared with the analytical solutions and the diffusion coefficient is determined.

#### **3.4.1 Simulation of Thermal Equilibrium State**

The simulation results after 1000 iterations are shown in Figures 3.2, 3.3, 3.4, 3.5 and 3.6. Figures 3.2 and 3.3 illustrate the speed distribution of the particles at thermal equilibrium states for relativistic and non-relativistic cases, respectively. The simulation results (the dot points in Figures 3.2 and 3.3) are checked against the relativistic Boltzmann (the curves in Figure3.2) and the non-relativistic Maxwell-Boltzmann distribution (the curves in Figure3.3). It is found that the simulation results are consistent with the theoretical predictions.

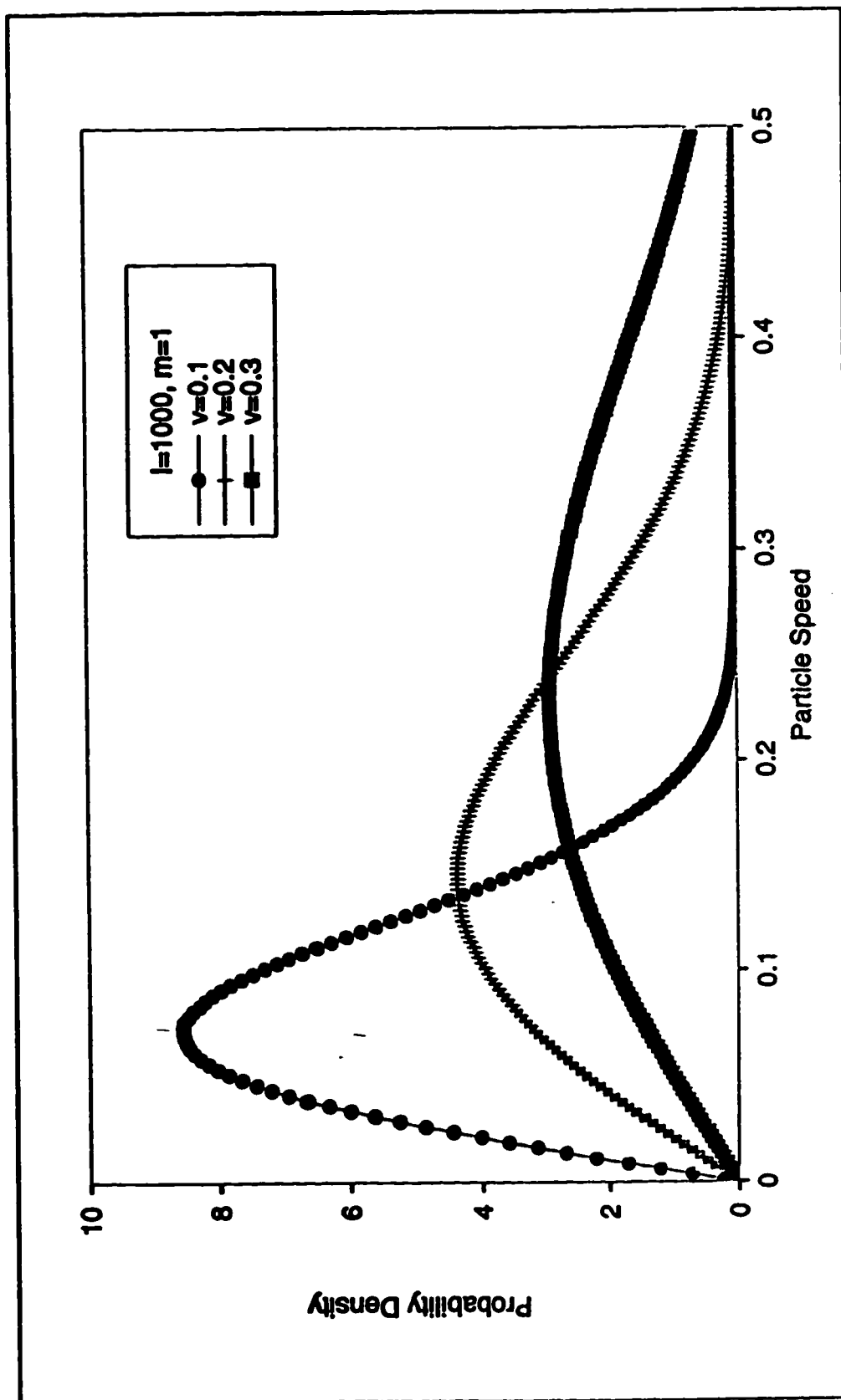


Figure 3.2 The speed distributions of particles after 1000 iterations. 6000 particles with the same mass and speed were initialized with random angles. Relativistic collision rules were applied in these simulations.

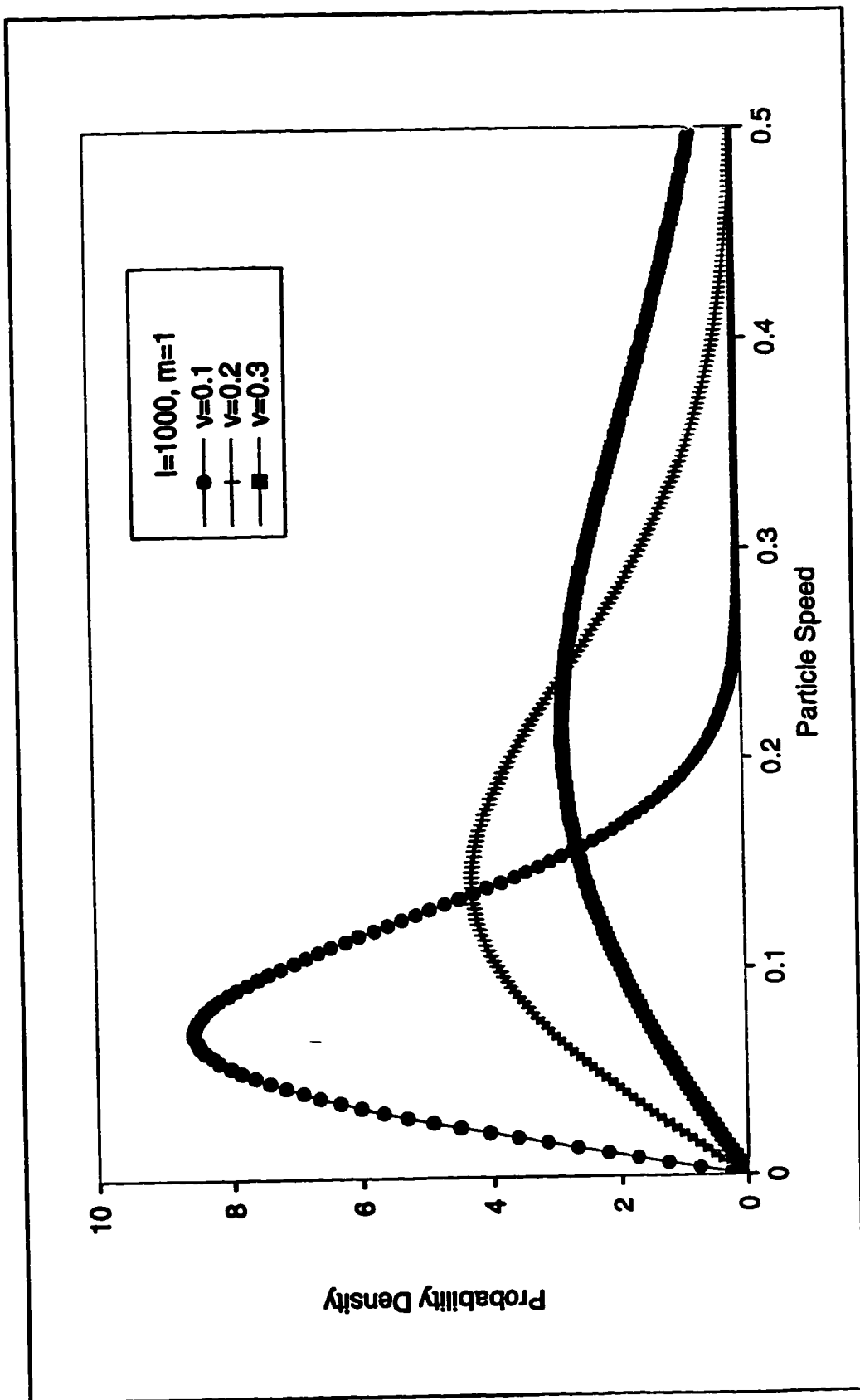


Figure 3.3 The speed distributions of particles after 1000 iterations. The initial configuration for the simulations was the same as in Figure 3.2. Non-relativistic collision rules were employed in these simulations.

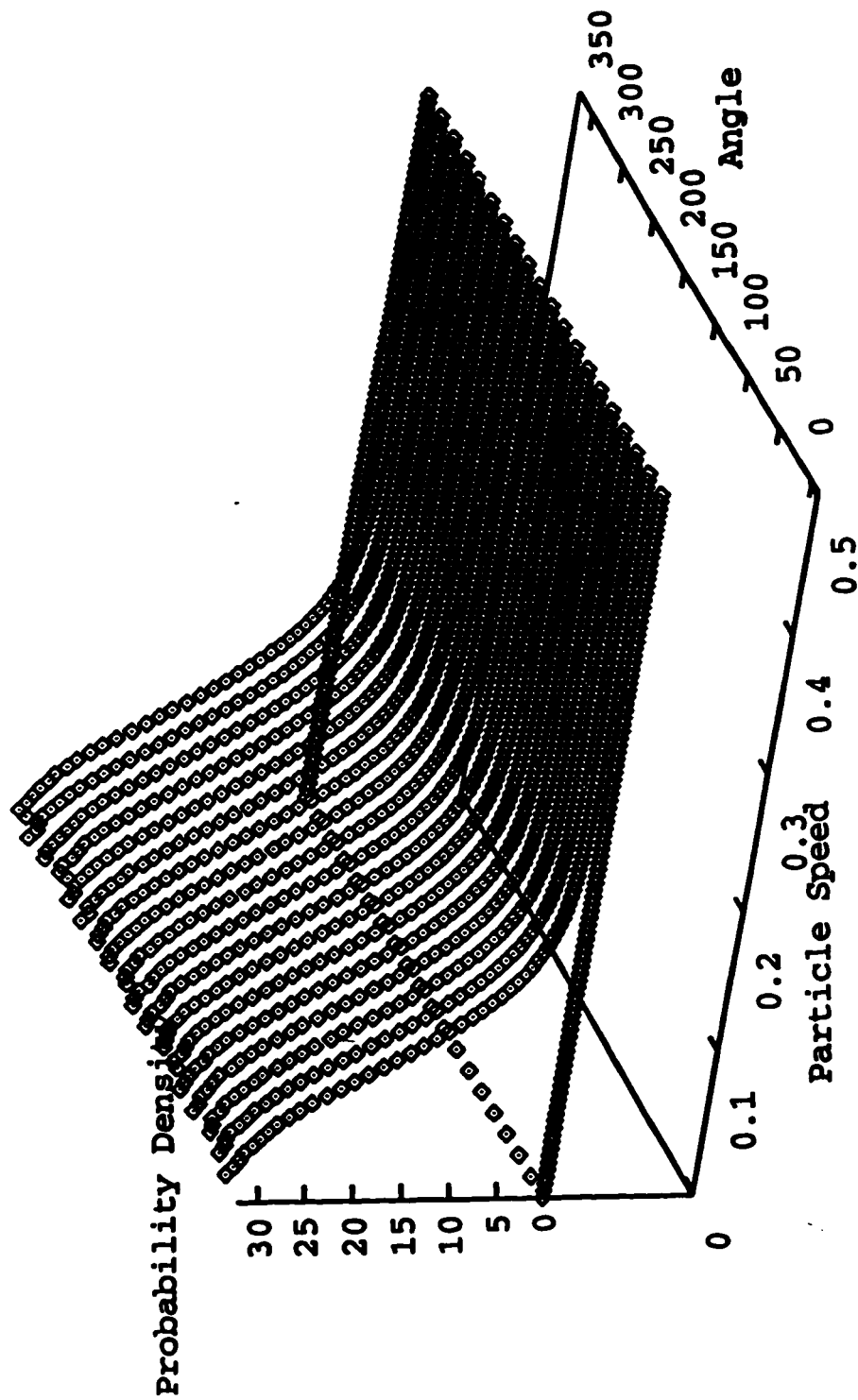


Figure 3.4 A plot of probability density of particles versus speed and angle after 1000 iterations. The speed distribution which is invariant with angle demonstrates that isotropy is maintained in the relativistic cases.

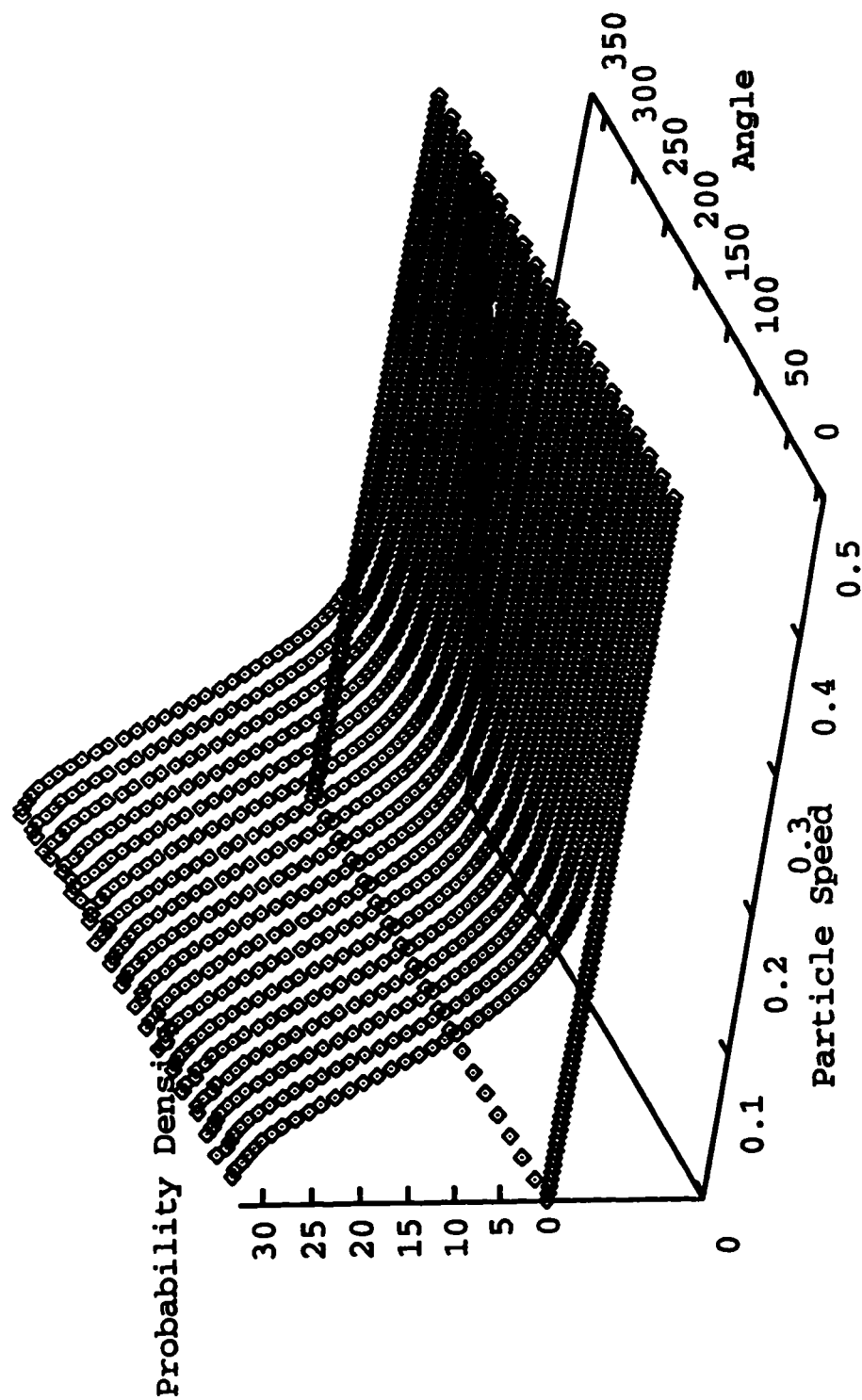


Figure 3.5 A plot of probability density of particles versus speed and angle after 1000 iterations. The speed distribution which is invariant with angle demonstrates that isotropy is maintained in the non-relativistic cases.

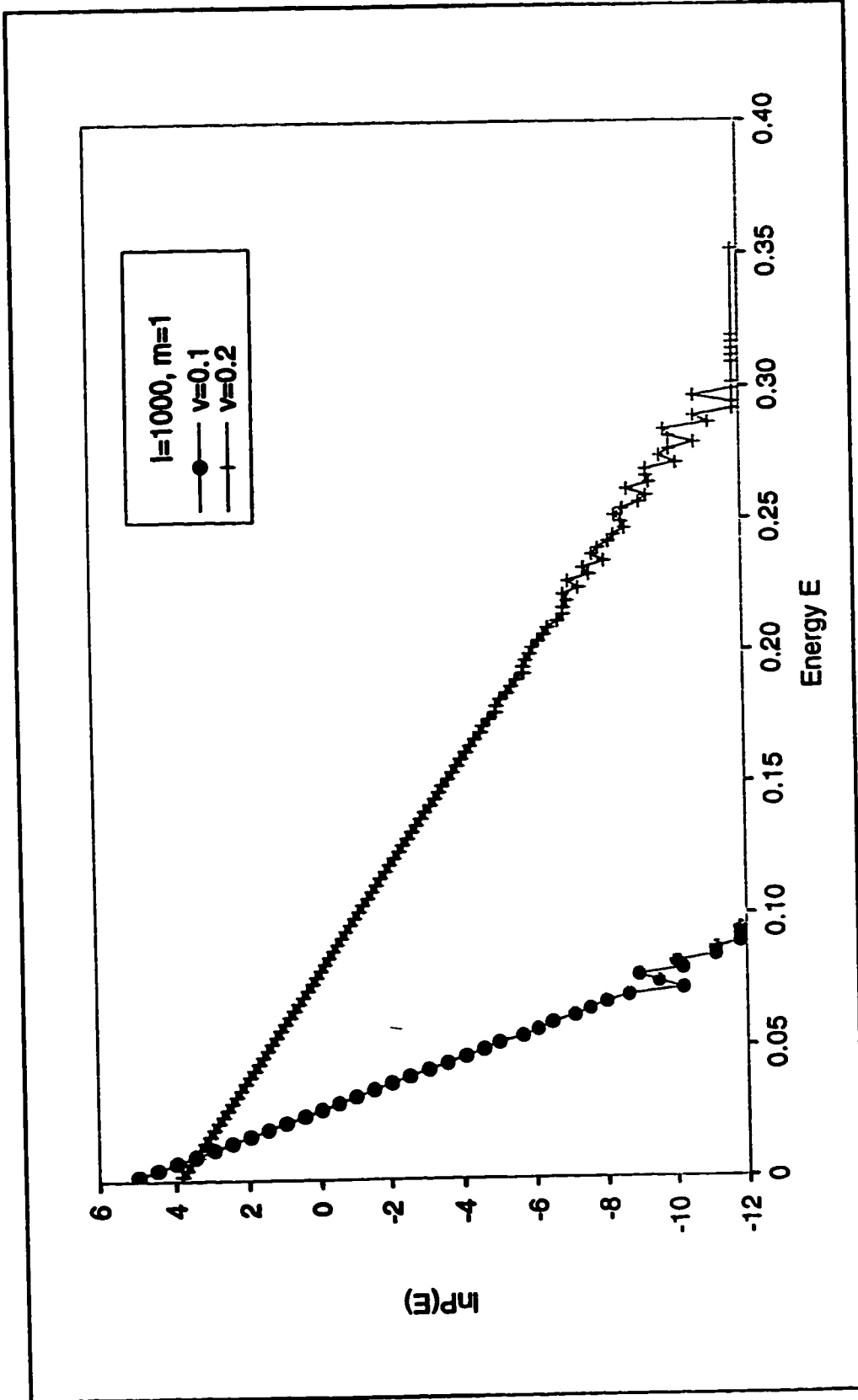


Figure 3.6 Corresponding plots of  $\ln(P(E))$  versus Energy  $E$  for the particle speed distributions with  $v_0=0.1$ , and  $0.2$  for Figure 3.3. The plots are straight lines as expected. Temperatures can be determined from the slopes of the lines.



For velocities much less than the speed of light, the two collision rules should provide identical results. As a check, the Boltzmann distributions in the relativistic and non-relativistic cases are compared. When overlaying Figure 3.3 on Figure 3.2, it is found that the distribution curves are identical for  $v=0.1$  and start to differ for  $v=0.2$ . This indicates that our collision rules for both relativistic and non-relativistic cases are consistent. The isotropy in the model is also maintained, i.e., the speed distribution is invariant with angle (Figures 3.4 and 3.5) for both the relativistic and the non-relativistic cases.

Figure 3.6 illustrates simulation results for  $m=1.00$  and  $v = 0.1$  and  $0.2$ , respectively, in the non-relativistic case. The plots of  $\ln(P(E))$  vs.  $E$  are straight lines as predicted. However, at very high energy, scattered points were observed. Such is the case because only a few particles reach these high energies, but a large number of particles are required for a valid statistical analysis. The corresponding simulation values for the intercept  $\ln(\beta)$ , slope  $-\beta$ ,  $\beta$  and  $T$  were computed (listed in Table 3.2) and were very close to the theoretical predictions (Table 3.1).

Table 3.2 Simulation values for beta, T, ln(beta) and -beta.

m	$v_0$	beta	T	ln(beta)	-beta
1.00	0.10	208.51	0.0048	5.34	-208.51
1.00	0.20	54.60	0.018	4.00	-54.60

The simulation results not only provide support for the validity of the model, but also indicate that thermal effects are incorporated in the model. Temperature can be altered by changing the particle velocities and determined from the particle velocities. Furthermore, the simulation results demonstrate that the relativistic and non-relativistic collision rules are consistent. Since the cases considered in the following analyses involve much lower velocities, the non-relativistic rules are adequate and are used in all the following simulations. It is emphasized that when the non-relativistic rules are used, 1 is no longer taken as the speed of light and the restriction for  $v \leq 1$  is lifted. However, it is noted that the present propagation rules require particle velocities to be not greater than 1. From the Boltzmann distribution simulation, it is found that, when initialized  $v \leq 0.2$ , the probability of a particle with a velocity larger than 1 is so remote that such events can be ignored. In most simulations not a single event of this type occurs and thus the chopping of such events is not required. It is also important to note that, in these simulations,

particle velocities are given in terms of lattice distance per time step. Since these distance and time steps are not specified and the velocity is in the dimensionless form, it is free to associate the simulation particle velocity, say  $v=0.1$ , with any physical velocity that one chooses.

### **3.4.2 Simulation of Initialization of Thermal Equilibrium State**

The simulation results are shown in Figures 3.7, 3.8, 3.9 and 3.10. Figure 3.7 shows the speed distribution of particles with  $m=1$  and  $\beta=200$  and  $50$  (corresponding to  $v=0.1$  and  $0.2$ ). To compare this distribution with the thermal equilibrium distribution, Figure 3.7 is compared with Figure 3.3. It is observed that the distribution curves in Figure 3.7 are very close to, although not as smooth as, the thermal equilibrium distribution curves in Figure 3.3. The noise in Figure 3.7 is expected because this is a “snapshot” of an equilibrium distribution. Figure 3.8 shows the speed distribution of particles with  $m=2$ . The distribution curves are identical to those in Figure 3.7, as expected, since  $m$  is not a factor affecting the distribution curves. Figure 3.9 shows the corresponding plots of  $\ln(P(E))$  vs.  $E$  for the

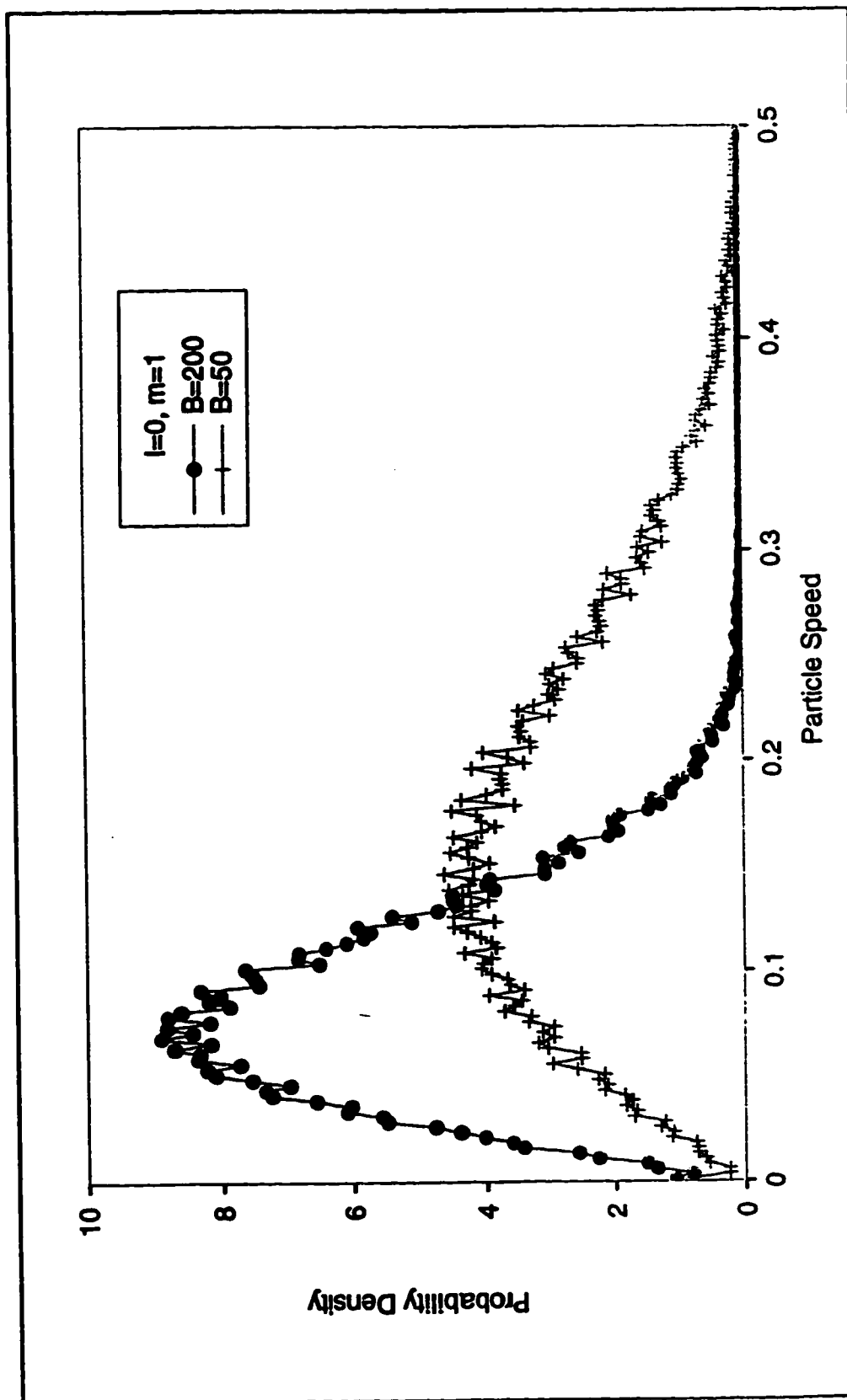


Figure 3.7 Initialization of a thermal equilibrium state with 60000 particles with  $m=1$ ,  $\beta=200$  and 50. The speed distribution curves represent "snapshots" of a thermal equilibrium state.

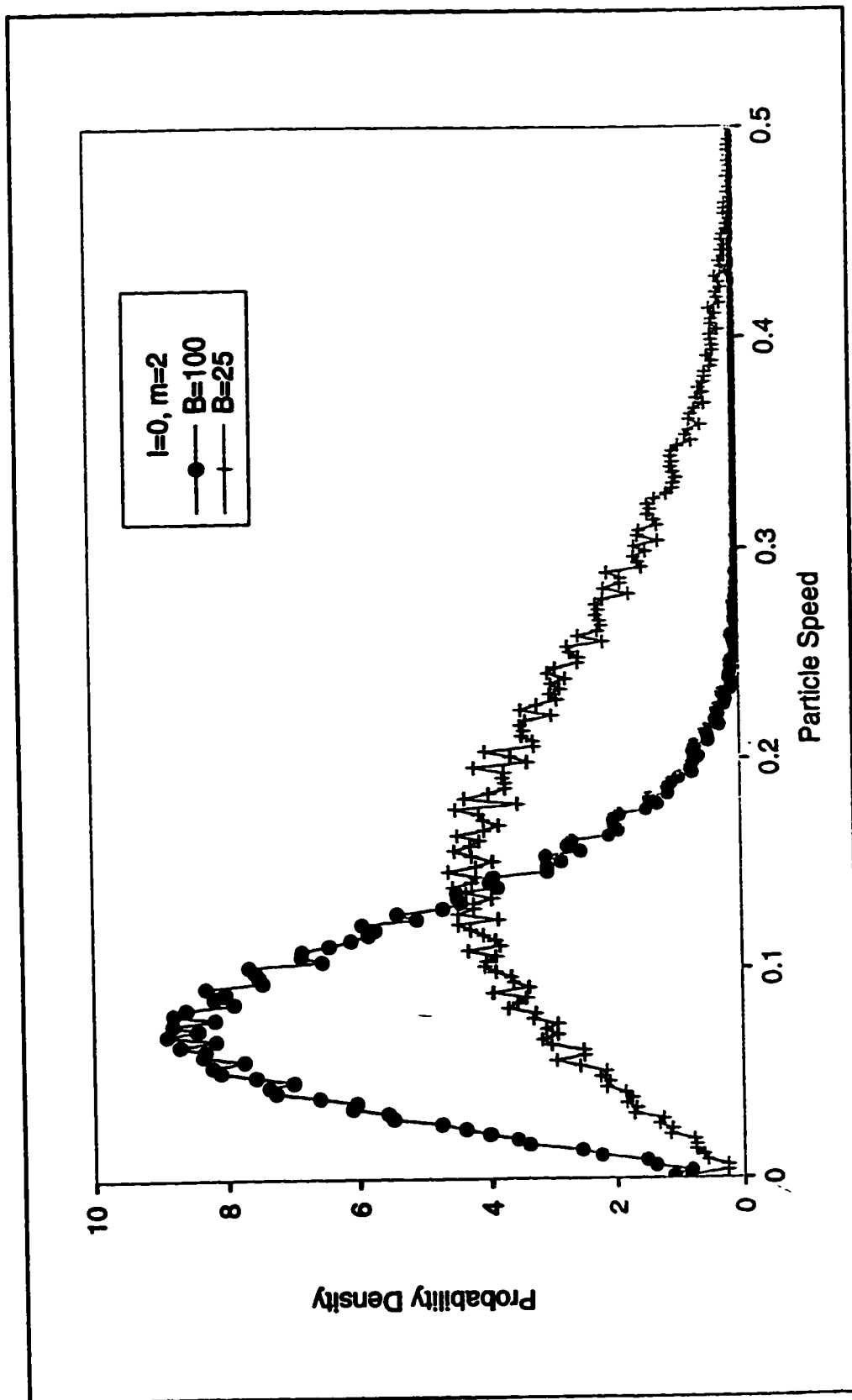


Figure 3.8 Initialization of a thermal equilibrium state with 60000 particles with  $m=2$ ,  $\beta=100$  and 25. The speed distribution curves represent "snapshots" of a thermal equilibrium state.

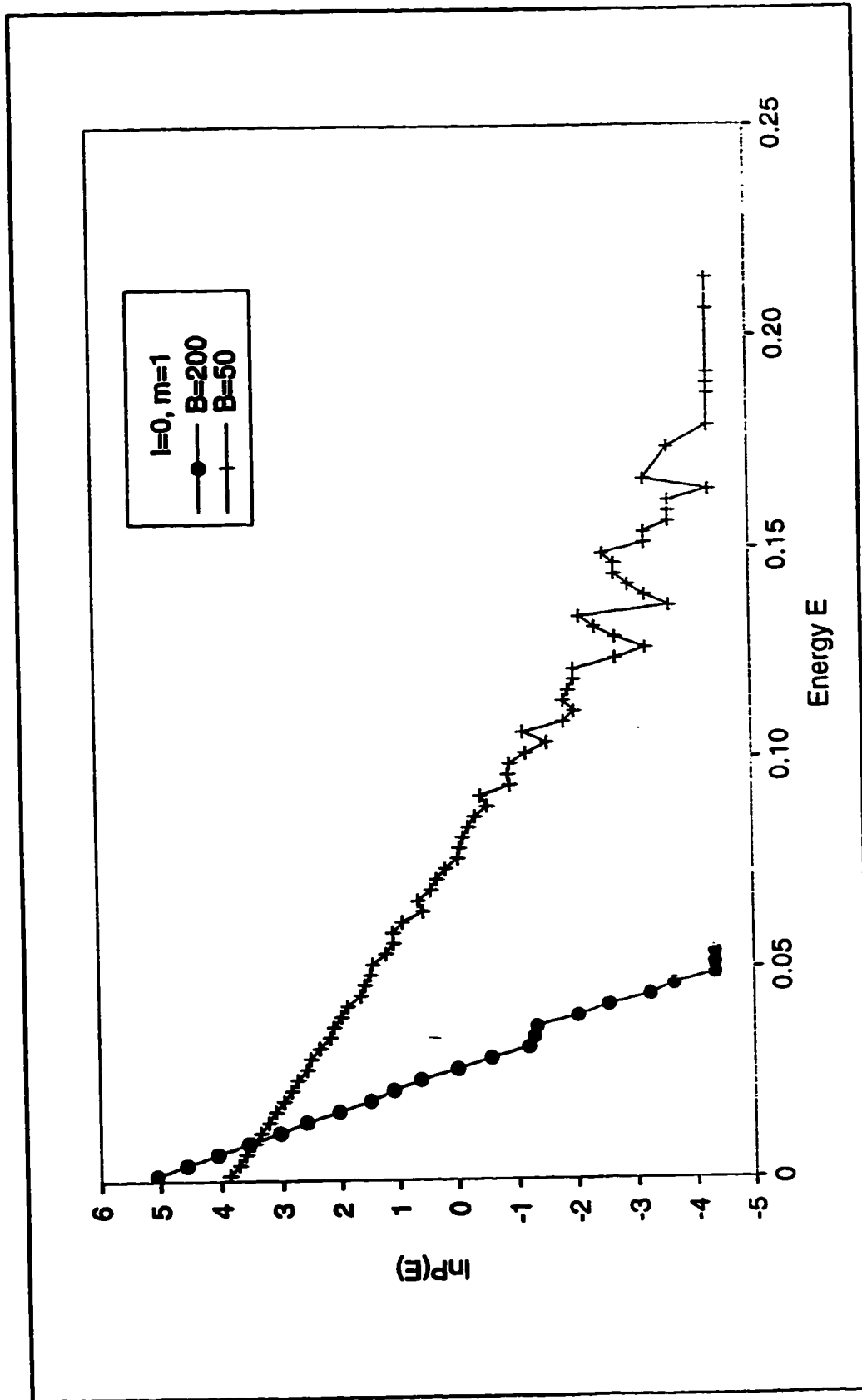


Figure 3.9 Corresponding plots of  $\ln(P(E))$  versus Energy  $E$  for Figure 3.7. Temperatures can be determined from the slopes of the lines.

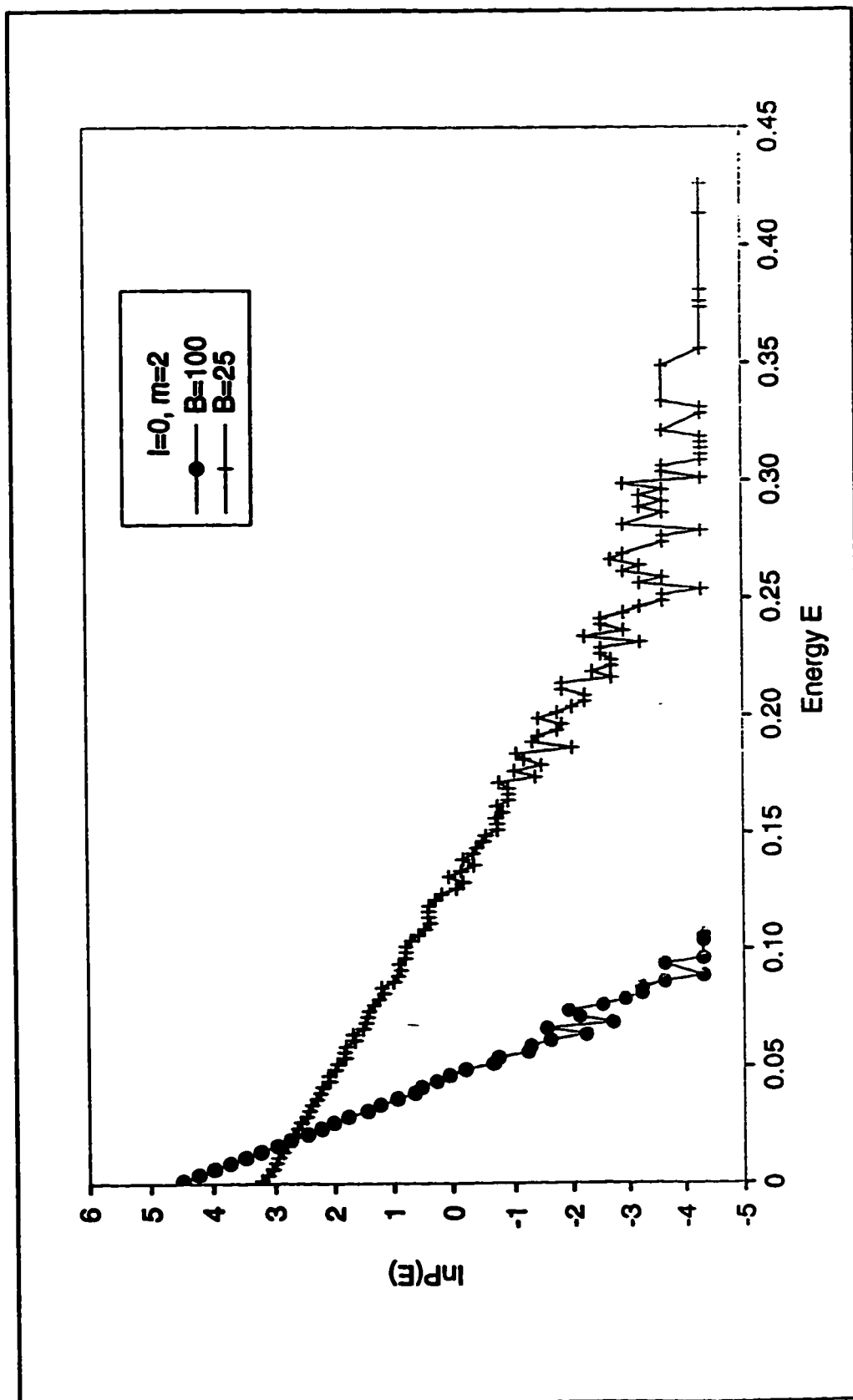


Figure 3.10 Corresponding plots of  $\ln(P(E))$  versus Energy  $E$  for Figure 3.8. Temperatures can be determined from the slopes of the lines.

speed distribution curves in Figure 3.7. The plots are straight lines, as expected. Also, the plots in Figures 3.9 and 3.6 are in close agreement (note the scale is different).

Figure 3.10 shows the corresponding plots of  $\ln(P(E))$  vs.  $E$  for the speed distribution curves in Figure 3.8. When comparing Figure 3.10 and 3.9, it is observed that the slopes of the plots in Figure 3.10 are lower than those in Figure 3.9. The reason for this is that for the same  $v$ , a larger mass generates a larger energy which results in a higher temperature and thus a smaller  $\beta$ . Again, these figures are plotted using different scales.

The simulation results indicate that the initialization of a thermal equilibrium state can be generated by the thermodynamic automaton model. The initialized speed distribution represents a “snapshot” of a thermal equilibrium distribution.

### **3.4.3 Simulation of Diffusion in a Tube**

Figure 3.11 indicates the evolution of concentration profiles at iterations of 0, 40, 80, 200, 400 and 700 for self-diffusion at a



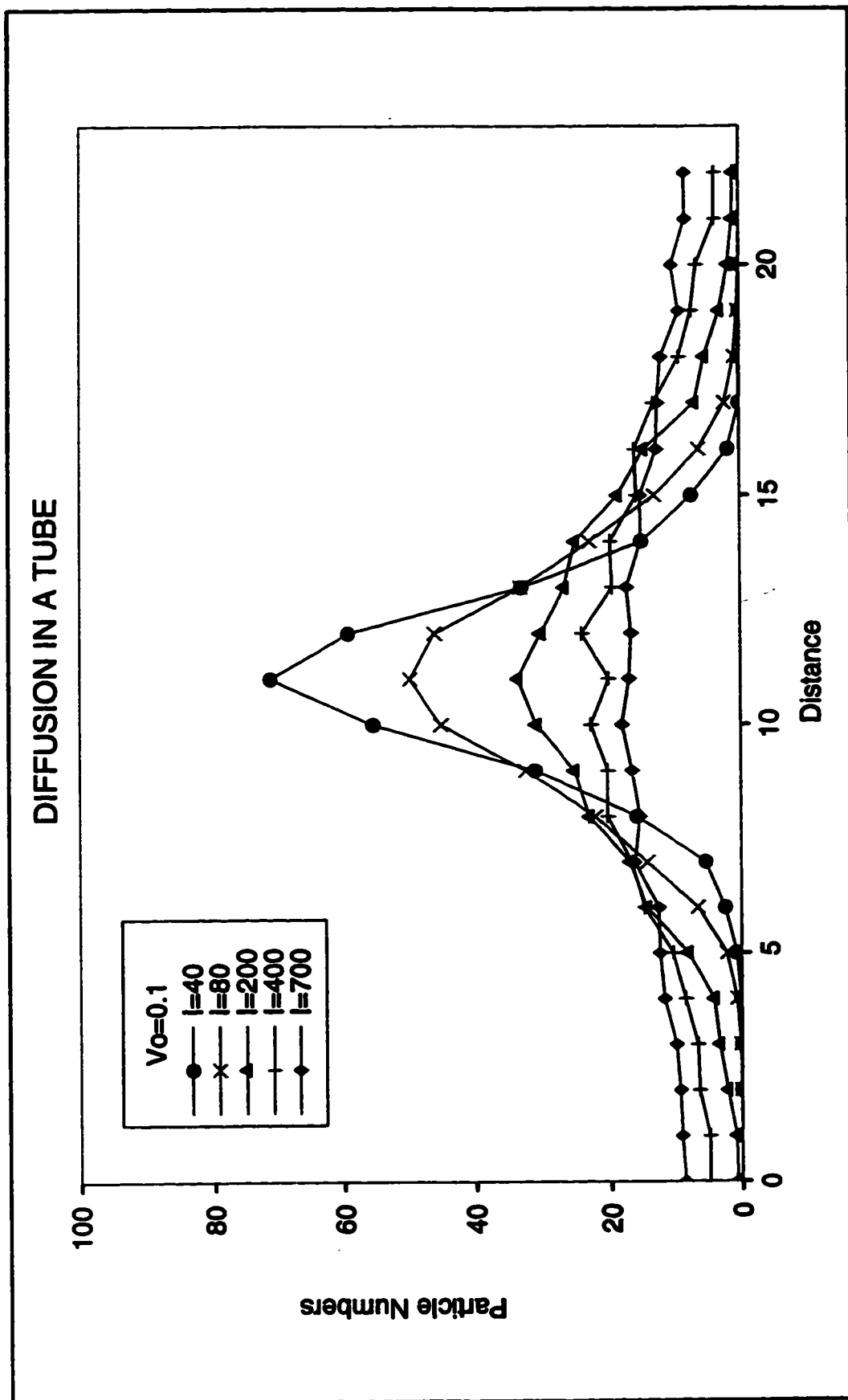


Figure 3.11 Simulation results of the evolution of concentration profiles at iterations of 0, 40, 80, 200, 400 and 700 for self-diffusion at a temperature of 0.005.

temperature of 0.005. Figure 3.12 shows nonlinear best fits of the evolution of the concentration profiles in Figure 3.11. When compared with the analytical solution (Figure 3.1), a close agreement can be noted.

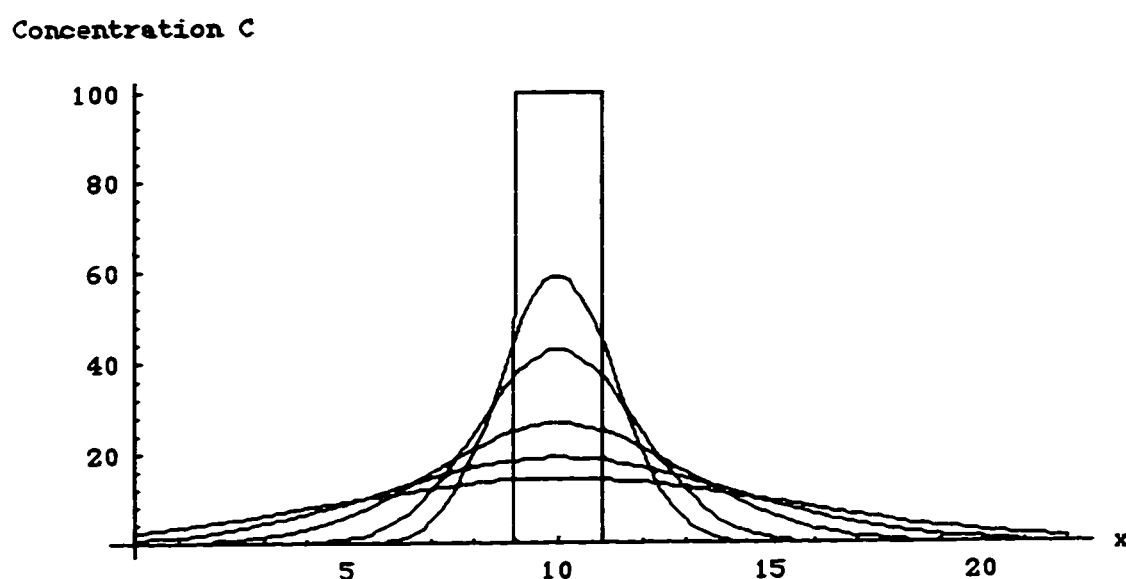


Figure 3.12 Nonlinear error function best fits of the evolution of concentration profiles in Figure 3.11.

The parameter ( $Dt$ ) was computed and is listed in Table 3.3. Knowing  $t$ , The diffusion coefficient of the diffusion process was calculated from the parameter  $Dt$  and is also listed in Table 3.3. The diffusion coefficient ( $0.021 \pm 0.004$ ) was constant and agreed with the theoretical prediction. Note that in the simulations, the unit of distance is specified by a lattice unit, the unit of time is specified by

an iteration unit and thus for the diffusion coefficient, the unit is lattice unit<sup>2</sup>/iteration unit.

Table 3.3 Diffusion coefficients of a diffusion process at different time steps at a temperature of 0.005.

Dt (Lattice unit <sup>2</sup> )	t (Iteration unit)	D (Lattice unit <sup>2</sup> /Iteration unit)
0.81	40	0.020
1.50	80	0.019
4.29	200	0.021
8.30	400	0.021
16.00	700	0.023

When the temperature was changed to 0.00005, the following simulation results were obtained. Figure 3.13 indicates the evolution of tracer concentration profiles at iterations of 0, 400, 700, 1000, 1180 and 2000 for self-diffusion at a temperature of 0.00005. Figure 3.14 shows the nonlinear best fits of the evolution of the concentration profiles in Figure 3.13. Again, when compared with the analytical solution (Figure 3.1), a close agreement is found.

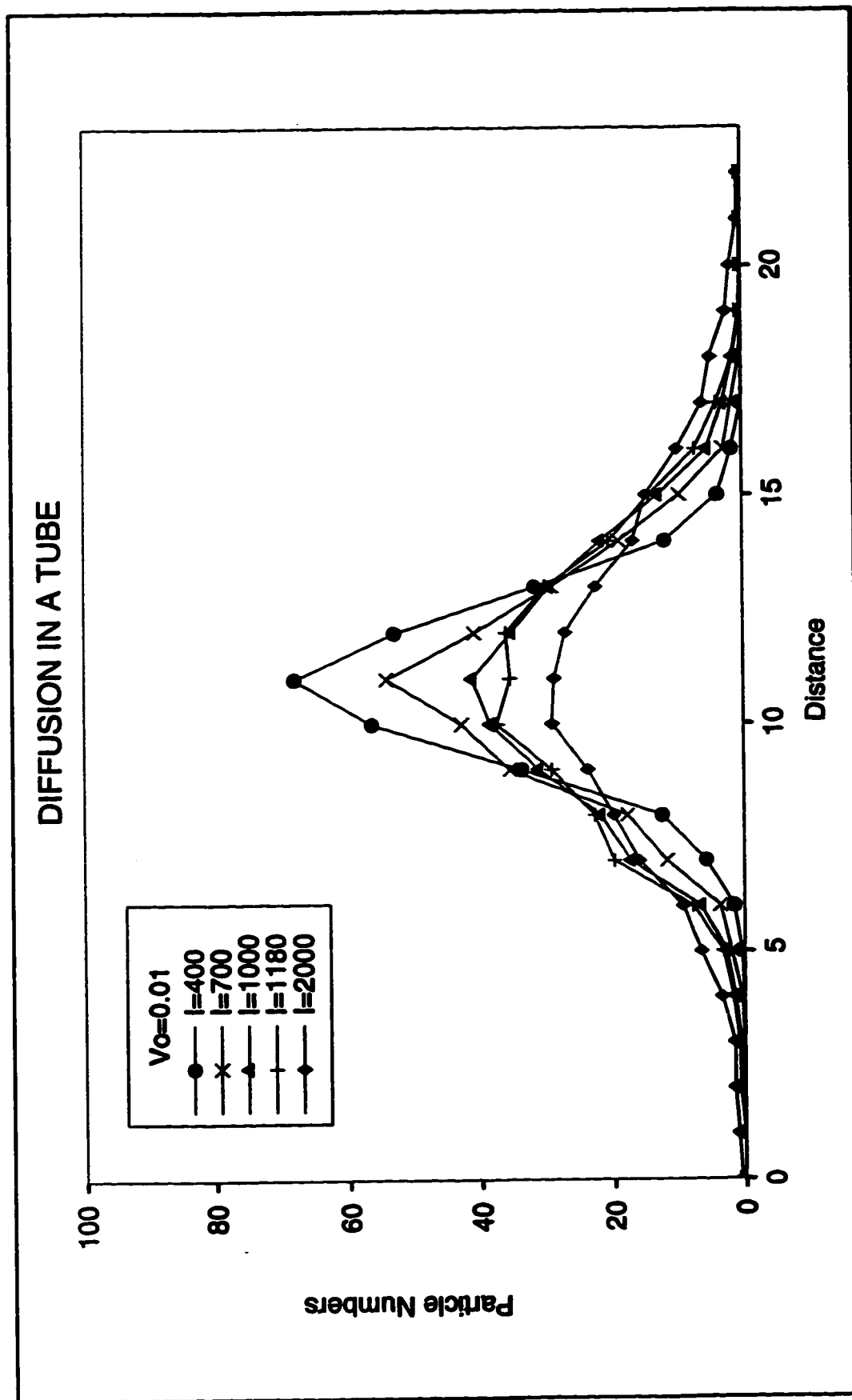


Figure 3.13 Simulation results of the evolution of concentration profiles at iterations of 0, 400, 700, 1000, 1180 and 2000 for self-diffusion at a temperature of 0.00005.

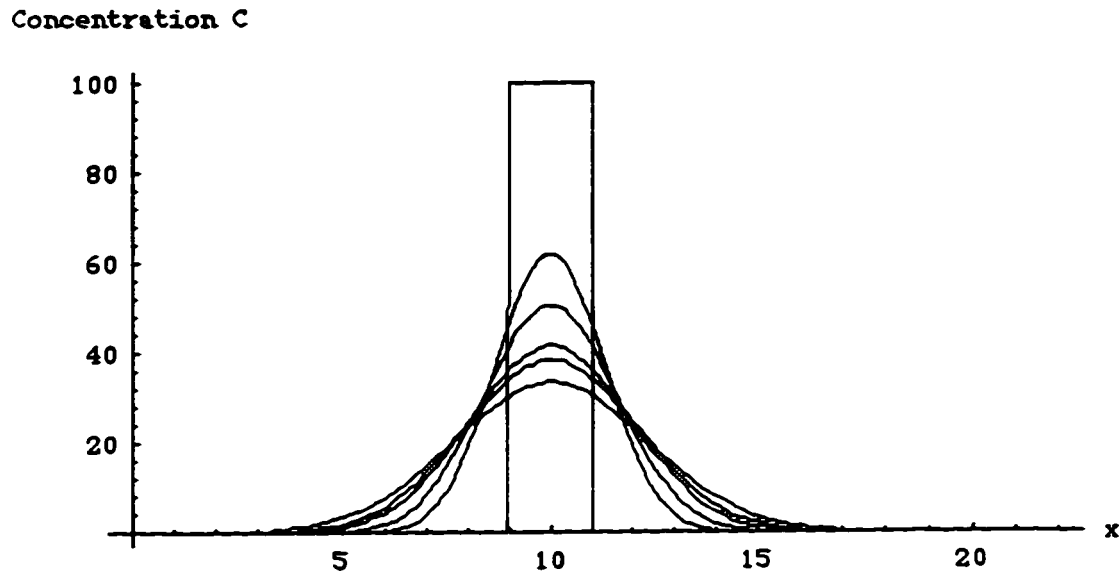


Figure 3.14 Nonlinear best fits of evolution of tracer concentration profiles in Figure 3.13.

The diffusion coefficient listed in Table 3.4 is also constant at different time steps. Due to the lower temperature, this coefficient ( $0.0016 \pm 0.0004$ ) is smaller than that ( $0.021 \pm 0.004$ ) in the previous modelling. It can be seen that the diffusion coefficient is controlled by temperature, i.e., it increases with an increase in temperature.

Table 3.4 Diffusion coefficients of the diffusion process at different time steps at a temperature of 0.00005.

Dt (Lattice unit <sup>2</sup> )	t (Iteration unit)	D (Lattice unit <sup>2</sup> /Iteration unit)
0.65	400	0.0016
1.07	700	0.0015
1.66	1000	0.0017
1.96	1180	0.0017
2.67	2000	0.0013

### 3.5 Conclusions

1. The thermal equilibrium state, initialization of thermal equilibrium state and diffusion in a tube were simulated by the thermodynamic automaton model. The simulation results were consistent with the theoretical predictions, thus providing support for the validity of the model.

2. Temperature is an internal property of the model, and can be determined from the particle velocity distribution by simulating the thermal equilibrium state.

3. The thermodynamic model is able to initialize a thermal equilibrium state. The initialized speed distribution represents a “snapshot” of a thermal equilibrium distribution.

4. The diffusion coefficient of a fluid can be determined by simulating diffusion in a tube.

### **3.6 Bibliography**

Carslaw, H.S. and Jaeger, J.C., 1959. Conduction of Heat in Solids. Oxford at the Clarendon Press. 50-54.

Landau, L.D. and Lifshitz, E.M., 1959. Fluid Mechanics. Pergamon Press. Addison-Wesley Publishing Company, Inc. 219-227.

Press, W.H., Teukolsky, S.A., Vetterling, W.T. and Flannery, B.P., 1992. Numerical Recipes in C. Second Edition. Cambridge University Press. 275-287.



## **CHAPTER 4**

### **FLOW SIMULATION USING A THERMODYNAMIC AUTOMATON MODEL**

#### **4.1 Introduction**

Plane Poiseuille flow is driven by an externally imposed pressure drop between two stationary flat walls. This flow process has been modeled by the conventional lattice gas FHP model (Frisch et al., 1986), with particle reversing applied to simulate an external force and no-slip boundary conditions employed at the walls (e.g. Rothman, 1988). Since the conventional model did not incorporate thermal effects, the influence of heat generated by viscous dissipation could not be addressed. Chen et al. (1989) utilized a multi-speed lattice model, an extension of the HLF model (D'Humières et al., 1986), to conduct an isothermal channel flow simulation with a no-slip boundary. Although temperature was included in their model, the effect of viscous heating was not observed. The objective of this study is to simulate a thermodynamic process of plane flow with a similar insulating no-slip boundary condition and to demonstrate the effect of viscous heat on the temperature of the fluid and thus the fluid viscosity.

Thermal boundary conditions which can be considered as a heat bath have been used in both molecular dynamics (Tenenbaum et al., 1982; and Trozzi and Ciccotti, 1984) and in a lattice gas simulation for heat conduction processes (Chopard and Droz, 1988; and Chen et al., 1989).

In this study, a new thermodynamic automaton model is used to simulate the channel flow with insulating and thermal boundary conditions. The coefficient of fluid viscosity is then determined.

In Section 4.2, the relevant theoretical background is provided. In Section 4.3, details of the model and simulation experiments are given. In Section 4.4, the simulation results are presented and discussed. Section 4.5 is devoted to conclusions.

## 4.2 Theoretical Background

During fluid flow processes, the shear viscosity,  $\mu$ , is defined as the ratio of the shearing stress to the rate of change of the shear strain.

$$\mu = \frac{\tau}{\frac{du}{dy}} \quad (4.1)$$

When flow occurs between two parallel plates at a separation distance of  $2h$ , the equation of motion for this flow is governed by the Navier-Stokes equation

$$\rho \frac{Du_x}{Dt} = -\frac{\partial p}{\partial x} + \mu \left[ \nabla^2 u_x + \frac{1}{3} \frac{\partial}{\partial x} (\nabla \cdot \vec{u}) \right] \quad (4.2)$$

where  $u_x$  is the fluid flow velocity in  $x$  direction,  $p$  is the pressure,  $\mu$  is the fluid viscosity and  $\rho$  is the fluid density.

For an incompressible fluid, the continuity equation is

$$\nabla \cdot \vec{u} = 0 \quad (4.3)$$

Substituting Equation (4.3) into (4.2), the Navier-Stokes equation reduces to

$$\rho \frac{Du_x}{Dt} = -\nabla p + \mu \nabla^2 u_x \quad (4.4)$$

Assuming steady flow and a no-slip boundary condition, one obtains the plane Poiseuille flow equation

$$u_x = -\frac{\nabla p}{\mu} \left( yh - \frac{y^2}{2} \right) \quad (4.5)$$

The negative sign offsets the negative value of  $\nabla p$ . Equation (4.5) indicates that the Poiseuille flow velocity under steady state conditions is a symmetric parabolic profile.

The flux of fluid is

$$Q = \int_0^{2h} u_x dy = -\frac{2h^3}{3\mu} \nabla p \quad (4.6)$$

and the mean velocity is

$$u_a = -\frac{h^2}{3\mu} \nabla p \quad (4.7)$$

The concept of viscous dissipation during flow can be understood readily from the energy equation (c.f. Kundu, 1990). In the above flow case, the energy equation is

$$\rho \frac{D}{Dt} \left( \frac{1}{2} u_x^2 \right) = \frac{\partial}{\partial y} (u_x \tau_{xy}) - \emptyset \quad (4.8)$$

where

$$\emptyset = 2\mu e_{xy} e_{xy} \quad (4.9)$$

The quantity  $\emptyset$ , which is proportional to  $\mu$ , represents the viscous dissipation of kinetic energy. Equation (4.8) dictates that there is a kinetic energy loss due to viscous dissipation. This loss is compensated by the pump action. When the plate boundaries serve

as insulators, viscous dissipation causes an increase in the fluid temperature. When the boundaries act as a heat bath, the heat generated by viscous dissipation is removed from the thermal boundary.

On the microscopic (molecular) scale, if particles in a system undergo random motion only, the net average random velocity of the particles is zero and this indicates no flow at the macroscopic scale. The thermal energy induced by the random motion defines temperature in the system, i.e.,  $E=kT$  (in 2D). If flow occurs in a certain direction, the net average velocity of the particles is no longer zero and a flow results at the macroscopic scale. In this case, a “flowing energy” caused by flow is superimposed on the thermal energy of the particles; thus the total energy is the sum of the “flowing energy” and the thermal energy.

The thermodynamic automata represent a “particle like” construction at an intermediate scale (meso-scale). Here the particles are packets of information which obey basic physical theory (e.g. conservation of momentum) at the meso-scale and this is found to be sufficient to yield consistency with the Boltzmann distribution and the Navier-Stokes equation at the macro-scale.

### 4.3 The Model and Simulation Experiments

The detailed description of the basic model is given in Chapter 2. One of the main features of the model is that, in contrast to the conventional lattice gas model, the particle velocities are not discrete but continuous.

To model plane flow, one requires pump action to generate the flow with boundary conditions. In order to mimic pump action (a pressure gradient), a constant momentum is added to each particle at each iteration. Furthermore, to facilitate the simulation process, the pump action is installed in every cell. No-slip boundary conditions can be attained as usual, i.e., by reversing the particle velocity when a particle hits the boundary. There are two ways of implementing thermal boundary conditions upon particles colliding with the boundary: (1) the particles are returned such that the particle velocities fit a characteristic Boltzmann distribution, and the particle velocity direction points to the interior of the lattice, ranging from 0 to 180 degrees; (2) all particles are returned with the same fixed velocity. The first method is adopted here.

Two main types of simulation experiments were performed:

1. Poiseuille flow with all conditions identical except the boundary conditions, i.e., no-slip boundary and thermodynamic boundary conditions.
2. fluid flow with thermal boundary conditions and the same pressure drop but different temperatures.

Experiment 1 was necessary to observe the difference between the boundary conditions. Experiment 2 was used to determine the fluid viscosity and the effects of temperature on fluid viscosity. The fluid viscosity can be computed in the conventional way (Rothman, 1988) by knowing the velocity profile and pressure drop. However, here, fluid viscosity is calculated by employing Equation (4.7). These experimental results were compared with theoretical predictions (Sears and Salinger, 1974).

In all the simulation experiments, 100 particles were initialized in each cell of a  $101 \times 11$  lattice with a thermal equilibrium state at a temperature of 0.005 (i.e. average velocity of particles is 0.1). Periodic boundary conditions were applied in the left and right boundaries of the lattice and no-slip or thermal boundaries were employed in the top and bottom boundaries. The pressure drops

were adjusted by the amount of momentum added to the particles at each of the iterations and the temperature by the average particle velocity of particles returned back from the top and bottom boundaries. For each row of the lattice, the flow velocity, mean flow velocity, total energy, thermal energy, and density of the particles were recorded at every other 200 iterations. Mathematica 2.2 was used for plotting.

The simulation codes were written in the C programming language and the simulation experiments were run with a super computer SP2 (Scalable Powerful Parallel Machine) located at the University of Alberta, Edmonton. In general, each experiment takes about 800 CPU minutes.



## **4.4 Results and Discussion**

In this section, simulation results for Experiment 1 is first presented. The two distinct thermal processes with insulating and thermodynamic boundary conditions are then compared. The fluid viscosity is calculated and the effect of temperature on fluid viscosity is discussed.

### **4.4.1 Simulation of the Thermal Dynamic Process of Plane Poiseuille Flow**

Simulation results for plane Poiseuille flow with no-slip (left column) and thermal boundary conditions (right column) are shown in Figure 4.1. Figure 4.1 indicates that, under no-slip boundary conditions (left column), the thermal energy (i.e. temperature) increases with time (top left graph), the mean flow velocity initially increases from zero to 1000 iterations and then decreases with increasing viscosity (middle left graph). However, for the thermodynamic boundary conditions (right column), the fluid thermal energy (i.e., temperature) initially decreases to a thermal equilibrium temperature at about 2000 iterations and then remains constant (top right graph) afterwards. The mean flow velocity

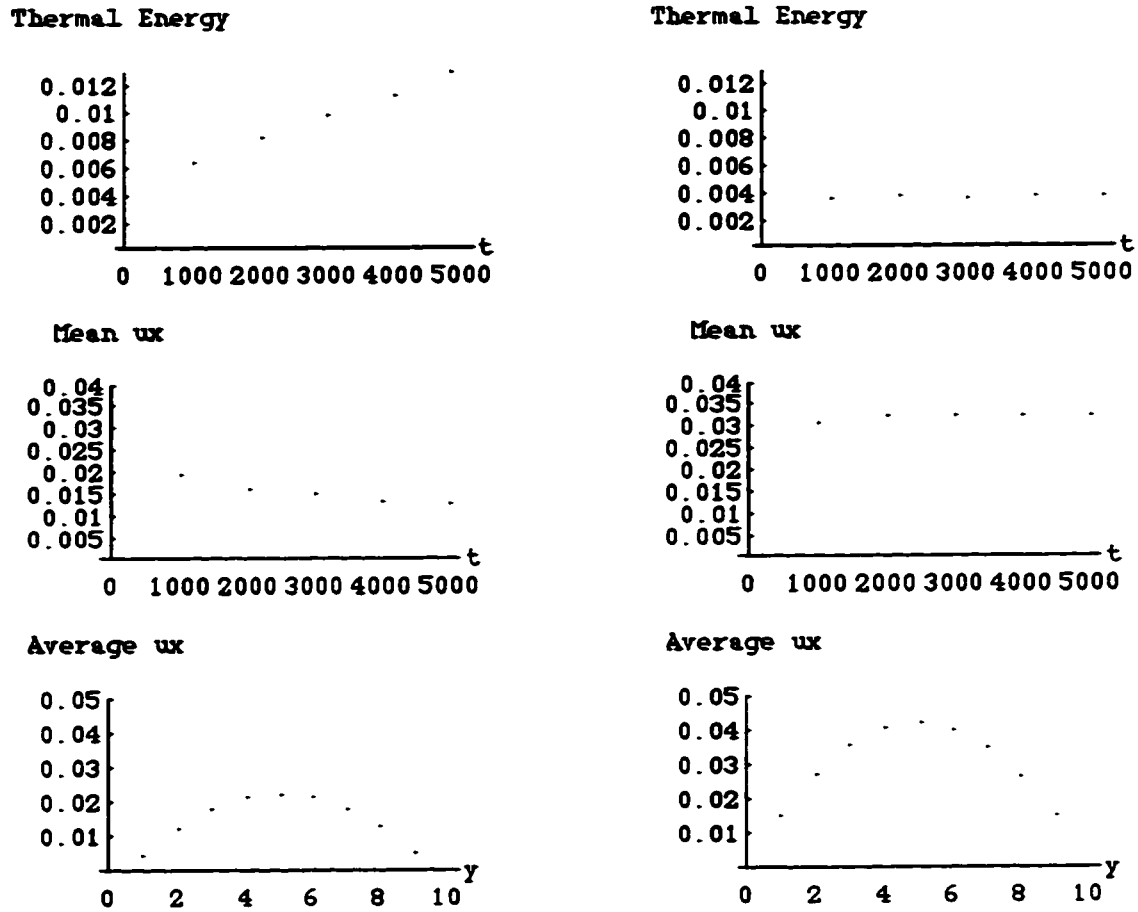


Figure 4.1 Simulation and comparison of thermal dynamic processes of plane Poiseuille flow with no-slip boundary conditions, i.e., thermal insulator (left column) and thermodynamic boundary conditions, i.e., heat bath (right column).

initially increases from zero to 1000 iterations and then keeps constant (middle right graph). Symmetric parabolic velocity distribution profiles for both conditions were observed, as expected. Row average velocities of particles vs. plate width ( $y$ ) at 5000

iterations were also shown in Figure 4.1 (bottom graphs) for illustration purposes.

The above processes can be explained as follows. The pumping action heats the fluid if the boundary is an insulator. The increase in temperature causes an increase of the fluid viscosity. Therefore, the mean flow velocity decreases with time. However, when the boundary is a heat bath, the extra heat caused by the pumping action is removed by the heat bath. Hence, the temperature does not change, so the fluid viscosity and the mean fluid flow velocity are constant.

In summary, the simulated thermodynamic processes are consistent with theoretical predictions and the implemented thermodynamic boundary appears to function very well.

#### **4.4.2 Fluid Viscosity Determination**

Fluid viscosity was determined from Equation (4.7) only for the thermodynamic boundary conditions where a steady state can be established. To make the computation more accurate, the averages of the mean flow velocity and the temperature from 2000 to 5000

iterations were calculated. The results for Experiment 2 are shown in Table 4.1 which lists the values of fluid viscosity against temperature (T) and  $\sqrt{T}$  as well as the associated parameters.

Table 4.1 Calculated fluid viscosity based on Experiment 2.

mean flow pressure velocity (lu/it)	drop $\mu/(\text{lu} \cdot \text{it})^2$	dynamic viscosity ( $\mu/(\text{lu} \cdot \text{it})$ )	T	$\sqrt{T}$
0.03245	0.0001	0.02568	0.003672	0.06059
0.02322	0.0001	0.03588	0.006793	0.08242
0.01586	0.0001	0.0525	0.01336	0.1155

where lu=lattice unit, it=iteration unit and  $\mu$ =mass unit. Temperature (T) were determined from the thermal energy by assuming the Boltzmann constant  $k=1$ .

Figure 4.2 is the corresponding plot of the fluid viscosity vs.  $\sqrt{T}$ . It illustrates that the fluid dynamic viscosity is proportional to  $\sqrt{T}$ .

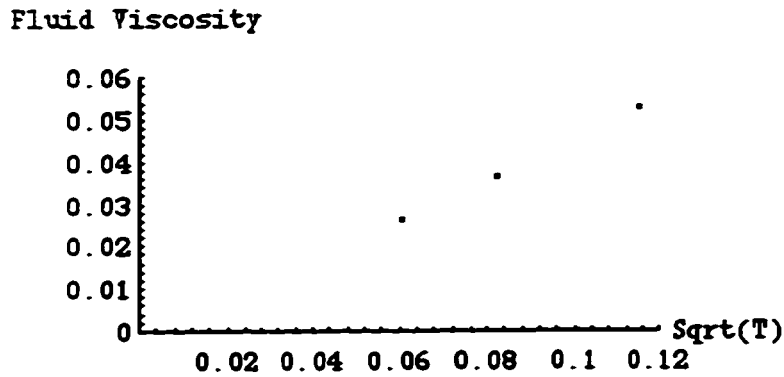


Figure 4.2 Fluid viscosity vs.  $\sqrt{T}$ . Viscosity is proportional to  $\sqrt{T}$ .

Existing physical theory (Sears and Salinger, 1974) indicates that shear viscosity is a strong function of temperature. For gases, the dynamic viscosity is proportional to  $\sqrt{T}$  since the random thermal speed is proportional to the  $\sqrt{T}$ , and so is the momentum transport. However, for liquids, the viscosity decreases with temperature since the shear stress is caused mainly by the cohesive forces between the liquid molecules. The thermodynamic automaton model is a gas model, thus the shear viscosity should be proportional to  $\sqrt{T}$ . The simulation experimental results (Figure 4.2) are consistent with these theoretical predictions. Note, a gas and a liquid both obey the Navier-stokes equation. If a gas behaves in an

incompressible fashion and the temperature is held constant, then both gas and liquid's behaviour is identical.

## 4.5 Conclusions

1. The thermodynamic automaton model simulates thermal processes in plane Poiseuille flow.

2. The simulation results clearly demonstrated that (1) for the no-slip boundary conditions, the excess heat generated by viscous dissipation causes the fluid temperature to increase, thus altering the fluid viscosity; (2) for the thermal boundary conditions, the viscous heat is removed by the thermal boundary and a steady state is achieved.

3. Fluid viscosity determined from the simulation is approximately proportional to  $\sqrt{T}$ . This finding is consistent with theoretical predictions for a gas. Furthermore, this temperature dependence of viscosity is identical to the predictions of physical theory (Sears and Salinger, 1974).

## 4.6 Bibliography

Chen, S., Lee, M., Zhao, K.H. and Doolen, G.D., 1989. A Lattice Gas Model with Temperature. *Physica D* 37, 42-59.

Chopard, B. and Droz, M., 1988. Cellular Automata Model for Heat Conduction in a Fluid. *Physics Letters A*, V. 126, No. 8,9. 476-480.

D'Humières, D., Lallemand, P. and Frisch, U., 1986. Lattice Gas Model for 3D Hydrodynamics. *Europhys. Lett.*, Vol. 2, No. 4, 291-297.

Frisch, U., Hasslacher, B. and Pomeau, Y., 1986. Lattice-Gas Automata for the Navier-Stokes Equation. *Physical Review Letters*, Vol. 56, No. 14, 1505-1508.

Kundu, P.K., 1990. *Fluid Mechanics*. Academic Press, Inc. San Diego. California.

Rothman, D.H., 1988. Cellular-Automata Fluids: A Model for Flow in Porous Media. *Geophysics*, Vol. 53, No. 4, 509-518.



Sears, F.W. and Salinger, G.L., 1974. Thermodynamics, Kinetic Theory, and Statistical Thermodynamics. Addison-Wesley Publishing Company. 281-291.

Tenenbaum, A., Ciccotti, G, and Gallico, R., 1982. Stationary Nonequilibrium States by Molecular Dynamics. Fourier's Law. Physical Review A, Vol. 25, No. 5, 2778-2787.

Trozzi, C. and Ciccotti, G., 1984. Stationary Nonequilibrium States by Molecular Dynamics. II. Newton's Law. Physical Review A, Vol. 29. No. 2, 916-925

## **CHAPTER 5**

### **THERMODYNAMIC AUTOMATON SIMULATIONS OF FLUID FLOW, DIFFUSION AND DISPERSION IN POROUS MEDIA**

#### **5.1 INTRODUCTION**

Fluid flow, diffusion and dispersion in porous media are important processes in fields such as hydrogeology, biology, soil science, petroleum engineering and geophysics. The practical importance of these processes in oil production and ground water contamination is the primary reason for this study.

With the aid of a powerful computer, automata simulations can be a useful tool for the investigation of these flow phenomena. Some recent studies on this topic are described by Gutfraind and Hansen (1995), Gao and Sharma (1994 a and b) and Somers (1993).

In the description given in this thesis, a thermodynamic automaton which incorporates fluid-solid collisions to mimic a porous medium is developed, and fluid flow, diffusion and dispersion in a porous medium are simulated with this model.

Section 5.2 contains the relevant theoretical background. Section 5.3 provides details of the model and simulation experiments. Section 5.4 presents the simulation results and associated discussion. Section 5.5 provides the conclusions.

## 5.2 Theoretical Background

By performing experiments of single phase fluid flow in a vertical column of sand, the French engineer Henry Darcy (1856) first discovered that the volumetric flow rate of fluid through a porous medium is directly proportional to the applied pressure drop and is inversely proportional to the fluid viscosity. This empirical relationship is the so-called Darcy's law. Later on, theoretical derivations of Darcy's law were provided by a number of researchers (e.g. Newman, 1977 and Whitaker, 1986a). In one dimension, Darcy's law is given by the simple equation

$$q = -\frac{K}{\mu} \frac{dp}{dx} \quad (5.1)$$

where

$q$  = volumetric flow rate/unit area,

$K$  = permeability of the porous medium,

$\frac{dp}{dx}$  = applied pressure drop,

$\mu$  = fluid viscosity.

The permeability  $K$  of the porous medium is defined as the capability of porous media to allow a fluid to flow through. It is a fundamental property of the geometry of a porous medium.

Balasubramanian et al. (1987) made a detailed study of Darcy's law using lattice-gas hydrodynamics. They obtained an effective Darcy's

law by allowing a damping term (a function of velocity) in the Navier-Stokes equation. That is,

$$\mu \frac{d^2 u}{dx^2} - \frac{\mu}{K} u = \frac{1}{\rho} \frac{dp}{dy} \quad (5.2)$$

Here,  $u$  is the flow velocity,  $\rho$  is the density,  $p$  is the pressure,  $\mu$  is the fluid viscosity, and  $K$  is the permeability of the medium. Using the Boltzmann approximation, they showed that the permeability is inversely proportional to the density of the solid scatterers.

For steady two-phase flow in homogeneous porous media, the governing equations of motion are given by de la Cruz and Spanos (1983), Whitaker (1986b), Kalaydjian (1987) and Eastwood (1992).

$$Q_{11}\bar{q}_1 - Q_{12}\bar{q}_2 = -\bar{\nabla}p_1 + \rho_1 g \quad (5.3)$$

$$Q_{22}\bar{q}_2 - Q_{21}\bar{q}_1 = -\bar{\nabla}p_2 + \rho_2 g \quad (5.4)$$

where  $Q$  is the mobility ratio,  $q$  is the flow rate,  $\bar{\nabla}p$  is the pressure gradient,  $\rho$  is the density of a fluid, and subscripts 1 and 2 refer to phases 1 and 2, respectively.

Diffusion occurs from high to low concentration areas due to molecular motion. For a fluid diffusing in a long tube, the diffusion equation is

$$\frac{\partial C}{\partial t} = D \frac{\partial^2 C}{\partial x^2} \quad (5.5)$$

where,  $C$  = concentration of the tracer,

$D$  = diffusion coefficient.

Solutions of this equation are related to the symmetric Gauss function. The diffusion coefficient can be determined from a plot of concentration profiles at various times.

When diffusion occurs in a porous medium, the apparent diffusion coefficient  $D_a$  is used in the diffusion equation (Equation (5.5)). The permeability  $K$  of the porous medium and the apparent diffusion coefficient,  $D_a$ , are related (Barrer, 1951) by

$$K = -D_a \frac{dC}{dx} \quad (5.6)$$

The apparent diffusion coefficient  $D_a$  measured in porous media is less than the molecular coefficient  $D$  as measured in a tube.

Perkins and Johnston (1963) reviewed diffusion and dispersion in porous media and pointed out that the ratio of  $\frac{D_a}{D}$  is approximately 0.6 to 0.7 for packs of unconsolidated granular material. For both cemented and unconsolidated porous rock, the ratio can be expressed as

$$\frac{D_a}{D} = \frac{1}{F\eta} \quad (5.7)$$

where  $F$  is the formation electrical resistivity factor, and  $\eta$  is the porosity of the porous medium.

Dispersion has been referred to as the spreading of a tracer released into a flowing fluid (Bear, 1988; and Baudet et al., 1989). Cyr et al. (1988) used "dispersion" to describe the broadening of the transition zone (immiscible displacements) and mixing zone (miscible displacements) in porous media. Dispersion includes two important mechanisms, i.e., molecular diffusion and mechanical mixing due to fluid velocity gradients. Dispersion in porous media is traditionally modeled by a conventional convection-diffusion equation where the molecular diffusion coefficient is replaced by a dispersion tensor. For one-dimensional flow, it is given by

$$\frac{\partial C}{\partial t} + v_x \frac{\partial C}{\partial x} = D_l \frac{\partial^2 C}{\partial x^2} \quad (5.8)$$

where  $v_x$  = mean velocity in the  $x$  direction,

$D_l$  = longitudinal dispersion coefficient.

Solutions of this equation are available for various initial and boundary conditions (Bear, 1972). Usually, the solution of this equation is related to the Gauss-error function. The longitudinal dispersion coefficient, generally assumed to be constant, may be determined using the breakthrough times for concentration values

of. for example, 0.16 and 0.84 (note, usually the width of the transition zone is defined by the distance between  $x$  at concentration 0.84 and  $x$  at concentration 0.16).

Udey and Spanos (1993) used a new approach to describe dispersion by demanding consistency with the equations for immiscible two phase flow with zero surface tension. Under a high flow rate regime where diffusion is negligible, they obtained a concentration equation which differs from the standard convection-diffusion equation in that non-constant apparent dispersion coefficients were used. They found that their analysis fits experimental data better.

When the porous medium is heterogeneous, the dispersion coefficient is space dependent. Thus a Fokker Planck equation (Risken, 1984), which contains non-constant drift and dispersion coefficients, should be used to model the dispersion process.

### 5.3 The Model and Simulation Experiments

The basic model was described in Chapter 2. Simulations of thermal boundary conditions and pump action to generate flow were described in Chapter 4.

The porous medium can now be introduced into the model in a straightforward fashion. When details of the effect of pore structure are important (for instance, the effect of pore structure on the distribution of the wetting and non-wetting phases in porous media), a pore-scale model can be constructed by introducing actual solid structures into the lattice. When a fluid particle encounters the solid matrix, a no-slip boundary is applied. Rothman (1988) applied this method to construct pore structure in a conventional lattice gas model and thus integrated the microstructure of the porous medium into his permeability calculation. However, it has been shown by Stauffer (1991) that massive computation is needed for realistic implementation of the pore-scale model.

When viewing porous media at a much larger scale (megascopic scale), the porous media can be modeled by allowing a probability for a solid collision at each cell in the lattice. The permeability is adjusted by changing that probability, and heterogeneity can be incorporated by allowing that probability to change in space. Although this approach does not allow us to see the details of the pore structure, it does permit us to simulate flow at the megascopic scale without computational difficulty. Gao and Sharma (1994a and



b) adopted this method in a conventional lattice gas automaton to simulate fluid flow and dispersion in heterogeneous porous media. However, a no-slip boundary condition was applied in their simulations. In this study, the porous medium at the megascopic scale is modelled. In the programming, for each particle in a cell, a random number is generated. If the random number is larger than the solid probability in that cell, the fluid particle is allowed to undergo a solid collision; moreover, that particle is not permitted another collision until it moves out of that cell. The rest of the fluid particles which do not collide with the solid randomly collide with each other.

Three main types of simulation experiments were conducted:

1. one-phase flow in porous media.
2. diffusion in porous media.
3. dispersion in porous media.

As a first step, Darcy flow is simulated and the simulation results is compared with theoretical predictions. Also, the effects of permeability and flow velocity on flow types, i.e., from Darcy flow (flat velocity profile) to plane Poiseuille flow (parabolic velocity profile) is investigated. The simulation experiments were performed by changing the permeability (solid probability) or pressure drop.

Simulations of Experiment 2 are carried out with different permeabilities to investigate the effects of permeability on the apparent diffusion coefficient. To ascertain the effects of the solid

probability (SP, the probability of collision with a solid object) distribution on diffusion, four different types of solid distribution but with the same mean SP (0.5) were employed. They are (1) homogeneous, i.e., the SP is the same (0.5) at every cell; (2) a Boltzmann distribution, the SP distribution fits a Boltzmann function at the range of 0.1 to 0.9; (3) a step function distribution, the SP distribution fits the step function from 0.1 to 0.9 and (4) a double Boltzmann distribution, the SP distribution fits a function obtained by adding two Boltzmann functions with peaks at 0.385 and 0.588.

Experiment 3 is performed by combining fluid flow and diffusion experiments in porous media. Different flow rates and SP distribution are applied in order to observe the effect of flow rate and SP distribution on dispersion. For fluid-solid collisions, both the no-slip boundary and thermal boundary conditions were applied. In addition, to check if a different SP distribution changes the gross permeability of a porous medium, one-phase flow experiments are conducted with both a homogeneous SP and the double Boltzmann distribution.

The initial set up of the simulations was almost the same for each experiment; that is, 100 particles were initialized in each cell of a  $101 \times 11$  lattice with a thermal equilibrium state at a temperature of 0.005 (particle velocity being 0.1). For the diffusion simulation, periodic boundary conditions were applied at the top, bottom, left and right boundaries of the lattice. For Darcy flow and dispersion modeling, thermal boundaries were utilized at the top and bottom

boundaries of the lattice to remove the extra heat caused by pump action. A tracer is initialized at the centre (3 columns) of the lattice for diffusion and dispersion modeling. The average flow velocity of each row of the lattice over 2000 to 5000 iterations was computed and the distribution of particle numbers for each column was recorded at 100 iteration intervals.

The simulation codes were written in C and simulation experiments were run with the SP2. Generally, it takes about 6 CPU hours to run a simulation.

## 5.4 Results and Discussion

In this section, the experimental results for one-phase flow is first presented, and the simulation results are compared with theoretical predictions. Then, the simulation results for diffusion in porous media is presented, and the effect of permeability and heterogeneity on apparent diffusion coefficients is discussed. Finally, the simulation results for dispersion in porous media is presented, and the effects of flow rates and different boundary conditions on dispersion are analyzed.

### 5.4.1 One Phase Flow in Porous Media

Figure 5.1 shows the simulation results for Darcy flow. It can be seen that for the same pressure drop (0.0005), a decrease in the SP (solid probability) results in an increase in the flow rate and thus an increase in permeability. The velocity profile for plane Poiseuille flow is parabolic, but for Darcy flow (Figure 5.1) it is flat due to the solid collisions. Balasubramanian et al. (1987) also obtained a flat velocity profile for Darcy flow from their numerical experiments.

Table 5.1 shows simulation results for Darcy flow with the same permeability ( $SP=0.1$ ) but different pressure drops. A straight line (Figure 5.2) is obtained when the simulation data points are plotted and connected in Table 5.1. These simulation results were consistent with the predictions of Darcy's law.

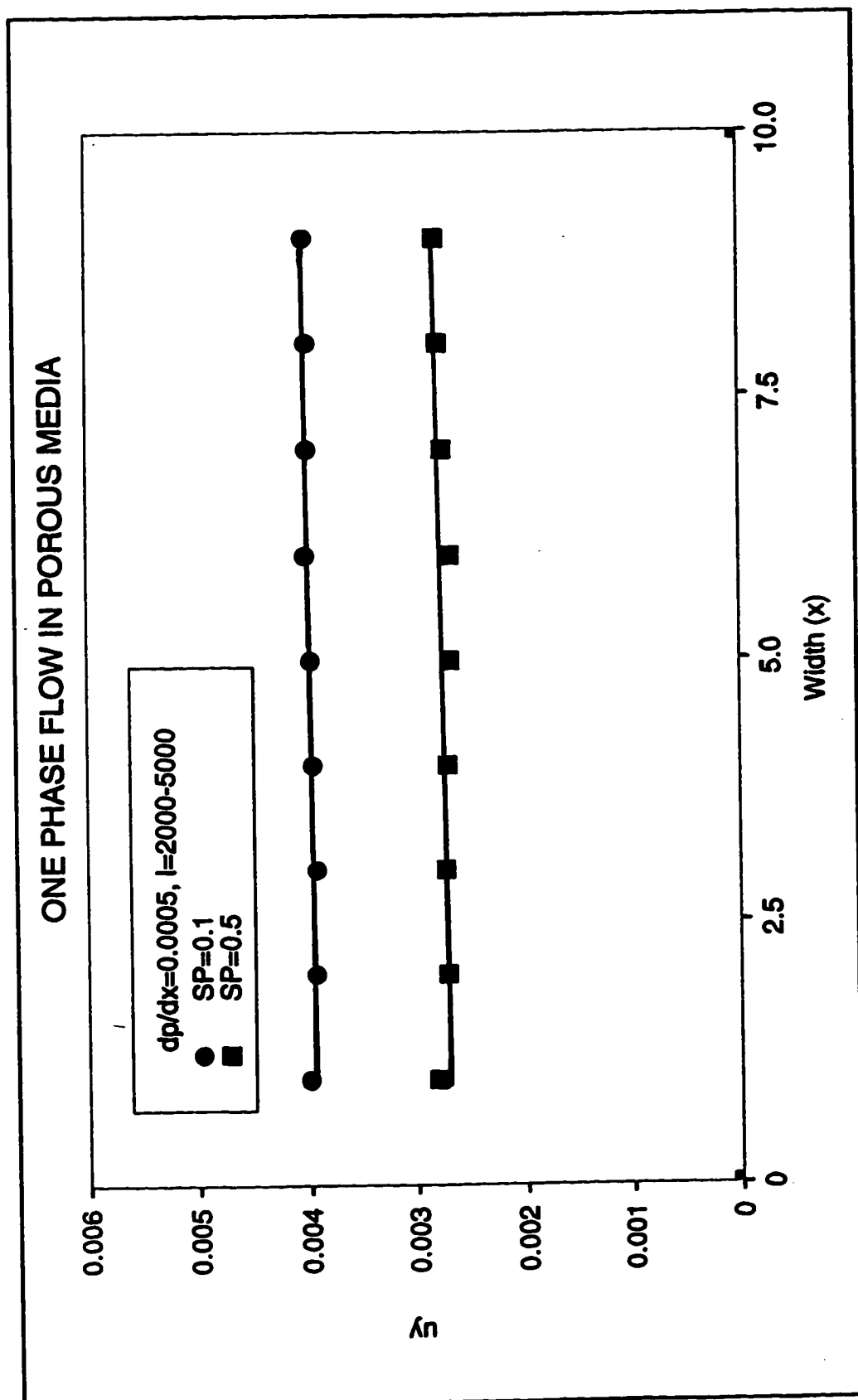


Figure 5.1 Flow velocity profiles with two different probabilities of a solid collision at lattice sites (0.1 and 0.5).

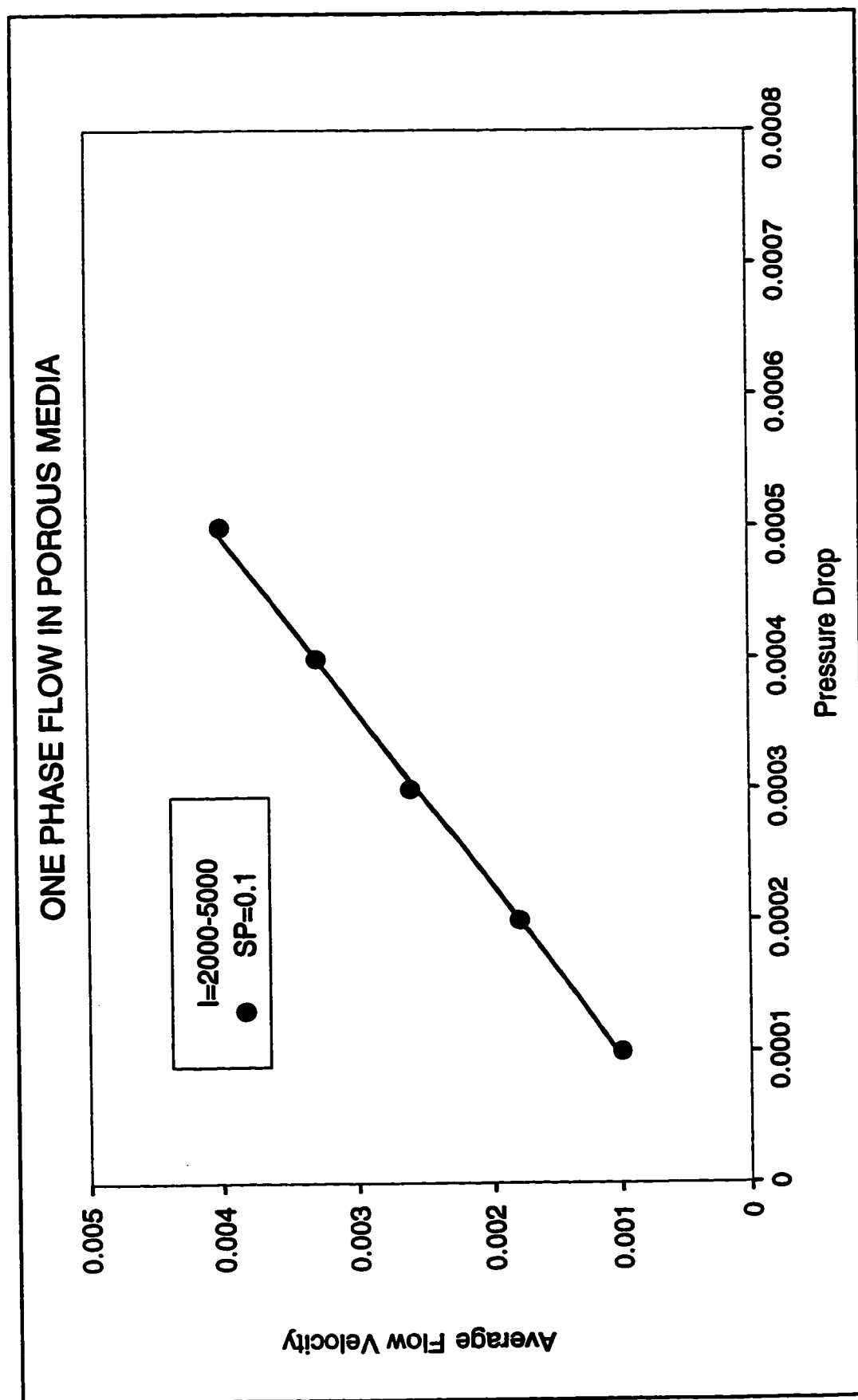


Figure 5.2 Flow velocity vs. pressure drop for one phase flow in a porous medium.

Table 5.1 Average flow rate vs. pressure drop.

pressure drop	average flow rate
-----	-----
0.0001	0.0010
0.0002	0.0018
0.0003	0.0026
0.0004	0.0033
0.0005	0.0040
-----	-----

Figure 5.3 illustrates that an increase in permeability (decrease in SP) results in a flow velocity profile change from flat to parabolic. At the limit of SP being zero, Plane Poiseuille Flow (Figure 5.4) is obtained. Figures 5.5 and 5.6 demonstrate that when the flow velocity is reduced to a small value, the velocity profiles are erratic. These simulation results can be explained as follows. From Equation (5.2), when the permeability  $K$  is small, the second term on the LHS of the equation is the dominant term and thus the velocity profile is flat. However, when  $K$  is large, the first term is the dominant term so the velocity profile is parabolic. When  $K$  is fixed and the flow velocity  $u$  is very small, the two terms are of the same order of magnitude; thus, the interaction of the two terms causes the velocity profile to be erratic.

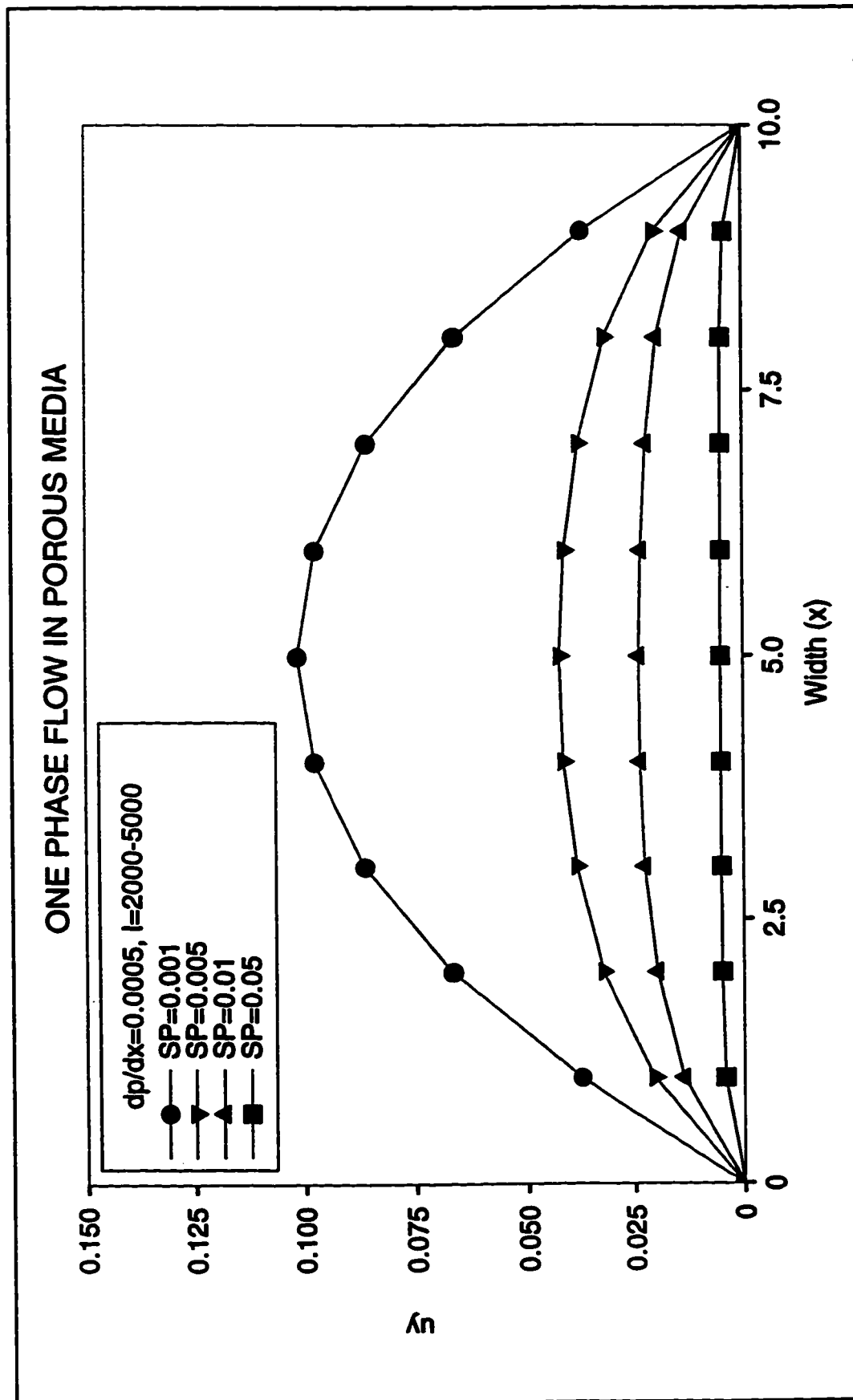


Figure 5.3 The change of flow velocity profiles with changes in  $1/\text{permeability}$ .



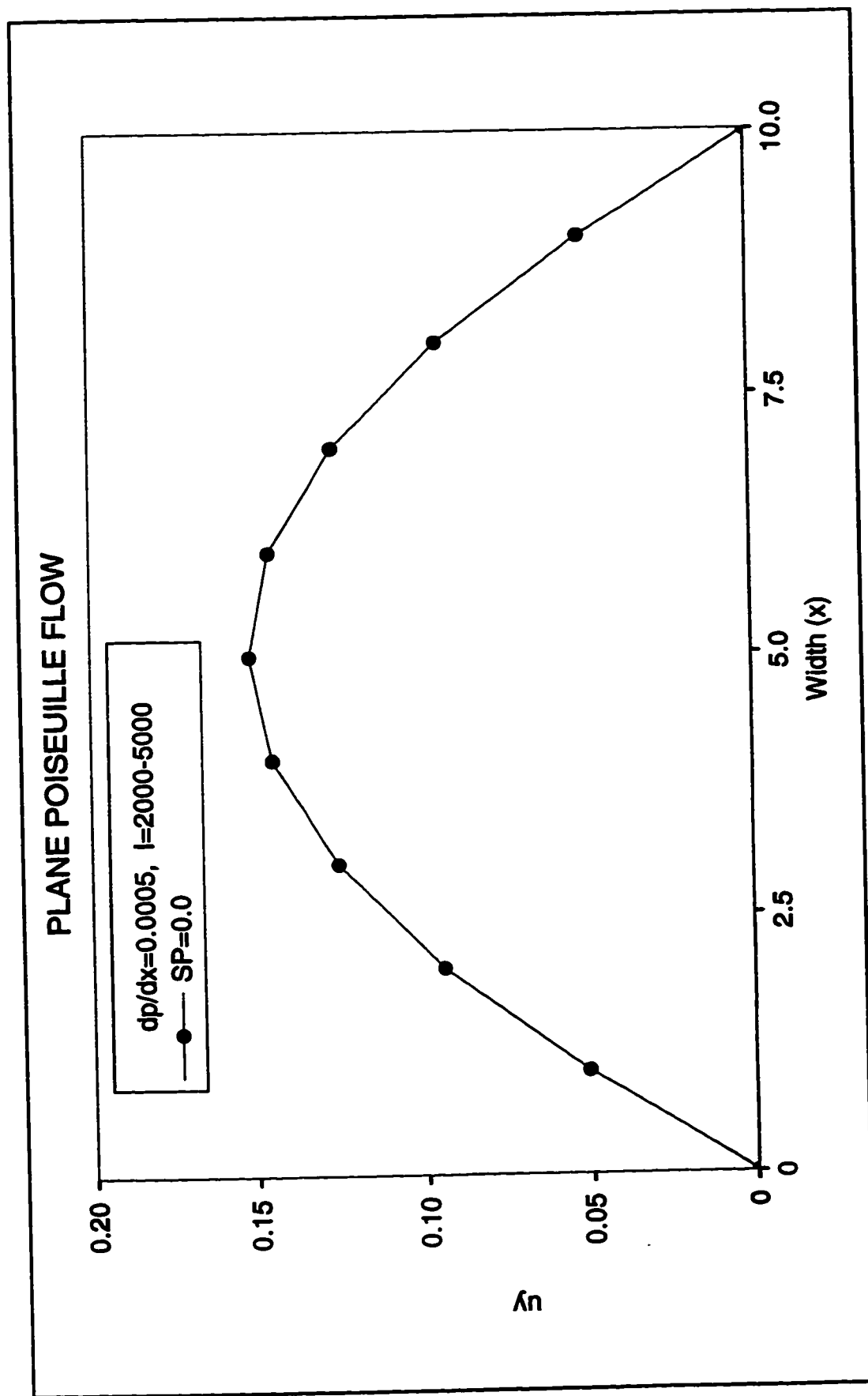


Figure 5.4 A flow velocity profile with the probability of a solid collision being zero.

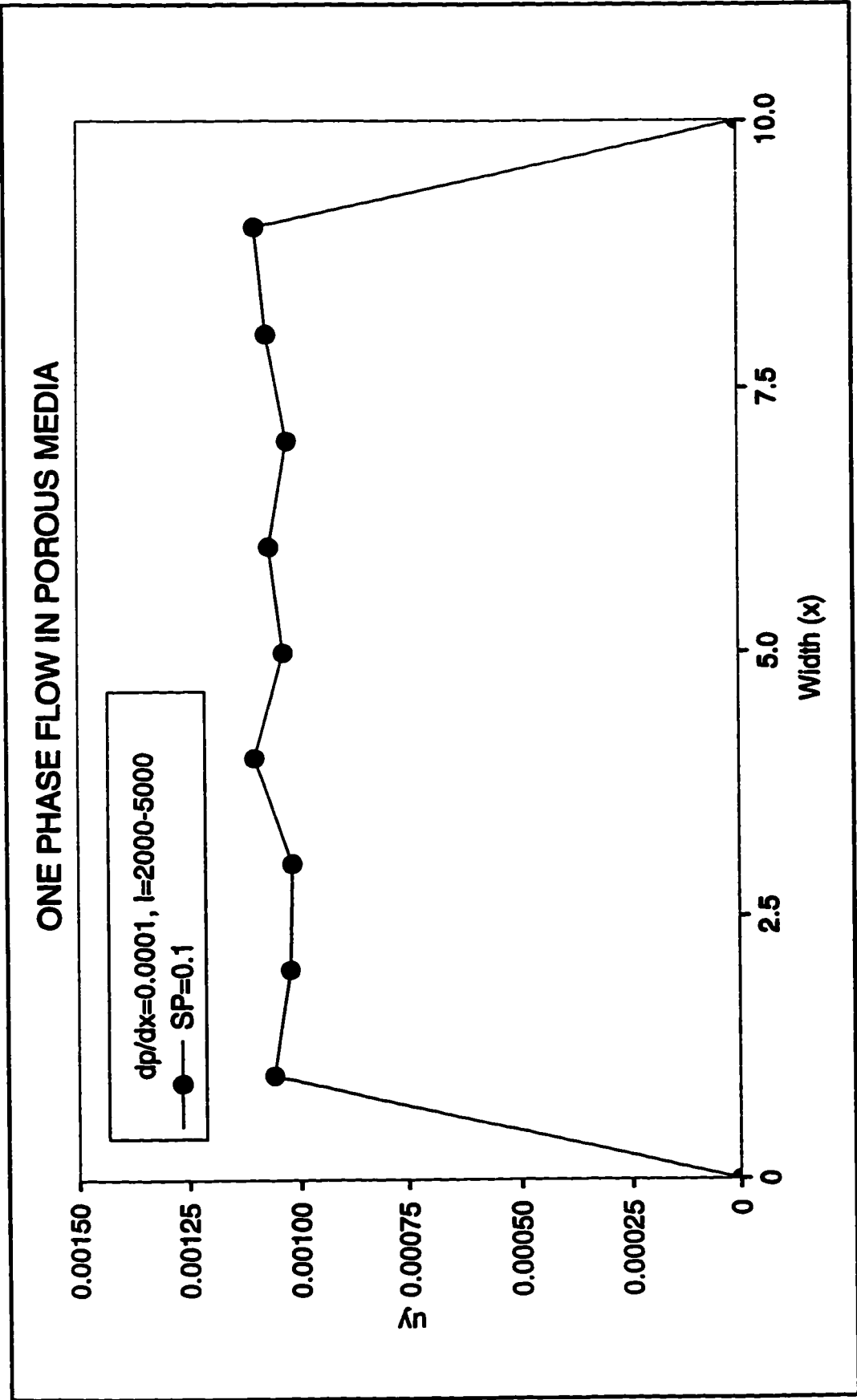


Figure 5.5 A flow velocity profile with a low flow velocity (0.001).

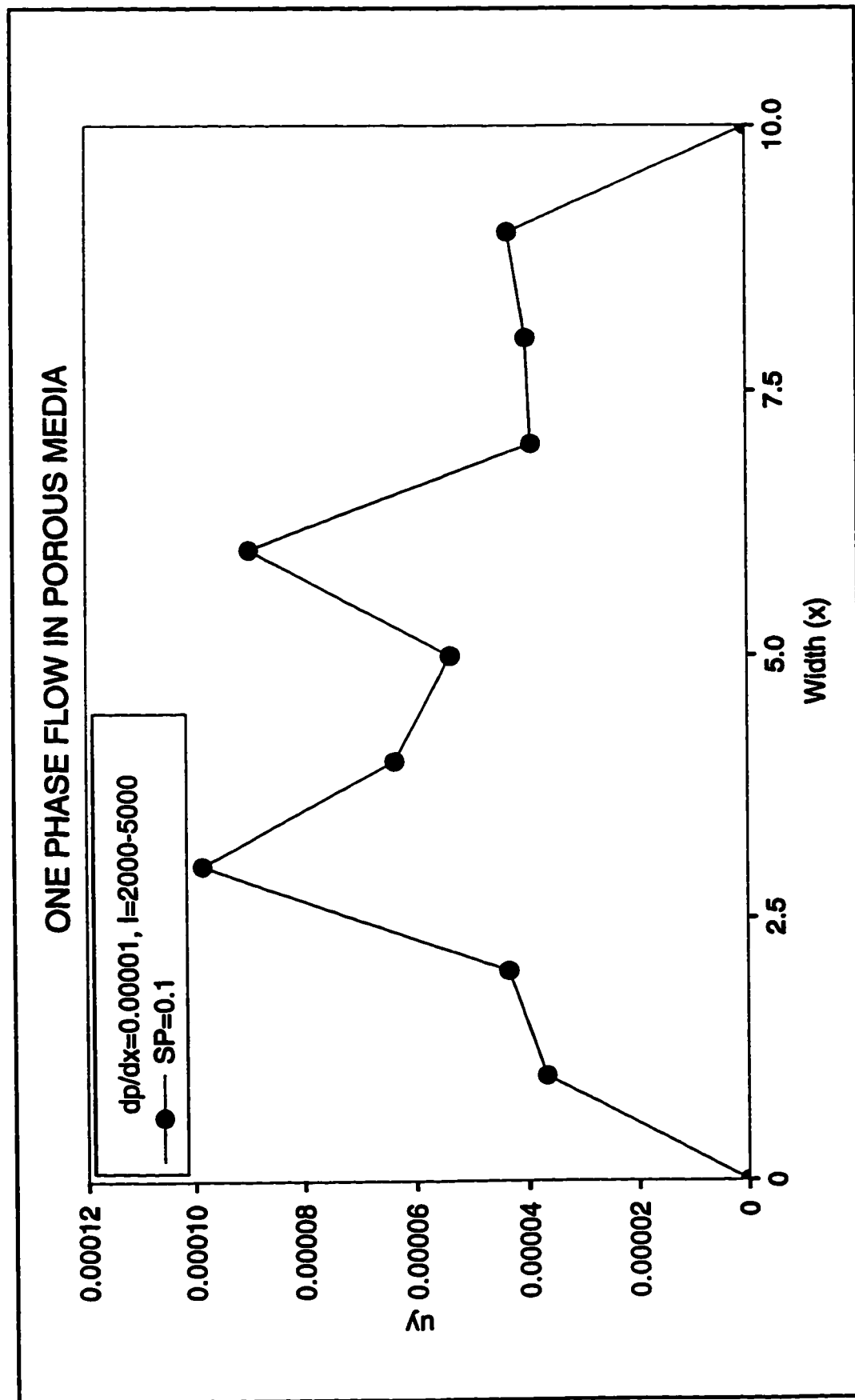


Figure 5.6 A flow velocity profile with a very low flow velocity (0.000006).

#### 5.4.2 Diffusion in Porous Media

As mentioned in Section 5.3, the initial configuration for the diffusion simulation is that the tracer (100 particle/cell) is initialized in the centre of the lattice (Columns 49, 50 and 51). The tracer then spreads sideways with time. Figure 5.7 shows the simulation results at 200 iterations for a homogeneous porous medium (SP is the same in every cell on the lattice) with different permeabilities or SP. Figure 5.7 indicates that the larger the SP, the lower the permeability and the lower the diffusion coefficient. This is consistent with the predictions of Perkins and Johnston (1963). The concentration profiles with a symmetric Gaussian distribution centered on the lattice agree with the solution of the diffusion equation (Equation (5.5)).

Figure 5.8 shows the simulation results after 500 iterations for porous media with different SP distributions (i.e. heterogeneity) but the same mean SP. Figure 5.8 indicates that the diffusion process for porous media with the SP distribution of a Boltzmann function, a step function and a double Boltzmann function is similar to that for homogeneous media. It is expected that a threshold may exist where the diffusion process for heterogeneous porous media starts to differ from that for the homogeneous porous media. The effects of heterogeneity are also constrained by the 2D modeling.

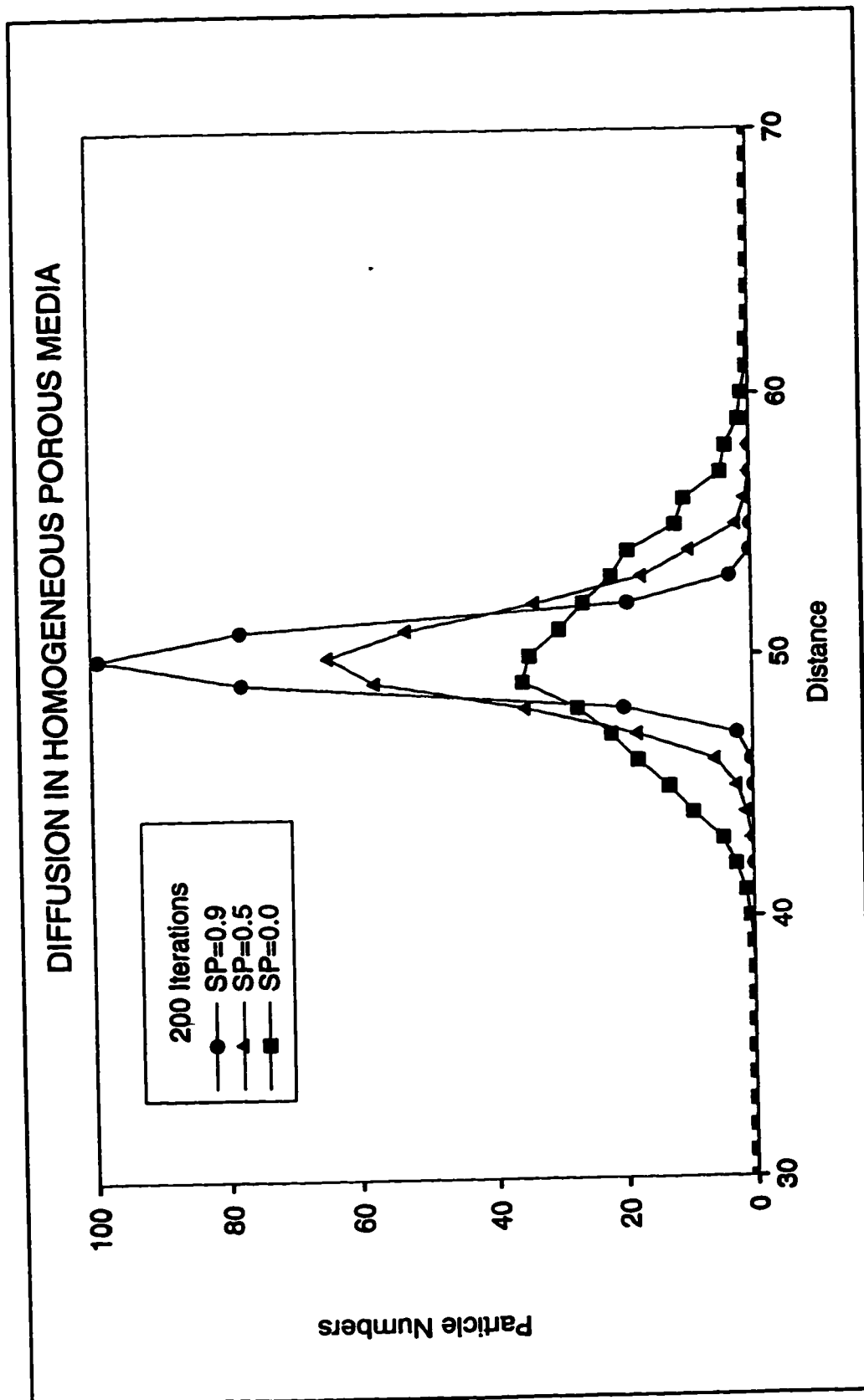


Figure 5.7 Diffusion in a homogeneous porous medium. The concentration profiles are plotted after 200 iterations with the probabilities of a solid collision being 0.9, 0.5 and 0.0.

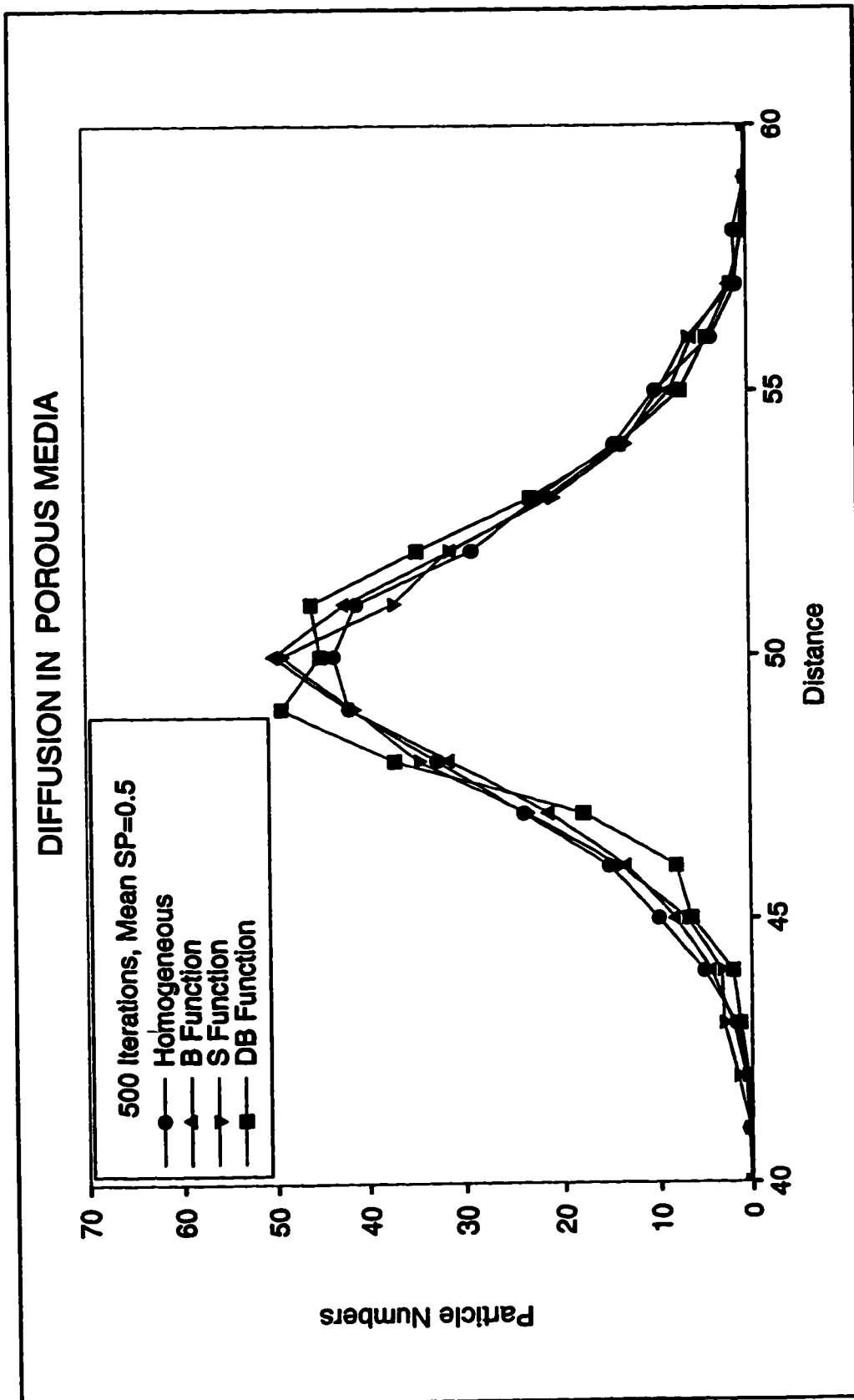


Figure 5.8 Comparison of diffusion in porous media with different distributions of the probability of a solid collision but the same mean probability of a solid collision.

### 5.4.3 Dispersion in Porous Media

Figure 5.9 illustrates the simulation results at 1500 iterations for dispersion in both homogeneous and heterogeneous porous media, where no-slip boundary conditions are applied for fluid-solid collisions. The figure illustrates that with an increase in the flow velocity from 0 to 0.012, the tracer spreads faster and the centre of the concentration profiles shifts further to the right. The simulation result of a dispersion increase with an increase in fluid velocity is consistent with theoretical predictions. Gao and Sharma (1994b) obtained similar simulation results by using a conventional lattice gas model.

Figure 5.10 shows the simulation results at 1500 iterations for dispersion in both homogeneous and heterogeneous porous media, where thermal boundary conditions are applied for fluid-solid collisions. One-phase flow in both homogeneous and heterogeneous porous media was conducted with the same pressure drop (0.005). It was observed that the same flow rate (0.020) is generated. Thus, both homogeneous and heterogeneous porous media have the same permeability. When comparing Figures 5.9 and 5.10, it is found that, at a low flow rate due to a small pressure drop ( $dp/dx=0.0005$ ), there is no significant difference between the concentration profiles under both no-slip and thermal boundary conditions. However, when a high pressure drop is applied (0.005), the concentration profiles under thermal boundary conditions move faster but are less flattened than those obtained using no-slip boundaries. The

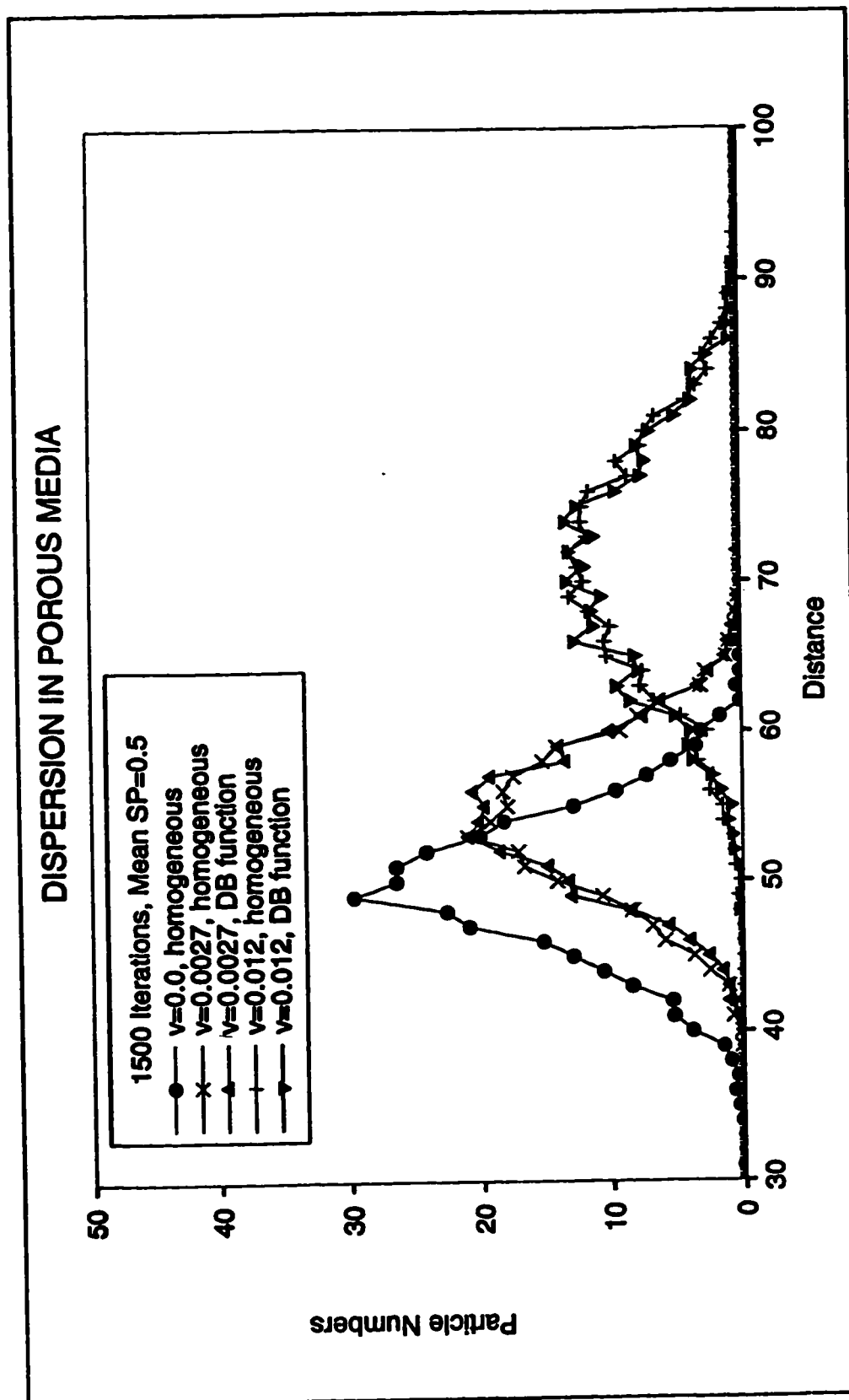


Figure 5.9 Dispersion in porous media with a no-slip boundary condition for the solid collision. The concentration profiles are plotted after 1500 iterations with different flow rates and different distributions of the probability of a solid collision.



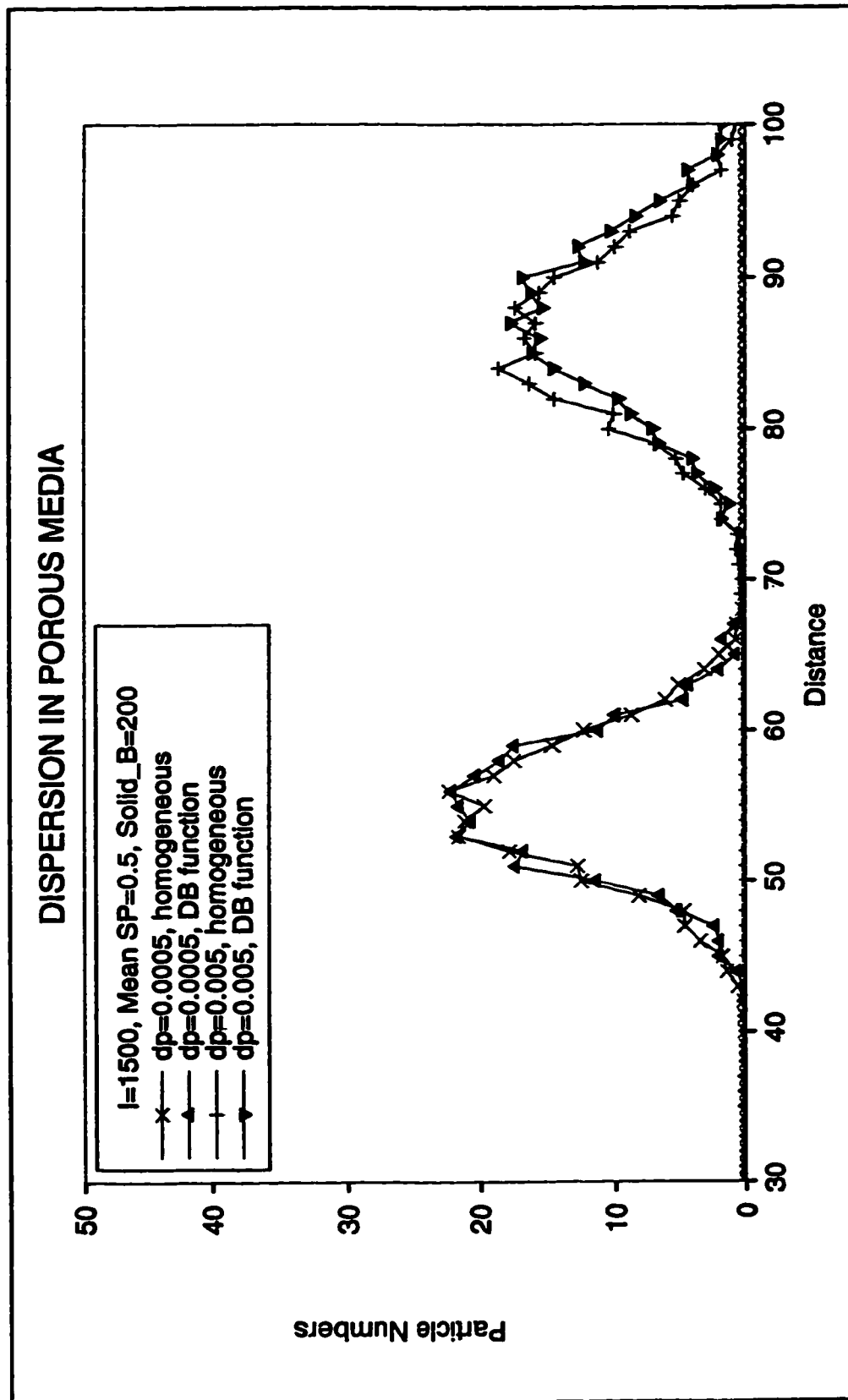


Figure 5.10 Dispersion in porous media with a thermal boundary condition for the solid collision. The concentration profiles are plotted after 1500 iterations with different flow rates and different distributions of the probability of a solid collision.

justification is as follows. As in the case of plane Poiseuille flow under both the no-slip and thermal boundary conditions, when a small pressure drop is applied, i.e., a small amount of momentum is added to each particle at each iteration, the viscous dissipation effect is small and the temperature is relatively constant. The diffusion coefficient and flow rates of the fluid under both boundary conditions are almost the same. This results in the same dispersion. In contrast, when a high pressure drop is applied, i.e., a large amount of momentum is added to each particle at each iteration, the fluid temperature increases for the no-slip boundary condition but remains constant for the thermal boundary condition. The temperature increase results in a low flow rate of the fluid (high viscosity) and a large diffusion coefficient. That is why the concentration profiles with the no-slip boundary condition move slower but spread faster than those with the thermal boundary condition.

Figures 5.9 and 5.10 also indicate that the SP distribution (i.e. heterogeneity) of the porous medium did not affect the dispersion process significantly. Again, the effects of heterogeneity on dispersion may be limited by the threshold below which the effects of heterogeneity are negligible, and by 2D modeling. Also, this appears to be associated with the restriction that macroscopic phase separation is not allowed and that the pore structure effect is not simulated properly. This final point is analyzed in more detail in the next chapter (Chapter 6).

### 5.5. Conclusions

1. A thermodynamic automaton model for modeling fluid flow, diffusion and dispersion in porous media was constructed. This model included fluid solid collisions to mimic a porous medium and thermal boundary conditions for the solid matrix in the porous medium.

2. Darcy flow was simulated. The simulation results are consistent with the predictions of Darcy's law. The change of types of velocity profile (flat, parabolic and erratic) is affected by permeability and flow velocity and is consistent with theoretical predictions.

3. Diffusion in porous media was modeled. The simulation results indicate that (1) the apparent diffusion coefficients decrease with a decrease in permeability; (2) small scale heterogeneity did not affect the diffusion process significantly.

4. Dispersion in porous media was modeled. The simulation results indicate that (1) dispersion increases with an increase in flow velocity; (2) thermal boundary conditions for a solid should be used to model dispersion processes in order to maintain a constant temperature; and (3) small scale heterogeneity did not affect the dispersion process significantly. It may be limited by the threshold and 2D modeling. Also, it may be related to the constraint that macroscopic phase separation is not allowed, and that the pore structure is not properly simulated.

## 5.6. Bibliography

Balasubramanian, K., Hayot, F., and Saam, W.F., 1987. Darcy's Law from Lattice-Gas Hydrodynamics. *Phys. Rev. A*. Vol. 36, No. 5, 2248-2253.

Barrer, R.M., 1951. *Diffusion in and through Solids*. Cambridge University Press. 1-4.

Baudet, C., Hulin, J.P., Lallemand, P. and d'Humieres, D., 1989. Lattice-Gas Automata: A Model for the Simulation of Dispersion Phenomena. *Phys. Fluids A*. Vol. 1, No. 3, 507-512.

Bear, J., 1972. *Dynamics of Fluids in Porous Media*. Published by American Elsevier Company Ltd., 579-582.

Cyr, T.J., de la Cruz, V. and Spanos, T.J.T., 1988. An Analysis of the Viability of Polymer Flooding as an Enhanced Oil Recovery Technology. *Transport in Porous Media*. Vol. 3, 591-618.

Darcy, H., 1856. *Les Fontaines Publiques de la Ville Dijon*, Dalmont, Paris.

de la Cruz, V. and Spanos, T.J.T., 1983. Mobilization of Oil Ganglia, *AIChE J.*, Vol. 29, No. 7, 854-858.

Gao, Y. and Sharma, M.M., 1994a. A LGA Model for Fluid Flow in Heterogeneous Porous Media. *Transport in Porous Media*. Vol. 17, 1 - 17.

Gao, Y. and Sharma, M.M., 1994b. A LGA Model for Dispersion in Heterogeneous Porous Media. *Transport in Porous Media*. Vol. 17, 19 - 32.

Gutfraind, R. and Hansen, A., 1995. Study of Fracture Permeability Using Lattice Gas Automata. *Transport in Porous Media*. Vol. 18, 131 - 149.

Eastwood, J.E., 1992. Thermomechanics of Porous Media. Ph.D dissertation. University of Alberta, Edmonton. 76-86.

Kalaydjian, F., 1987. A Macroscopic Description of Multiphase Flow in Porous Media Involving Spacetime Evolution of Fluid/Fluid Interface. *Transport in Porous Media*. Vol. 2, 537-552.

Newman, S.P., 1977. Theoretical Derivation of Darcy's Law. *Acta. Mech.*, Vol. 25, 153.

Perkins, T.K. and Johnston, O.C., 1963. A Review of Diffusion and Dispersion in Porous Media. *Society of Petroleum Engineers Journal*, Vol. 3, No. 1, 70-84.

Risken, H., 1984. The Fokker-Planck Equation. Springer-Verlag Berlin Heidelberg. 4-8.

Rothman, D.H., 1988. Cellular-Automaton Fluids: A Model for Flow in Porous Media. Geophysics, Vol. 53, No. 4, 509-518.

Somers, J.A., 1993. Direct Simulation of Fluid Flow with Cellular Automata and the Lattice-Boltzmann Equation. Applied Scientific Research. Vol. 57, Nos. 1-2, 127-133.

Stauffer, D., 1991. Computer Simulations of Cellular Automata. J. Phys. A: Math, Gen. Vol. 24, 909-927.

Udey, N. and Spanos, T.J.T., 1993. The Equations of Miscible Flow with Negligible Molecular Diffusion. Transport in Porous Media. Vol. 10, 1 - 41.

Whitaker, S., 1986a. Flow in Porous Media I: A Theoretical Derivation of Darcy's Law. Transport in Porous Media. Vol. 1, 3-25.

Whitaker, S., 1986b. Flow in Porous Media II: The Governing Equations for Immiscible, Two-Phase Flow, Transport in Porous Media. Vol. 1, 105-125.

## **CHAPTER 6**

### **AUTOMATON SIMULATION OF DISPERSION IN POROUS MEDIA WITH ENHANCED RULES**

#### **6.1 Introduction**

Dispersion in porous media is simulated at two different scales i.e. the macroscopic scale (pore scale) and the megascopic scale (scale of hundreds of pores). Pore scale modeling requires massive computation but does allow us to see the details of the pore structure and its effect on dispersion. In contrast, large scale modeling overcomes some of the computational difficulties but does not provide the details of the pore structure. Nevertheless, the two scales should provide consistent results. That is, large scale simulation should integrate pore structure effects on dispersion and reflect the "message" imbedded at the pore scale.

Gao and Sharma (1994) carried out a large scale simulation on dispersion with a no-slip boundary for the solid. Large scale modeling on dispersion has been modelled in this study (see Chapter 5) with both a no-slip and a thermal boundary for the solid. It appears that pore structure was not properly incorporated in the previous modeling. Also, some information was missing. For example, the displacing and displaced fluid were assumed to be totally mixed at the "particle level" and thus macroscopic phase separation was not allowed. Also, like the case of immiscible displacement, the wetting phase surrounds and collides with the solid matrix. The displaced fluid in miscible flooding behaves as a wetting phase and

collides with the solid matrix unless it is totally mixed with the displacing fluid at the particle level. In addition, when the invading and invaded fluids have different viscosities, the mixing zone will have a different viscosity. To reflect the viscosity effect on dispersion, the fluid particle can be indexed as to whether it is in the mixing zone or not, and the particle collision probability can be adjusted accordingly. Since a tracer used in a dispersion simulation has the same viscosity as the displaced fluid, the effect of viscosity on dispersion does not arise. Finally, a theoretical study (see Chapter 7) indicates that there is a pressure difference between the displacing and the displaced fluids at the same megascopic volume elements represented by a lattice site. However, the pressure difference was zero in our previous modeling was assumed.

In this study, simulate dispersion in porous media at the pore scale is first simulated and the pore structure effect on dispersion is demonstrated. Then the rules in the large scale modeling are modifies to incorporate pore scale information, including phase separation, pore structure effects and the pressure difference between the displacing and displaced fluids.

Section 6.2 contains the relevant theoretical background. Section 6.3 provides details of the models at the pore scale and megascopic scale with the enhanced rules as well as simulation experiments. Section 6.4 presents the simulation results and associated discussion. Section 6.5 provides the conclusions.



## **6.2 Theoretical Background**

Dispersion and theories accounting for dispersion in porous media are presented in Section 5.2. Recently, the laboratory experimental results of Sternberg et al. (1996) provided evidence indicating that the conventional convection diffusion equation fails to adequately predict dispersion in porous media.

Theoretically, two approaches (equations) have been used to replace the convection diffusion equation when describing dispersion. One approach involves the use of nonlocal equations (Edelen, 1976) which allow information from the whole region to be included to determine the effect at any particular point in the system. This approach incorporates memory of the past history of the flow. The other approach is the equation derived by Udey and Spanos (1993) under the condition of negligible diffusion. The Buckley Leverett solution provides a simple analytical solution (Spanos et al., 1988).

### 6.3 The Model and Simulation Experiments

A large scale (mega-scale) model for dispersion simulation is given in Chapter 5. Here, a pore scale model is first constructed. Then the mega-scale model with enhanced rules are modified to incorporate the pore scale information.

The pore scale model can be constructed by introducing actual solid structures into the lattice. When a fluid particle encounters the solid matrix, a thermal solid boundary condition is applied. That is, when fluid particles collide with the solid, they simply bounce back under the condition that particle speeds fit a characteristic Boltzmann distribution. Here, the fluid particles are not allowed to stay in solid cells. Following conventional practice, a “tube model”, i.e., a bundle of tubes is used to represent porous media. The tube model is chosen so that one can control permeability by adjusting tube radii. These models, although simple, do reflect some effects of pore structure on dispersion. Two “tube models” with the same gross permeability (41.67) but different pore structures (channel thicknesses) are designed as illustrated in Figure 6.1.

Model A consists of five tubes with the same diameter (10). It is homogeneous at both the macro-scale and the mega-scale. Model B consists of six tubes with different diameters (3x5, 2x10, 15). It has the same permeability as that of Model A at the mega-scale. The two models are used to represent two cores with the same permeability but different pore structures. For simplicity, model A is called a

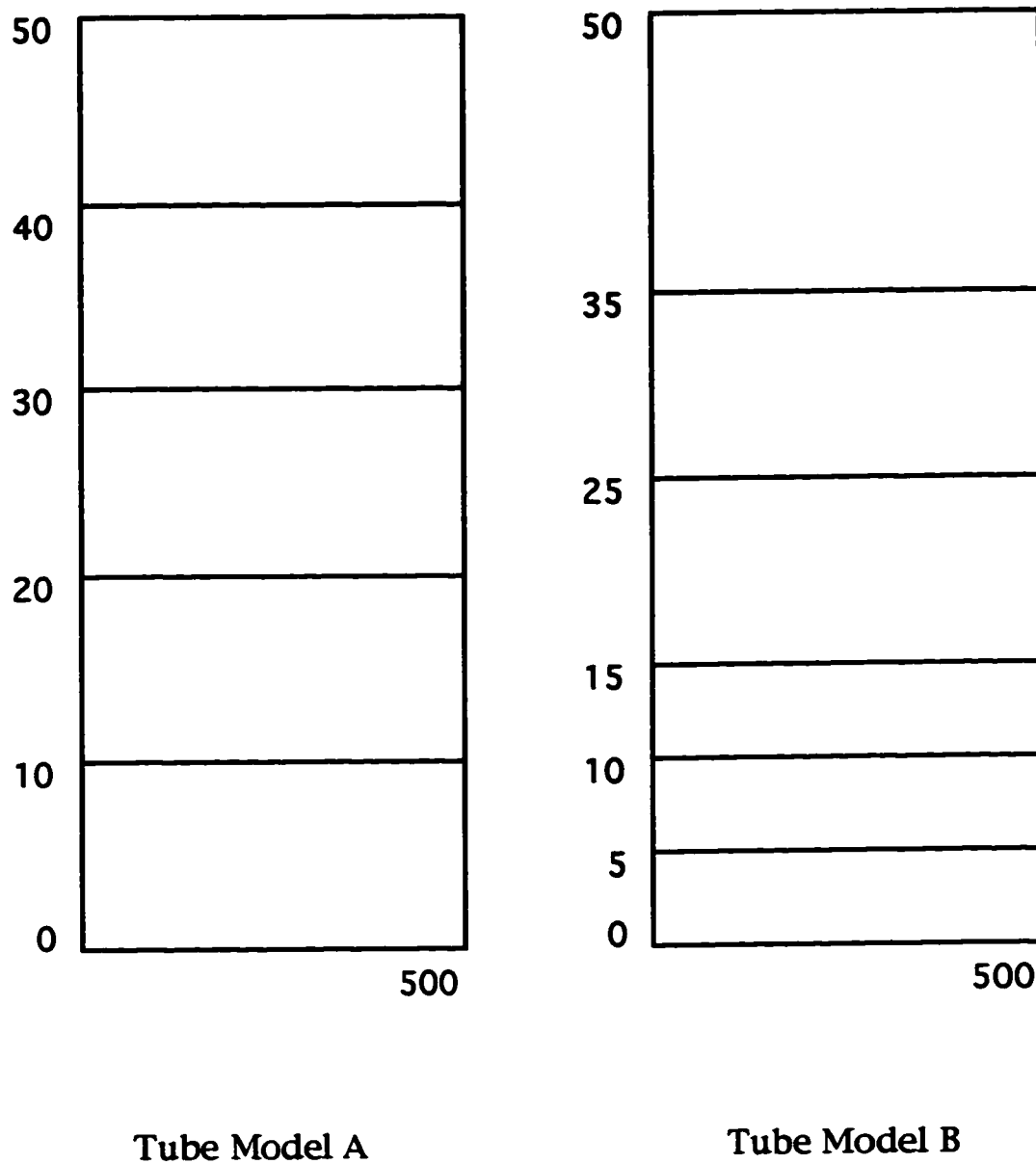


Figure 6.1 Schematic diagram of tube models A and B.

homogeneous model (HO) and model B a heterogeneous model (HE).

For a thermodynamic automaton model constructed to simulate a porous medium at the mega-scale, viscosity related effects can be introduced through the collision rules. Namely, an increase in the number of fluid-fluid particle collisions results in an increase in momentum transfer. Pore structure effects can be introduced by adjusting the particle velocity directions after collisions. To incorporate the pore scale information in the large (mega) scale modeling, previous rules for the simulation are modified as follow:

(1) B (blue) and R (red) are used to represent displacing and displaced particles. Further,  $B_0$  and  $B_1$  are used to represent the displacing fluid particle in the segregated and mixing zones respectively, and the same for  $R_0$  and  $R_1$ .

(2) since  $B_0$  and  $R_0$  are in a segregated region,  $B_0$  is not allowed to collide with  $R_0$ . Thus,  $B_0$  can only collide with  $B_0$ ,  $B_1$ , and  $R_1$ . Moreover,  $B_0$  becomes  $B_1$  when  $B_0$  collides with  $R_1$ . The same rules are applied to  $R_0$  accordingly.

(3) when  $B_0$  collides with  $R_1$  and in the central mass frame, if the rotation angle is greater than 90 degrees but less than 270 degrees, a random number is generated. When the random number is less than a flipping probability, the direction of the two particles are reversed. The pore structure effect can be incorporated by changing the flipping probability. In this model, the flipping probability is set to be either 0 or 1.

(4) for fluid-solid collisions, the distribution of displacing (B) and displaced (R) fluids, i.e., displaced fluid surrounding the solid matrix

(and thus colliding with the solid), is reflected by setting the priority of the fluid-solid collision as  $R_0 > R_1 > B_1 > B_0$ .

(5) to maintain the same permeability, in each cell, the total number of fluid particles colliding with the solid should be the total number of fluid particles  $N (R_0 + R_1 + B_1 + B_0)$ , multiplied by the solid collision probability  $P$  in that cell.

(6) to implement the pressure difference between the displacing and displaced fluids, instead of adding the same amount of momentum to both of the displacing and displaced particles, different amounts of momentum are partitioned to the different types of particles according to the following equations:

$$m_2 v_2 - m_1 v_1 = \beta' (n_2 - n_2') \quad (6.1)$$

$$n_2 m_2 v_2 + n_1 m_1 v_1 = (n_2 + n_1) m v \quad (6.2)$$

Here  $m$  is the mass,  $v$  is the velocity,  $n$  is the particle number at the present time in a cell and  $n'$  is the particle number at the previous time. The parameter  $\beta'$  is the beta factor (BF) which can be determined experimentally. The subscripts 1 and 2 refer to fluid 1 and 2, respectively. Equation (6.1) comes from the dynamic pressure difference between the displacing and displaced fluids (see Equation (7.36) in Chapter 7). That pressure difference is associated with the concentration (particle number) changing with time. Equation (6.2) indicates that the total momentum added in a cell is the same as if only one phase existed in the cell.

Two main types of simulation experiments were conducted:

1. dispersion in pore scale models (tube models).
2. dispersion in mega-scale models with the enhanced rules.

Simulations of Experiment 1 are carried out to analyze the effects of pore structure and temperature on dispersion. Four simulations are run at the same pressure drop ( $dp/dx=0.005$ ), and the same permeability (41.67) but at a different initial particle velocity ( $v_0$ ), temperature ( $1/B$ ) and with models having different pore structures.

The parameters of the simulations are as follows:

- (1.1)  $v_0 = 0.1$ ,  $B=200$ , HO.
- (1.2)  $v_0 = 0.1$ ,  $B=200$ , HE.
- (1.3)  $v_0 = 0.01$ ,  $B=20000$ , HO.
- (1.4)  $v_0 = 0.01$ ,  $B=20000$ , HE.

The initial set up for the above runs was the same i.e. a  $500 \times 50$  lattice was used with 20 particles in each cell. Blue particles were assigned to the left part (Columns 0 to 199) and the right part (Columns 301 to 500) and red particles to the middle part (Columns 200 to 300). Thermal boundary conditions were applied for the solid boundary (tube walls).

For Experiment 2, eight simulations are run at the same pressure drop ( $Dp=0.005$ ), temperature ( $T=1/200$ ), initial particle velocity ( $v_0=0.1$ ) and mean solid probability ( $SP=0.5$ ) but with different values of BF, flipping probabilities (FP) and with models having homogeneous (HO) and heterogeneous (HE) SP distributions. The parameters of the simulations are as follows:

- (2.1)  $FP=0$ ,  $BF=0$ , HO.
- (2.2)  $FP=0$ ,  $BF=0$ , HE (DB function).
- (2.3)  $FP=0$ ,  $BF=0.001$ , HO.

- (2.4)  $FP=0$ ,  $BF=0.001$ , HE (DB function).
- (2.5)  $FP=0$ ,  $BF=0.01$ , HO.
- (2.6)  $FP=0$ ,  $BF=0.01$ , HE (DB function).
- (2.7)  $FP=1$ ,  $BF=0.01$ , HO.
- (2.8)  $FP=1$ ,  $BF=0.01$ , HE (DB function).

The initial configuration for Experiment 2 was the same, i.e., a  $200 \times 10$  lattice was used with 100 particles in each cell. The  $B_0$  particles were assigned to Columns 0 to 85 and 115 to 200, and the  $R_0$  particles to Columns 94 to 106. In order to mimic the mixing zone, the  $B_1$  particles were assigned to Columns 86 to 89 and 111 to 114 and the  $R_1$  particles to Columns 90 to 93 and 107 to 110. Thermal boundary conditions were applied when fluid particles hit a solid.

The simulation codes were written in C and the simulation experiments were run with the SP2. Generally, it takes several CPU hours to run a simulation. The structure of the automaton model allows it to be solved efficiently on parallel computers. This will enable large three dimensional simulations to be accomplished in the future.

## 6.4 Results and Discussion

In this section, the simulation results for dispersion at the pore scale is first presented and discussed. Then, the simulation results for dispersion at mega-scale is presented and discussed.

### 6.4.1 Pore Scale Dispersion Simulation

Figure 6.2 depicts the simulation results at 300 iterations for Experiment 1. The four curves in Figure 6.2 show the distribution of particle numbers of tracer for Experiments (1.1), (1.2), (1.3) and (1.4) respectively. It is observed that under the same temperature condition, dispersion in a heterogeneous model is larger than that in a homogeneous model. The reason for this is that in the heterogeneous model, the tracer moves faster in the larger tubes and slower in the smaller tubes. This causes more dispersion in the heterogeneous model than in the homogeneous model because of the different local fluid flow velocities in the heterogeneous model. The double peaks observed in the concentration profiles for the heterogeneous model results from the separation of the flow in the high permeability tubes from those in the low permeability tubes. If a gradual change in tube diameters is used, then this effect should vanish.

When comparing the simulation results at different temperatures (Figure 6.2), it is observed that the tracer moves faster at the low temperature (high beta (B)) due to the low fluid viscosities. However,



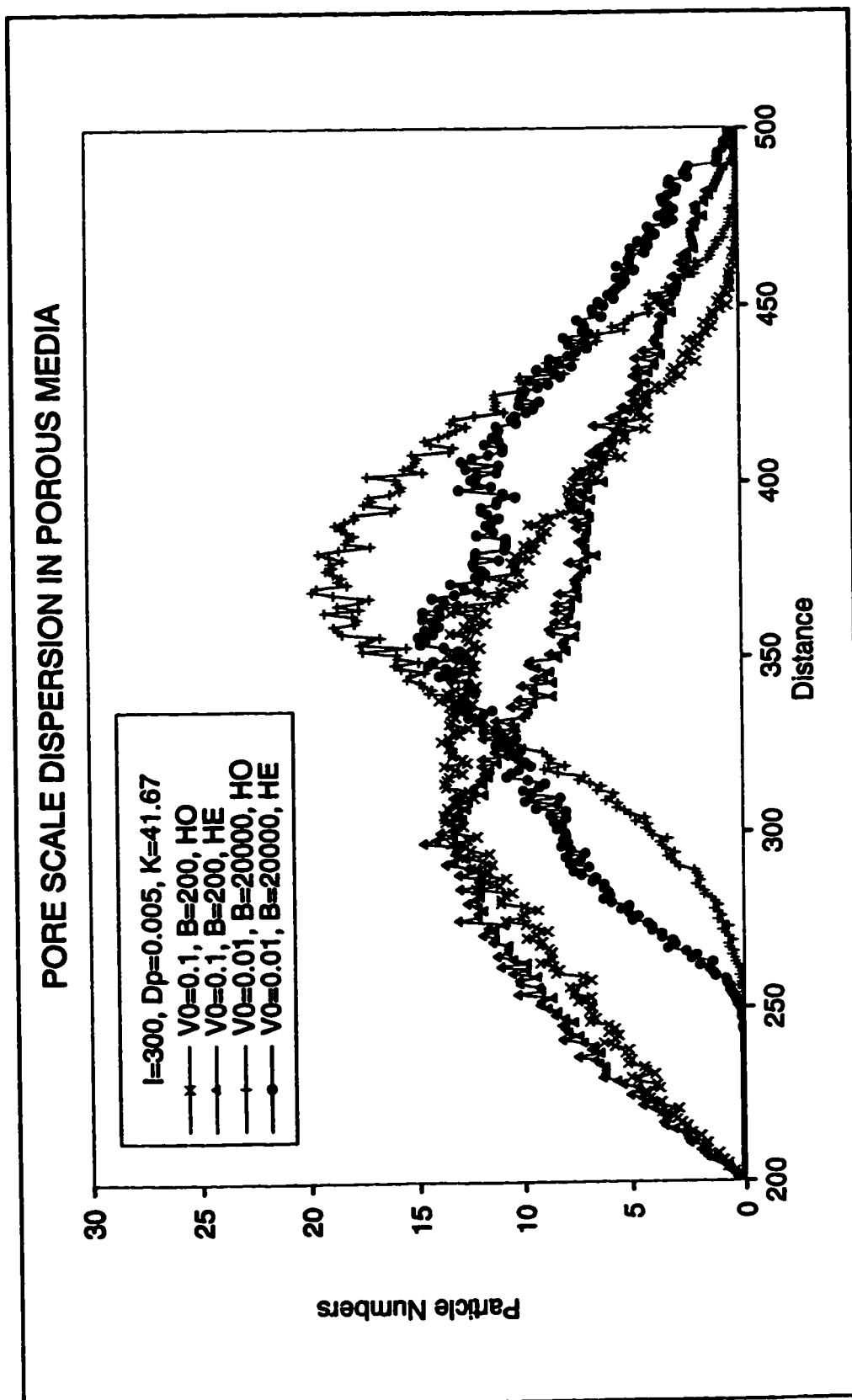


Figure 6.2 Pore scale dispersion in both the homogeneous and heterogeneous porous media models shown in Figure 6.1. The concentration profiles are plotted after 300 iterations and at two different temperatures.

the tracer at the high temperature (low B) spreads more because of the high diffusion coefficient. These simulation results are as expected.

In summary, pore scale dispersion simulations clearly demonstrate the pore structure effects on dispersion. That is, a core with continuous paths connecting large pores “promotes” dispersion. It also indicates that dispersion is affected by the diffusion coefficient and flow rates.

#### **6.4.2 Mega-Scale Dispersion Simulation**

As mentioned in Section 6.3, the initial configuration for the dispersion experiments is that the red particles (tracer) are initialized in the centre of the lattice (Columns 90 to 110) and the blue particles in the rest of the cells of the lattice. When flow starts, there are two miscible displacement fronts, i.e., a left front with blue particles displacing red particle, and a right front with red particles displacing blue particles.

Figures 6.3, 6.4 , 6.5 and 6.6 show the simulation results (distribution of red particle number at 1500 iterations) for Experiments (2.1) and (2.2), (2.3) and (2.4), (2.5) and (2.6), and (2.7) and (2.8), respectively. It can be seen that dispersion in the heterogeneous model is larger than that in the homogeneous model.

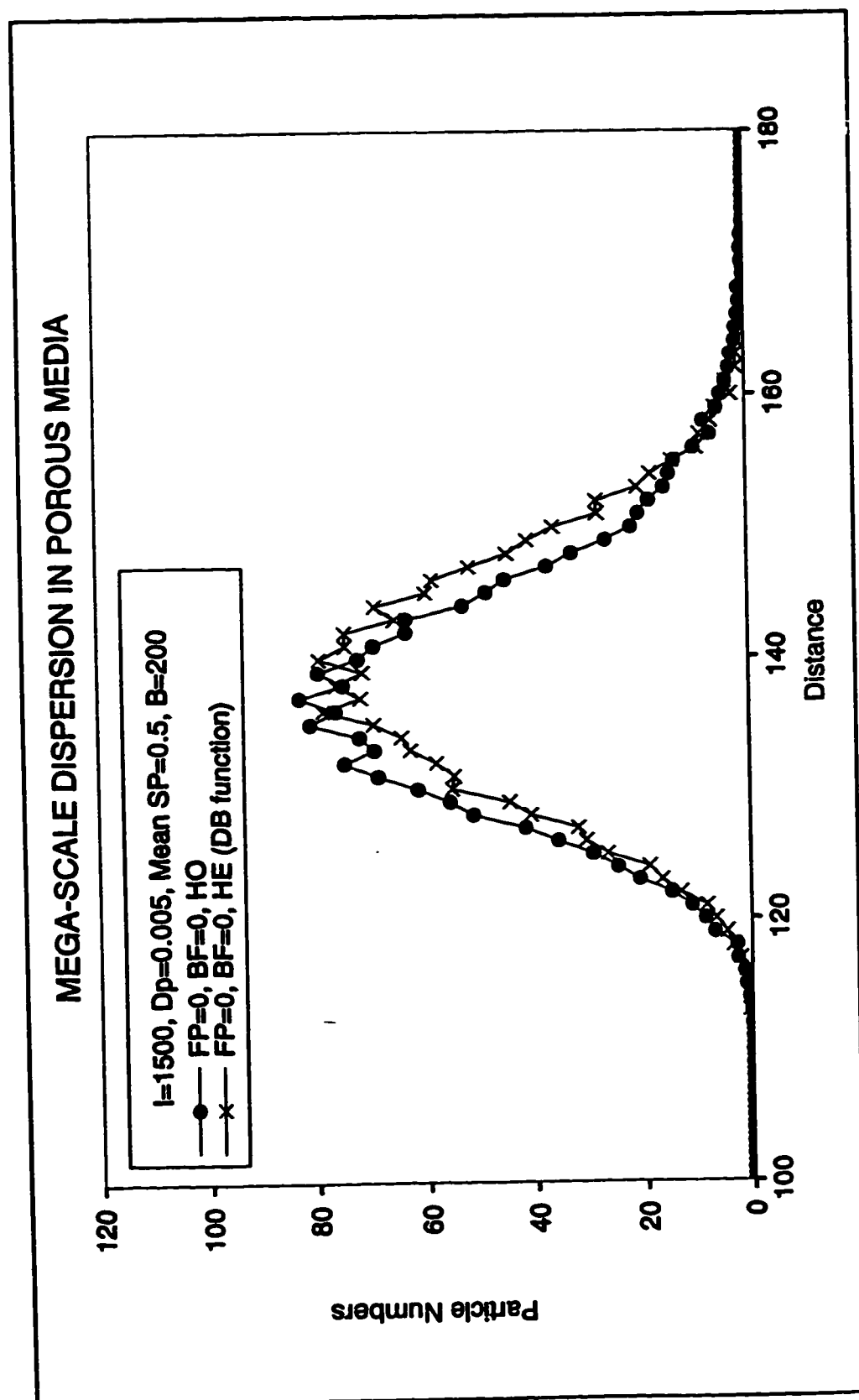


Figure 6.3 Mega-scale dispersion in both a homogeneous and a heterogeneous porous medium with both the flipping probability and the beta factor being zero. The concentration profiles are plotted after 1500 iterations.

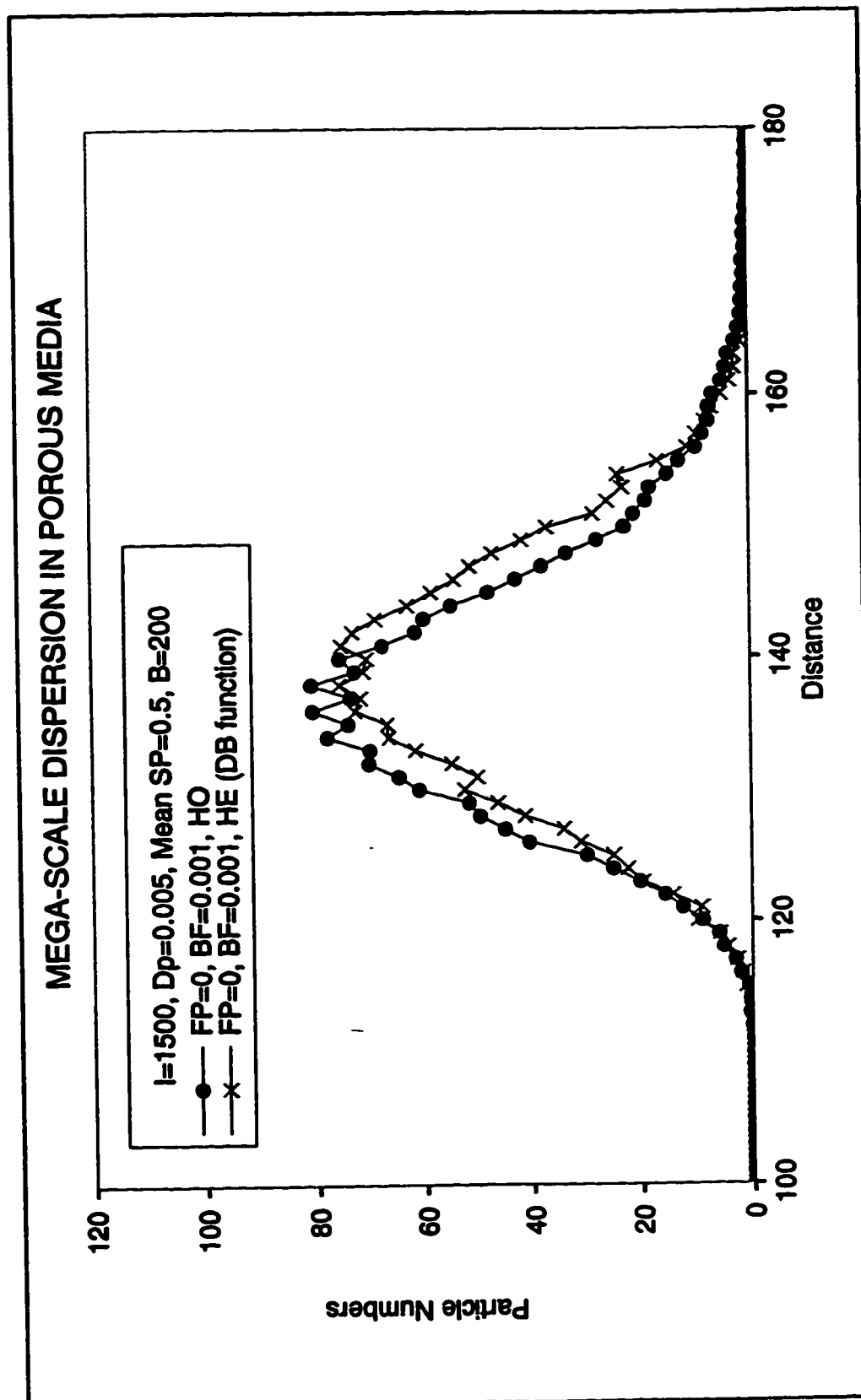


Figure 6.4 Mega-scale dispersion in both a homogeneous and a heterogeneous porous medium with the flipping probability being zero and the beta factor being 0.001. The concentration profiles are plotted after 1500 iterations.

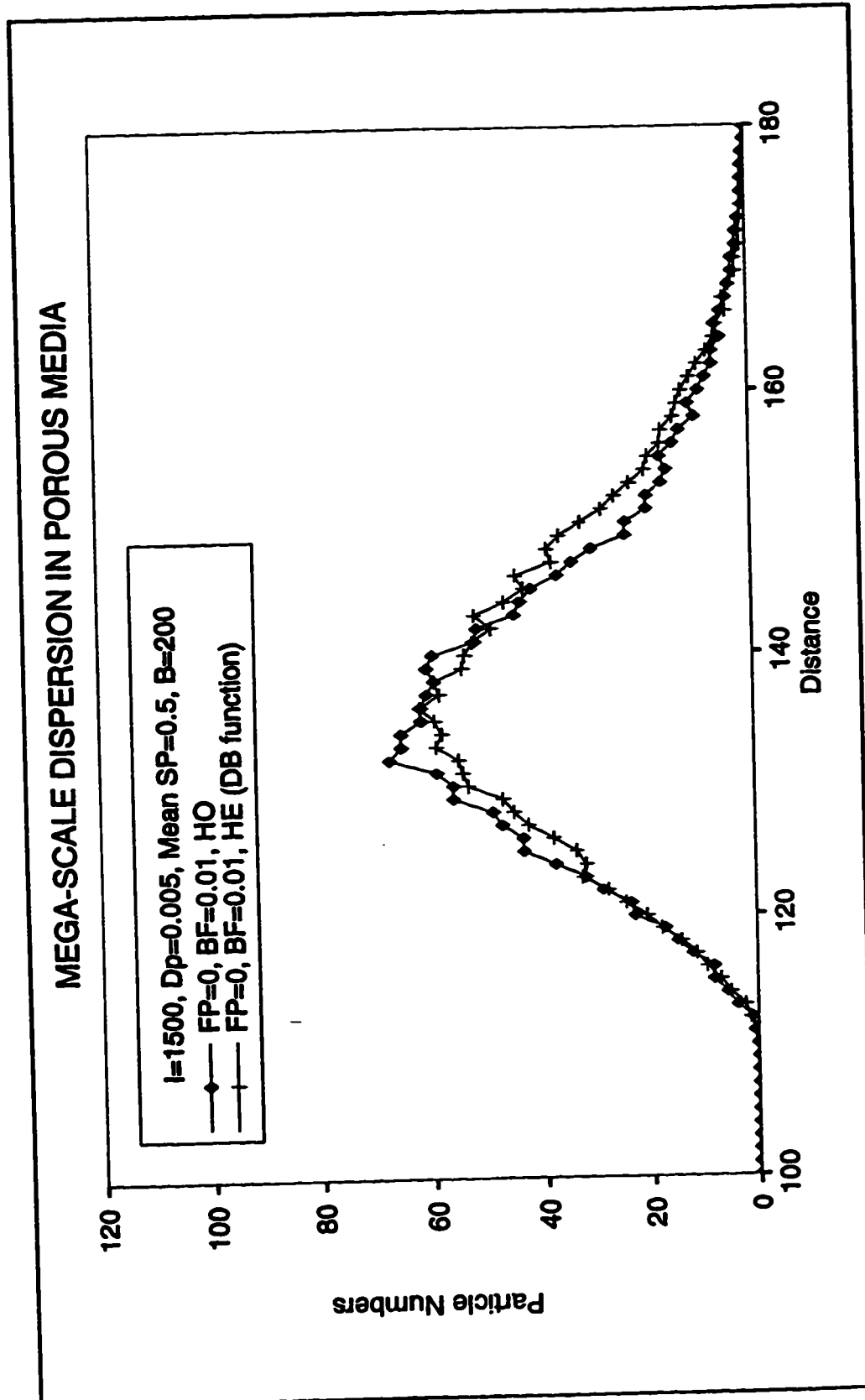


Figure 6.5 Mega-scale dispersion in both a homogeneous and a heterogeneous porous medium with the flipping probability being zero and the beta factor being 0.01. The concentration profiles are plotted after 1500 iterations.

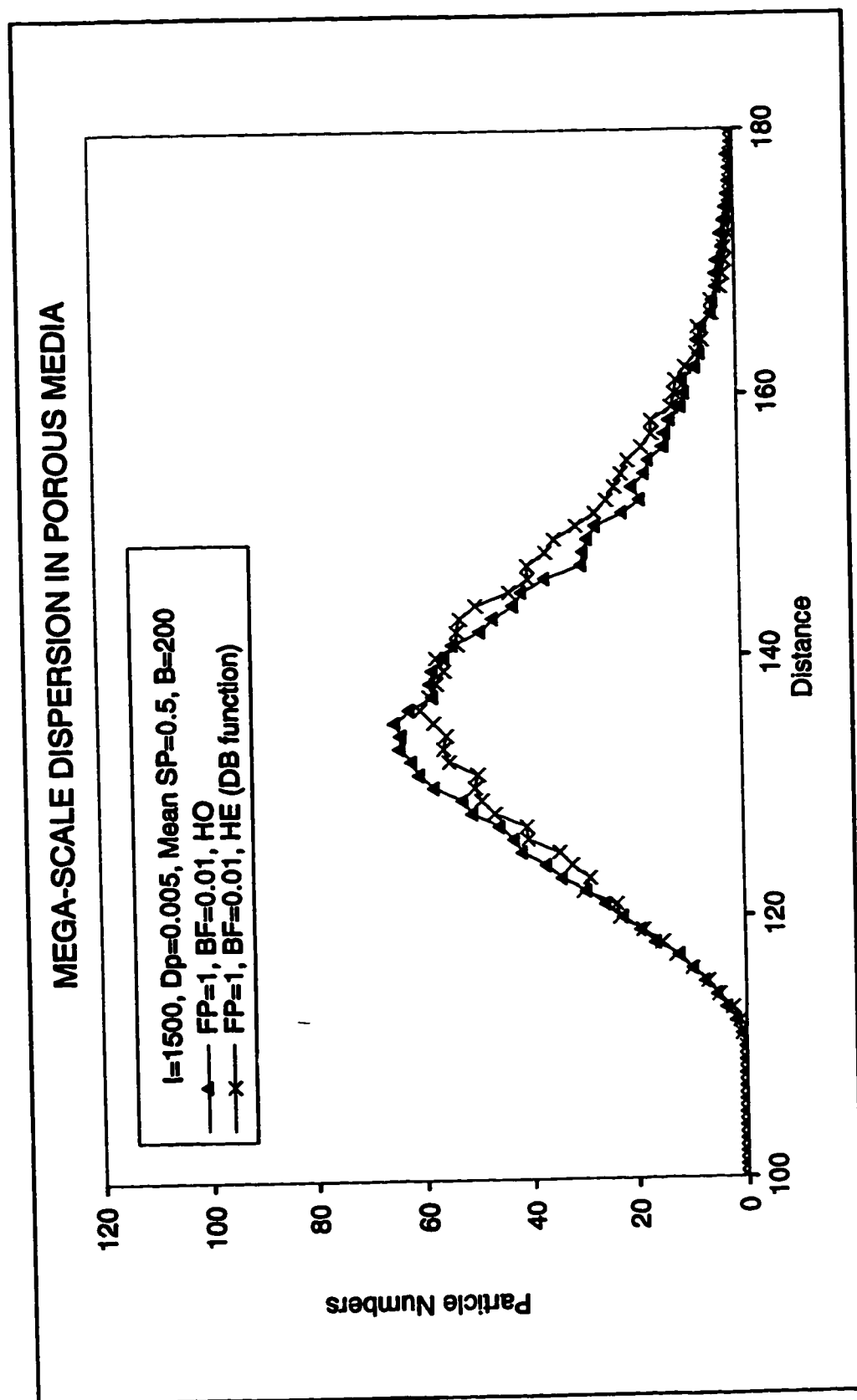


Figure 6.6 Mega-scale dispersion in both a homogeneous and a heterogeneous porous medium with the flipping probability being 1 and the beta factor being 0.01. The concentration profiles are plotted after 1500 iterations.

To study the effects of the value of beta factor (BF) on the dispersion, Figure 6.3 is compared with Figures 6.4 and 6.5. It is observed that an increase in the value of BF, increases dispersion. Moreover, when the value of BF is increased to 0.01, the concentration profiles are not symmetric around the displacement velocity which indicates an asymmetry in the breakthrough curves and an early breakthrough. This simulation result is consistent with both the theoretical predictions (Udey and Spanos, 1993) and experimental results (Brigham, 1974).

A comparison of Figures 6.5 and 6.6 indicates that the value of the flipping probability did not play an important role in reflecting the pore structure. That is, the effect of flipping probability was suppressed by some unknown factors or may be limited by 2D modelling or the nature of the gas model.

## 6. 5 Conclusions

1. Dispersion in porous media was simulated at both the pore scale and the mega-scale with enhanced rules.
2. Pore structure effects on dispersion are clearly demonstrated by pore scale modeling. That is, dispersion increases in a porous medium which consists of continuous paths connected by large pores.
3. Additional rules were added in mega-scale modeling to allow macroscopic phase separation, to reflect the fact that the solid has a preference to collide with the displaced fluid, to incorporate pore structure in porous media and to allow for pressure difference between the displacing and displaced fluids. The simulations results indicate dispersion in the heterogeneous model is larger than that in the homogeneous model. Further, when the value of BF is properly chosen ( $BF=0.01$ ), the concentration profile is not symmetric which indicates an early breakthrough. This simulation result is consistent with both theoretical predictions (Udey and Spanos, 1993) and experimental results (Brigham, 1974).



## 6.6 Bibliography

Brigham, W.E., 1974. Mixing Equations in Short Laboratory Cores. Soc. Petrol. Eng. J. Vol. 14, 91-99.

Edelen, D.G.B, 1976. Nonlocal Field Theories. In Continuum Physics (edited by Eringen), Vol. 4, Academic Press, New York.

Gao, Y. and Sharma, M.M., 1994. A LGA Model for Dispersion in Heterogeneous Porous Media. Transport in Porous Media. Vol., 17.19-32.

Spanos, T.J.T., de la Cruz, V. and Hube, J., 1988. An Analysis of the Theoretical Foundations of Relative Permeability Curves. AOSTRA Journal of Research, Vol. 4, 181-192.

Sternberg, S.P.K., Cushman, J.H. and Greenkorn, R.A., 1996. Laboratory Observation of Nonlocal Dispersion. Transport in Porous Media, Vol. 23, 135-151.

Udey, N. and Spanos, T.J.T., 1993. The Equations of Miscible Flow with Negligible Molecular Diffusion. Transport in Porous Media. Vol. 10. 1-41.

## **CHAPTER 7**

### **MEGASCOPIC CAPILLARY PRESSURE<sup>1</sup>**

#### **7.1 Introduction**

One of the problems that must be overcome in communicating information about transport processes in porous media is to assure that the terminology being used is clearly defined. Certainly two of the most inconsistently defined terms in relation to porous media are concentration and capillary pressure. The origin of the confusion with these terms is associated with the fact that in both cases one has pore scale and megascopic scale (scale of hundreds of pores) quantities with the same name yet distinctly different physical origins. The pore scale concentration refers to the mass fractions of phases mixed at the molecular scale whereas megascopic concentration refers to the mass fractions of phases mixed at larger scales as well. The pore scale capillary pressure describes the pressure difference across actual fluid interfaces whereas megascopic capillary pressure describes the difference between the megascopic (i.e., averaged) pressures of the fluid phases. In this Chapter the concept of megascopic capillary pressure is discussed. These definitions of capillary pressure and megascopic capillary pressure have been presented previously by Bear and Bachmat (1990). They use the term

---

<sup>1</sup> A version of this chapter has been published, de la Cruz, Spanos and Yang, 1995, Transport in Porous Media, 19: 67-77.

capillary pressure to describe the pressure difference across actual fluid interfaces at the pore scale and the term macroscopic capillary pressure to describe what we refer to here as megascopic capillary pressure, i.e., the difference between volume averaged pressures of the fluid phases. In this study the discussion is restricted to a megascopically homogeneous and isotropic porous medium in which all pores are connected.

The concept of capillary pressure in porous media as defined above has been thoroughly reviewed by a number of authors (e.g., Dullien, 1991; Barenblatt et al., 1990; Bear and Bachmatt, 1990; Lenormand and Zarcone, 1983; and de Gennes, 1983). Megascopic capillary pressure, however, depends on the megascopic variables and thus its connection to the pore scale capillary pressure is sometimes difficult to delineate (cf. Barenblatt et al., 1990, Bear and Bachmatt, 1990, and Bentsen, 1994). In the present analysis we attempt to obtain an understanding of megascopic capillary pressure by considering the incompressible limit of the equations of compressible fluid flow through porous media. Here the equations for compressible fluid flow through porous media have been constructed from the well understood equations and boundary conditions at the pore scale. Furthermore, one may make use of the thermodynamic understanding (de la Cruz et al., 1993) of the parameters and variables which describe such compressible deformations when considering this limit. This turns out to be an important consideration because the pressure equations for each of the fluid phases takes on an indeterminate

form in this limit, and the equation which defines the process under consideration is not independent of the continuity equations in this limit. It is observed that these three equations can be combined, when taking the incompressible limit of the system of equations describing the fluid motions, to yield a single process dependent relation. This new equation is a dynamical capillary pressure equation which completes the system of equations for incompressible multiphase flow.

In section 7.2 we write out a complete system of equations for the flow of two compressible fluids through a porous medium. It is assumed that both phases are completely connected and thermomechanical coupling is unimportant. The incompressible limit of these equations is observed to remove one first-order saturation constraint, and to yield an indeterminate form for the pressure equation for each fluid. For incompressible phases one loses two densities as variables; thus, when considering each of the equations in isolation, one ends up one equation short of a complete system.

In section 7.3 the incompressible limit of the pressure equations is considered in more detail. It is demonstrated that the limit of the difference of these two equations yields an equation which completes the system. In the appendix a more general construction of this equation is discussed.

## 7.2 The Flow of Two Compressible Fluids

The megascopic parameters which are considered in this paper are associated with steady flow in rigid porous media. A porous medium is envisaged here as a rigid incompressible matrix whose pores are fully connected and are filled with viscous compressible fluids. For ease of reference we collect together the system of equations proposed by de la Cruz and Spanos (1983 and 1989), on which the following analysis is based. The equations presented here are generalized to include bulk viscosity (Hickey et al., 1995) and inertial terms are ignored.

Equations of motion

$$[\mu_1 \nabla^2 \mathbf{v}_1 + (\xi_1 + 1/3 \mu_1) \nabla(\nabla \cdot \mathbf{v}_1)] + \nabla \left[ \frac{\xi_1}{\eta_1^0} \frac{\partial \eta_1}{\partial t} \right] - (Q_{11} \vec{q}_1 - Q_{12} \vec{q}_2) = \vec{\nabla} p_1 \quad (7.1)$$

and

$$[\mu_2 \nabla^2 \mathbf{v}_2 + (\xi_2 + 1/3 \mu_2) \nabla(\nabla \cdot \mathbf{v}_2)] + \nabla \left[ \frac{\xi_2}{\eta_2^0} \frac{\partial \eta_2}{\partial t} \right] - (Q_{22} \vec{q}_2 - Q_{21} \vec{q}_1) = \vec{\nabla} p_2 \quad (7.2)$$

Equations of continuity

$$\frac{1}{\rho_1^0} \frac{\partial}{\partial t} \rho_1 + \frac{1}{\eta_1^0} \frac{\partial}{\partial t} \eta_1 + \nabla \cdot \mathbf{v}_1 = 0 \quad (7.3)$$

$$\frac{1}{\rho_2^0} \frac{\partial}{\partial t} \rho_2 + \frac{1}{\eta_2^0} \frac{\partial}{\partial t} \eta_2 + \nabla \cdot \mathbf{v}_2 = 0 \quad (7.4)$$

### Pressure equations

$$\frac{1}{K_1} \frac{\partial}{\partial t} p_1 = -\nabla \cdot \mathbf{v}_1 - \frac{1}{\eta_1^0} \frac{\partial}{\partial t} \eta_1 \quad (7.5)$$

$$\frac{1}{K_1} \frac{\partial}{\partial t} p_2 = -\nabla \cdot \mathbf{v}_2 - \frac{1}{\eta_2^0} \frac{\partial}{\partial t} \eta_2 \quad (7.6)$$

### Saturation equation

$$\frac{\partial \eta_1}{\partial t} = \delta_2 \nabla \cdot \mathbf{v}_2 - \delta_1 \nabla \cdot \mathbf{v}_1 \quad (7.7)$$

The variables  $\mathbf{v}_i$  are megascopic average quantities. It is important to understand that  $\nabla \cdot \mathbf{v}_i$ , for instance, does not represent solely the rate of solid dilation, as in the case of a single fluid component. It also incorporates the net flux of a fluid phase into a volume element due to a change in saturation. Here the continuity equation (7.3) describes how this causes (dynamical) changes in the proportioning of materials by mass. The porosity equation (7.7) describes the specific process which is being considered (c.f. de la Cruz et al., 1993). Thus in general the parameters  $\delta_1$  and  $\delta_2$  for drainage like processes can differ from those for imbibition like processes. It is also possible that  $\delta_1$  and  $\delta_2$  given by (7.24) and (7.25) for quasi-static compression are different from the imbibition and drainage sets. In the present analysis it will be assumed that when the effect of surface tension can be neglected these three sets of  $\delta$ 's for quasi-static processes coincide.

If one now restricts the analysis to the case of incompressible, slow, steady flow then one can eliminate the Brinkman term and the bulk viscosity terms from the equations of motion. In this case the saturation equation can be constructed from the continuity equations and thus it is no longer an independent equation. Also the pressure equations each take an indeterminate form. As a result, one is now left with eight equations ((7.1), (7.2), (7.3) and (7.4)) and nine unknowns ( $\vec{v}_1$ ,  $\vec{v}_2$ ,  $p_1$ ,  $p_2$ , and  $\eta_1$ ). An empirical solution to this problem has been supplied by the Leverett (1941) J function.

$$J(s) = \frac{p_c}{\alpha} \left( \frac{K}{P} \right)^{1/2} \quad (7.8)$$

When this relation is plotted against the saturation of the wetting fluid it is observed that imbibition and drainage data yield two distinctly different curves (c.f. Scheidegger, 1974). A physical explanation of the type of dynamical relation required has been given by a number of authors (e.g. Marle 1982, and Eastwood, 1992) based on the grounds that the static capillary pressure equation is a zeroth order constraint rather than a first order equation which is required to make the system complete. These authors have attempted to write out the most general form for the dynamic pressure relationship between incompressible phases which includes parameters which must be determined experimentally. In the present analysis we take a different approach: since the system of equations for compressible phases

is complete the incompressible limit of these equations is considered.

The following system of equations

Equations of motion

$$(Q_{11} \vec{q}_1 - Q_{12} \vec{q}_2) = -\vec{\nabla} p_1 \quad (7.9)$$

and

$$(Q_{22} \vec{q}_2 - Q_{21} \vec{q}_1) = -\vec{\nabla} p_2 \quad (7.10)$$

along with equations (7.3), (7.4), (7.5), (7.6) and (7.7), describe the motion of two compressible fluids very close to the incompressible limit described above.



### 7.3 A Megascopic Capillary Pressure Equation

Now using equation (7.7) to eliminate  $\frac{\partial \eta_1}{\partial t}$  and  $\frac{\partial \eta_2}{\partial t}$  from the pressure equations (7.5) and (7.6) one obtains

$$\frac{1}{K_1} \frac{\partial}{\partial t} p_1 = \left( \frac{\delta_1}{\eta_1^0} - 1 \right) \nabla \cdot \mathbf{v}_1 - \frac{\delta_2}{\eta_1^0} \nabla \cdot \mathbf{v}_2 \quad (7.11)$$

$$\frac{1}{K_2} \frac{\partial}{\partial t} p_2 = -\frac{\delta_1}{\eta_2^0} \nabla \cdot \mathbf{v}_1 + \left( \frac{\delta_2}{\eta_2^0} - 1 \right) \nabla \cdot \mathbf{v}_2 \quad (7.12)$$

Now let  $K_1, K_2 \rightarrow \infty$ , but keeping  $K_2/K_1 = \text{fixed}$  (this assumption assures that the fluids are interacting phases in the incompressible limit as opposed to the solid phase, say, which simply imposes external constraints in this limit by virtue of the conditions  $K_s/K_1 \rightarrow \infty, \mu_s \rightarrow \infty$ ). Then from (7.5) and (7.6)

$$\frac{1}{\eta_1^0} \frac{\partial}{\partial t} \eta_1 + \nabla \cdot \mathbf{v}_1 = O\left(\frac{1}{K}\right) \quad (7.13)$$

$$\frac{1}{\eta_2^0} \frac{\partial}{\partial t} \eta_1 - \nabla \cdot \mathbf{v}_2 = O\left(\frac{1}{K}\right) \quad (7.14)$$

From (7.13) and (7.14) one obtains

$$\eta_1 \nabla \cdot \mathbf{v}_1 + \eta_1 \nabla \cdot \mathbf{v}_2 = O\left(\frac{1}{K}\right) \quad (7.15)$$

and from (7.15) and (7.7) one obtains

$$\frac{\partial \eta_1}{\partial t} = -\eta_1^0 \left( \frac{\delta_2}{\eta_2^0} + \frac{\delta_1}{\eta_1^0} \right) \nabla \cdot \mathbf{v}_1 + O\left(\frac{1}{K}\right) \quad (7.16)$$

Now comparing (7.13) and (7.16) one obtains

$$\frac{\delta_2}{\eta_2^0} + \frac{\delta_1}{\eta_1^0} = 1 + O\left(\frac{1}{K}\right) \quad (7.17)$$

If one uses these equations to describe a static compression of the fluids with zero surface tension then one obtains (setting  $\mu_s=0$  in the analysis of Hickey, 1994, and Hickey et al., 1995)

$$\delta_1 = \frac{K_1}{\left[ \frac{K_1}{\eta_1^0} + \frac{K_2}{\eta_2^0} \right]} \quad (7.18)$$

$$\delta_2 = \frac{K_2}{\left[ \frac{K_1}{\eta_1^0} + \frac{K_2}{\eta_2^0} \right]} \quad (7.19)$$

As stated previously, it will be assumed that the values of  $\delta_1$  and  $\delta_2$  are the same for quasi-static flow processes if surface tension ( $\alpha$ ) is zero. Then

$$\delta_1 = \frac{K_1}{\left[ \frac{K_1}{\eta_1^0} + \frac{K_2}{\eta_2^0} \right]} + \delta_1^\alpha \quad (7.20)$$

and

$$\delta_2 = \frac{K_2}{\left[ \frac{K_1}{\eta_1^0} + \frac{K_2}{\eta_2^0} \right]} + \delta_2^\alpha \quad (7.21)$$

where  $\delta_1^\alpha, \delta_2^\alpha$ , which  $\rightarrow 0$ , when  $\alpha \rightarrow 0$  are the pieces which distinguish a drainage like process from an imbibition like process. Upon substituting (7.20) and (7.21) into (7.17) one obtains

$$\frac{\delta_2^\alpha}{\eta_2^0} + \frac{\delta_1^\alpha}{\eta_1^0} = O\left(\frac{1}{K}\right) \quad (7.22)$$

Equation (7.22) is now interpreted to mean [the more general interpretation of equation (7.22) is considered in the appendix]

$$\delta_1^\alpha, \delta_2^\alpha = O\left(\frac{1}{K}\right) \quad (7.23)$$

which yields

$$\delta_1 = \frac{K_1}{\left[\frac{K_1}{\eta_1^0} + \frac{K_2}{\eta_2^0}\right]} + \frac{a_1}{K_1} + O\left(\frac{1}{K^2}\right) \quad (7.24)$$

$$\delta_2 = \frac{K_2}{\left[\frac{K_1}{\eta_1^0} + \frac{K_2}{\eta_2^0}\right]} + \frac{a_2}{K_2} + O\left(\frac{1}{K^2}\right) \quad (7.25)$$

Note that both incompressible fluid flow and local flow associated with fluid compressions were not present when relationships (7.18) and (7.19) were determined. Equation (7.23) is assumed to represent the process of incompressible fluid flow in the body of this Chapter and this assumption is evaluated in the appendix.

From (7.11), (7.24) and (7.25)

$$\frac{\partial p_1}{\partial t} = -\frac{K_1 K_2}{\eta_1^0 \eta_2^0 \left[ \frac{K_1}{\eta_1^0} + \frac{K_2}{\eta_2^0} \right]} \left[ \eta_1^0 \nabla \cdot \mathbf{v}_1 + \eta_2^0 \nabla \cdot \mathbf{v}_2 \right] + \frac{a_1}{\eta_1^0} \nabla \cdot \mathbf{v}_1 - \frac{K_1}{\eta_1^0} \frac{a_2}{K_2} \nabla \cdot \mathbf{v}_2 \quad (7.26)$$

Here the first term is an indeterminate form since  $[\eta_1^0 \nabla \cdot \mathbf{v}_1 + \eta_2^0 \nabla \cdot \mathbf{v}_2] = O\left(\frac{1}{K}\right)$  and its coefficient is  $O(K)$ . However this term also appears in

$$\frac{\partial p_2}{\partial t} = -\frac{K_1 K_2}{\eta_1^0 \eta_2^0 \left[ \frac{K_1}{\eta_1^0} + \frac{K_2}{\eta_2^0} \right]} \left[ \eta_1^0 \nabla \cdot \mathbf{v}_1 + \eta_2^0 \nabla \cdot \mathbf{v}_2 \right] + \frac{a_2}{\eta_2^0} \nabla \cdot \mathbf{v}_2 - \frac{K_2}{\eta_2^0} \frac{a_1}{K_1} \nabla \cdot \mathbf{v}_1 \quad (7.27)$$

Subtracting (7.27) from (7.26) one obtains

$$\frac{\partial(p_1 - p_2)}{\partial t} = \frac{a_1}{\eta_1^0} \left( 1 + \frac{\eta_1^0 K_2}{\eta_2^0 K_1} \right) \nabla \cdot \mathbf{v}_1 - \frac{a_2}{\eta_2^0} \left( 1 + \frac{\eta_2^0 K_1}{\eta_1^0 K_2} \right) \nabla \cdot \mathbf{v}_2 \quad (7.28)$$

Now define

$$\alpha_1 = \left[ \frac{K_1}{\eta_1^0} + \frac{K_2}{\eta_2^0} \right] \delta_1 - K_1 \quad (7.29)$$

$$\alpha_2 = \left[ \frac{K_1}{\eta_1^0} + \frac{K_2}{\eta_2^0} \right] \delta_2 - K_2 \quad (7.30)$$

and one may write

$$\frac{\partial(p_1 - p_2)}{\partial t} = \alpha_1 \nabla \cdot \mathbf{v}_1 - \alpha_2 \nabla \cdot \mathbf{v}_2 \quad (7.31)$$

Note  $\alpha_1$  and  $\alpha_2$  are of  $O(1)$ ; however, to measure them via  $\delta_1$  and  $\delta_2$  would pose difficult experimental problems because of the indeterminate forms of (7.24) and (7.25). It therefore appears that  $\delta_1$  and  $\delta_2$  have served their purpose in formally leading us to (7.31). Furthermore using (7.15) one may reduce (7.31) to

$$\frac{\partial(p_1 - p_2)}{\partial t} = \left( \alpha_1 + \frac{\eta_1^0}{\eta_2^0} \alpha_2 \right) \nabla \cdot \mathbf{v}_1 \quad (7.32)$$

or finally (from the continuity equation)

$$\frac{\partial(p_1 - p_2)}{\partial t} = -\beta \frac{\partial S_1}{\partial t} \quad (7.33)$$

where  $\beta = \left( \frac{\eta_0}{\eta_1^0} \alpha_1 + \frac{\eta_0}{\eta_2^0} \alpha_2 \right)$  may be taken as the new single parameter replacing the pair  $\delta_1$  and  $\delta_2$ . Here the parameter  $\beta$  which is a linear combination of  $\alpha_1$  and  $\alpha_2$  vanishes when  $\alpha=0$ , and is in general different for different processes. Equation (7.33) completes the system of equations for slow, incompressible, two phase flow.

If the assumption of quasi-static flow is relaxed and acceleration terms are allowed then a term of the form  $\beta' \frac{\partial^2 S_1}{\partial t^2}$  may also appear in Equation (7.33) yielding

$$\frac{\partial(p_1 - p_2)}{\partial t} = -\beta \frac{\partial S_1}{\partial t} + \beta' \frac{\partial^2 S_1}{\partial t^2} \quad (7.34)$$

Thus in the case of miscible flow,  $\beta=0$  and one obtains

$$\frac{\partial(p_1 - p_2)}{\partial t} = \beta' \frac{\partial^2 C_1}{\partial t^2} \quad (7.35)$$

or integrating with respect to time

$$p_1 - p_2 = \beta' \frac{\partial C_1}{\partial t} \quad (7.36)$$

Note that in this case, saturation of phase 1 ( $S_1$ ) has been replaced by the concentration of phase 1 ( $C_1$ ). The physical origins of Equation (7.36) are clear. If the concentration of one phase is increasing in a volume element during segregated, incompressible flow then an average pressure gradient must exist between the displacing and displaced phase. As a result the average pressure of the displacing phase must be greater than that of the displaced phase. The automata version of this equation for miscible flow is given by Equation (6.1) (see Chapter 6).

## 7.4 Conclusions

A process-dependent equation constraining megascopic capillary pressure, along with the equations of motion and the continuity equations is found to form a complete system of equations describing the immiscible flow of two incompressible fluid phases through porous media. A similar equation has been argued for in the case of miscible flow when the motion cannot be assumed to be quasi-static.

It has been observed in this analysis that each of the pressure equations for the component phases becomes indeterminate in the incompressible limit and the saturation equation (7.7) is not independent of the continuity equations in this limit. Thus the complete system of equations for compressible fluid flow through porous media appears to become incomplete in the incompressible limit. However, when the two pressure equations are combined with the saturation equation prior to taking the limit the resulting equation may be evaluated subject to the constraint that one specifies whether the phases are interacting (such as two fluid phases) or non interacting (such as a fluid and a rigid matrix). In the first case each phase still affects the other's motion in this limit and in the second case one phase simply imposes an external constraint on the other.

The requirement that one incorporate the process-dependent equation (7.7) into the pressure equations in order to evaluate

the incompressible limit, which yields equation (7.33), means that in specifying the parameter  $\beta$  one is selecting a specific process. Thus it appears that one must assign different values to  $\beta$  for imbibition and drainage if the nature of the connectivity of the non-wetting phase (at the pore scale) is different in the two processes.



## 7.5 Bibliography

Barenblatt, G.I., Entov V.M. and Ryzhik V.M., 1990. Theory of Fluid Flows Through Natural Rocks. Theory and Applications of Transport in Porous Media. Kluwer Academic Publishers. Dordrecht.

Bear, J. and Bachmat, Y., 1990. Introduction to Modeling of Transport Phenomena in Porous Media. Applications of Transport in Porous Media. Kluwer Academic Publishers, Dordrecht.

Bentsen, R., 1994. Effect of Hydrodynamic Forces on the Pressure-Difference Equation. Transport in Porous Media, Vol.17, 133-144.

de Gennes, P.G., 1983. Theory of Slow Biphasic Flows in Porous Media. Physico-Chem. Hydrodyn., Vol. 4, 175-185.

de la Cruz, V. and Spanos, T.J.T., 1983. Mobilization of Oil Ganglia. AIChE Journal, Vol. 29, 854-858.

de la Cruz, V. and Spanos, T.J.T., 1989. Thermomechanical Coupling during Seismic Deformations in a Porous Medium. Journal of Geoph. Res., Vol. 94, 637-642.

de la Cruz, V., P.N. Sahay and Spanos, T.J.T., 1993. Thermodynamics of Porous Media. Proc. R. Soc. Lond. A, Vol. 443, 247-255.

Dullien, F.A.L., 1992. Porous Media Fluid Transport and Pore Structure. Academic Press, San Diego.

Eastwood, J.E., 1992. Thermomechanics of Porous Media. Ph.D. Dissertation, Department of Physics, University of Alberta, Edmonton.

Hickey, C.J., 1994. Mechanics of Porous Media. Ph.D. Dissertation, Department of Physics, University of Alberta, Edmonton.

Hickey, C.J., Spanos, T.J.T. and de la Cruz, V., 1995. Deformation Parameters of Permeable Media. Geoph. Journ. Inter., Vol. 21, No. 2. 359-370.

Lenormand, R., Zarcone, C. and Sarr, A., 1983. Mechanisms of the Displacement of One Fluid by Another in a Network of Capillary Ducts. J. Fluid Mech, Vol. 135, 337-353.

Leverett, M.C., 1941. Capillary Behaviour in Porous Solids. Trans. AIME, Vol. 142, 152-169.

Marle, C.M., 1982. On Macroscopic Equations Governing Multiphase Flow with Diffusion and Chemical Reactions in Porous Media. Int. Journ. Eng. Sci., Vol. 20, 643-662.

Scheidegger, A.E., 1974. The Physics of Flow Through Porous Media. University of Toronto Press, Toronto.

## **CHAPTER 8 CONCLUSIONS**

In Chapter 2, a thermodynamic automaton model has been constructed. This model allows for a continuous distribution of particle velocities instead of the discrete particle velocities implemented in the conventional lattice gas models (Hardy, Pazzis and Pomeau, 1976 and Frisch, Hasslacher and Pomeau, 1986). The main advantages of this model are (1) it captures thermal effects; (2) relativistic effects can be incorporated; (3) there is no isotropy problem; and (4) it can be easily extended to 3D modeling. The disadvantage of this model is the relatively slow computational speed. Therefore, an extremely powerful computer is required.

In Chapter 3, the validity of the thermodynamic automaton model is checked by modeling the thermal equilibrium state and diffusion in a tube. The simulation results were consistent with the theoretical predictions, thus providing support for the validity of the model. Moreover, it is demonstrated that temperature is an internal property of the model and can be determined from the particle velocity distribution. The diffusion coefficient of a fluid can be determined by simulating diffusion in a tube.

In Chapter 4, some new functions such as "pump" and "thermal boundary" were added to the automaton model. Then the automaton model is used to simulate plane Poiseuille flow with a no-slip (insulator) and a thermal boundary (heat bath) condition. The

simulation results indicate that for the no-slip boundary, viscous dissipation causes the fluid temperature to increase and thus alter the fluid viscosity, and that for the thermal boundary condition, the viscous heat is removed by the thermal boundary and a steady state is achieved. Fluid viscosity determined from the simulation is proportional to  $\sqrt{\text{temperature}}$ . This result is identical to the predictions of physical theory (Sears and Salinger, 1974). Also, it clearly indicates that the automaton model is a gas model.

In Chapter 5, porous media, fluid-solid collisions and a thermal boundary for the solid matrix were introduced into the automaton model. Then the model is utilized to simulate one-phase flow, diffusion and dispersion in porous media at the megascopic scale. The simulation results show that (1) one-phase flow in porous media is consistent with the predictions of Darcy's law (1856); (2) the apparent diffusion coefficient decreases with a decrease in permeability; (3) small scale heterogeneity did not affect the diffusion process significantly; (4) dispersion increases with an increase in flow velocity; (5) thermal boundary conditions for the solid should be used to model dispersion processes in order to maintain a constant temperature; and (6) small scale heterogeneity did not affect the dispersion process significantly; it may be limited by the threshold below which the effect of heterogeneity are negligible, and by 2D modeling. Also, it may be related to the constraints that macroscopic phase separation is not allowed, and that pore structure is not properly simulated.

In Chapter 6, dispersion in porous media is simulated at both the pore scale and the mega-scale with enhanced rules which allow for macroscopic phase separation. These rules reflect the observation that the solid has a preference to collide with the displaced fluid. Also they incorporate pore structure through the propagation rules and pressure difference between the displacing and displaced fluids. Pore scale modeling clearly indicates the effects of pore structure on dispersion. That is, a pore structure with continuous paths connected by large pores increases dispersion. Mega-scale dispersion simulation indicates that when the beta factor (BF) from Equation (7.36) is properly chosen, the simulation results are consistent with both theoretical predictions and experimental results.

In Chapter 7, megascopic concentration and capillary pressure in porous media are discussed. It is found that megascopic concentration and capillary pressure have pore scale and megascopic quantities with the same name but different physical origins. A megascopic capillary pressure equation is derived, starting from the system of equations for compressible two-phase flow and taking the incompressible limit.

In this study, it has been demonstrated that automata simulation is a robust tool for modeling physical processes. Also, the power of the thermodynamic automaton in modeling physical processes including diffusion, fluid flow and dispersion in porous media has been illustrated. The potential application of this model can be extended to simulate immiscible flow including foamy oil flow (Boghosian et al.,

1996) and oil spreading where surface tension (Rothman and Keller, 1988) should be considered. However, a phase transition is required before the thermodynamic properties of liquids can be considered. This model may also be extended to 3D modeling. At present, the potential of the thermodynamic automaton seems to be very great.

.

## 8.1 Bibliography

Boghosian, B.M., Coveney, P.V. and Emerton, A.N., 1996. A Lattice-gas Model of Microemulsions. *Proc. R. Soc. Lond. A*. Vol. 452, 1221-1250.

Darcy. H., 1856. *Les Fontaines Publiques de la Ville Dijon*, Dalmont. Paris.

Frisch. U., Hasslacher, B. and Pomeau, Y., 1986. Lattice-Gas Automata for the Navier-Stokes Equation. *Physical Review Letters*, Vol. 56, No. 14, 1505-1508.

Hardy, J., de Pazzis, O. and Pomeau, Y., 1976. Molecular Dynamics of a Classical Lattice Gas Transport properties and Time Correlation Functions. *Physical Review A*, Vol. 13, No. 5, 1949-1961.

Rothman. D.H. and Keller, J.M., 1988. Immiscible Cellular-Automaton Fluids. MIT Porous Flow Project, Report No. 1, 1-10.

Sears. F.W. and Salinger, G.L., 1974. *Thermodynamics, Kinetic Theory, and Statistical Thermodynamics*. Addison-Wesley Publishing Company. 281-291.

## APPENDIX

A more general interpretation of Equation (7.22) yields

$$\delta_1^\alpha = \delta_1^{(o)\alpha} + O\left(\frac{1}{K}\right) \quad (\text{A1})$$

$$\delta_2^\alpha = \delta_2^{(o)\alpha} + O\left(\frac{1}{K}\right) \quad (\text{A2})$$

where

$$\frac{\delta_2^{(o)\alpha}}{\eta_2^0} + \frac{\delta_1^{(o)\alpha}}{\eta_1^0} = 0 \quad (\text{A3})$$

Thus

$$\delta_1 = \frac{K_1}{\left[\frac{K_1}{\eta_1^0} + \frac{K_2}{\eta_2^0}\right]} + \delta_1^{(o)\alpha} + \frac{a_1}{K_1} + O\left(\frac{1}{K^2}\right) \quad (\text{A4})$$

$$\delta_2 = \frac{K_2}{\left[\frac{K_1}{\eta_1^0} + \frac{K_2}{\eta_2^0}\right]} + \delta_2^{(o)\alpha} + \frac{a_2}{K_2} + O\left(\frac{1}{K^2}\right) \quad (\text{A5})$$

Upon substituting Equations (A4) and (A5) into Equations (7.11) and (7.12) one obtains

$$\frac{\partial p_1}{\partial t} = - \frac{K_1 K_2}{\eta_1^0 \eta_2^0 \left[ \frac{K_1}{\eta_1^0} + \frac{K_2}{\eta_2^0} \right]} \left[ \eta_1^0 \nabla \cdot \mathbf{v}_1 + \eta_2^0 \nabla \cdot \mathbf{v}_2 \right]$$



$$\frac{K_1}{\eta_1^0} \left[ \delta_1^{(0)\alpha} + \frac{a_1}{K_1} \right] \nabla \cdot \mathbf{v}_1 - \frac{K_1}{\eta_1^0} \left[ \delta_2^{(0)\alpha} + \frac{a_2}{K_2} \right] \nabla \cdot \mathbf{v}_2 \quad (\text{A6})$$

$$\frac{\partial p_2}{\partial t} = - \frac{K_1 K_2}{\eta_1^0 \eta_2^0 \left[ \frac{K_1}{\eta_1^0} + \frac{K_2}{\eta_2^0} \right]} \left[ \eta_1^0 \nabla \cdot \mathbf{v}_1 + \eta_2^0 \nabla \cdot \mathbf{v}_2 \right]$$

$$\frac{K_2}{\eta_1^0} \left[ \delta_1^{(0)\alpha} + \frac{a_1}{K_1} \right] \nabla \cdot \mathbf{v}_1 - \frac{K_2}{\eta_1^0} \left[ \delta_2^{(0)\alpha} + \frac{a_2}{K_2} \right] \nabla \cdot \mathbf{v}_2 \quad (\text{A7})$$

Upon subtracting Equation (A7) from Equation (A6) one obtains

$$\frac{\partial (p_1 - p_2)}{\partial t} = \left[ \frac{K_1}{\eta_1^0} + \frac{K_2}{\eta_2^0} \right] \left\{ \delta_1^{(0)\alpha} \nabla \cdot \mathbf{v}_1 - \delta_2^{(0)\alpha} \nabla \cdot \mathbf{v}_2 \right\} +$$

$$\left[ \frac{K_1}{\eta_1^0} + \frac{K_2}{\eta_2^0} \right] \left[ \frac{a_1}{K_1} \nabla \cdot \mathbf{v}_1 + \frac{a_2}{K_2} \nabla \cdot \mathbf{v}_2 \right] \quad (\text{A8})$$

but from Equation (A3)

$$\delta_2^{(0)\alpha} = - \frac{\eta_2^0}{\eta_1^0} \delta_1^{(0)\alpha} \quad (\text{A9})$$

and thus the first term in Equation (A8) becomes

$$\left[ \frac{K_1}{\eta_1^0} + \frac{K_2}{\eta_2^0} \right] \left\{ \eta_1^0 \nabla \cdot \mathbf{v}_1 + \eta_2^0 \nabla \cdot \mathbf{v}_2 \right\} \frac{\delta_1^{(0)\alpha}}{\eta_1^0} \quad (\text{A10})$$

which is an indeterminate form since

$$\left[ \frac{K_1}{\eta_1^0} + \frac{K_2}{\eta_2^0} \right] = O(K) \quad (\text{A11})$$

and

$$\left\{ \eta_1^0 \nabla \cdot \mathbf{v}_1 + \eta_2^0 \nabla \cdot \mathbf{v}_2 \right\} = O\left(\frac{1}{K}\right) \quad (\text{A12})$$

Thus, it is quite possible for  $\delta_1^\alpha$  and  $\delta_2^\alpha$  to contain terms of  $O(1)$ , but unless such terms vanish, the sought for equation remains in an indeterminate form. The additional complication which arises is that one must now evaluate the limit as  $K_1, K_2 \rightarrow \infty$  of the indeterminate form (A10). These terms could be required, for example, to account for flow processes which occur in seismic deformations but are not present in static compressions. However, in the incompressible limit, it must be kept in mind that when one specifies  $\eta_1^0 \nabla \cdot \mathbf{v}_1 + \eta_2^0 \nabla \cdot \mathbf{v}_2$  one cannot make both (A6) and (A7) determinate to  $O(1)$  and independent without making the system of equations overdetermined. Thus it is possible that this

generalization would not alter the form of the pressure equation (7.33) obtained previously, just the value of  $\beta$ .